Fall 1981

Water Wave Refraction with Non-Linear Theory

Im Sang Oh
Old Dominion University

WATER WAVE REFRACTION WITH NON-LINEAR THEORY

by

Im Sang Oh

B.S. February 1972, Seoul National University
Seoul, Korea

M.S. August 1976, Seoul National University
Seoul, Korea

A Dissertation Submitted to the Faculty of
Old Dominion University in partial fulfillment of the
Requirements for the Degree of

DOCTOR OF PHILOSOPHY

OCEANOGRAPHY

OLD DOMINION UNIVERSITY
OCTOBER, 1981

Approved by:

Chester E. Grosch (Director)

ABSTRACT

WATER WAVE REFRACTION WITH NON-LINEAR THEORY

Im Sang Oh
Old Dominion University, 1981
Director: Dr. Chester E. Grosch

Two different kinds of wave refraction models are formulated in the present study using Stokes' third order wave theory. One type of model is utilized in a parametric study employing several different topographies. Wave trajectories obtained from this model, when obtained by using first and third order wave theory with and without the consideration of energy dissipation, show considerable differences. These differences are examined in more detail for a bottom of constant slope: (1) An approximate 10% difference occurs between the refraction coefficients obtained using the first and the third order wave theory. (2) Considerably different ray trajectories are detected for a high wave steepness, and for a large incident angle due to intensive energy dissipation. (3) The refraction coefficient is found to decrease as the sea floor gets steeper. (4) The wave propagation directions, occurring near the wave breaking point, are found to be sensitive to both the wave steepness and incident angle. (5) Changes in wave breaking depth due to wave refraction and energy

dissipation show that the waves of large incident angle and of higher frequencies break in shallower water.

The second type of model uses power refraction theory; this provides a new approach for spectral transformation in shallow water. For this model, the deep water spectrum is supplied as an initial condition. This spectrum is then disassembled to component waves of individual wave height. The power transmitting line at a given water depth is determined by taking a vector sum of the powers of all the component waves, which have been exposed to refraction and energy dissipation. The spectra along this line of power flow are back calculated using these wave components. The spectra obtained from the above method are then compared to spectra from Hasselmann and Collins' model and remote sensing data. The model gives a reasonable result for relatively deeper water, but it does not reproduce the real conditions encountered by the irregular ocean floor region in which the water depth is very shallow. This disagreement seems to be caused mainly by the dissipation rate functions used in this model. Development of a new dissipation rate function is necessary for a better application of this model to shallow water region.

ACKNOWLEDGEMENTS

I am deeply grateful to Dr. Chester E. Grosch under whose supervision this research was carried out. Without his invaluable support, interest and encouragement, this study would not be possible.

Furthermore, I would like to express a great appreciation to my committee members, Drs. John C. Ludwick, Carvel H. Blair, and William D. Lakin for their guidance and criticism of this manuscript.

Special thanks are extended to former Graduate Program Director, Dr. Ronald E. Johnson, for his valuable discussions on administrative procedures, and for his assistance given during the formative stages of this research.

Appreciation is expressed to Mrs. Joan C. Grosch, Mrs. Abbie-Dora Blair, and Mrs. Roberta K. Johnson for their kindness and thoughtful giving of advice covering cooking to language.

I particularly want to express my gratitute to Dr. Jong Yul Chung, Seoul National University, Seoul, Korea not only for his academic advice, but also for his continuous encouragement throughout this study.

Mr. W. Douglas Morris provided the wave data used in this research. Richard B. Philips, then, converted this data into a readable format for the Old Dominion University computer. Deep gratitude goes to them.

I thank my fellow graduate students, Maria Cintia Piccolo, her husband, Gerardo M. E. Perillo, Joung Won Kim, Gregory V. Kopansky, Ian Anderson, and John W. Koster for their willingness to offer assistance and to lend a sympathetic ear to my problems.

Most of all, I give my deepest thanks and love to my wife, Kee Choon Kim, for her inestimatable patience, sacrifice, and love. Without her support and encouragement, I would have never seen this work through to completion.

I also give thanks, with all my heart, to my mother-in-law for taking care of our children, Soo-hyun and Joo-ho, while I was away from home for more than four years.

Finally, I wish to dedicate this dissertation to my family. Their support and encouragement throughout my education have given me the opportunity to expand my knowledge and to nurture my inquisitiveness towards life. Above all, my heartfelt gratitude is reserved for my parents.

TABLE OF CONTENTS

LIST OF TABLES

LIST OF FIGURES

Chapter 1

INTRODUCTION

It is usually more difficult to understand the transitional state of a physical phenomenon than the equilibrium state. The field of ocean gravity waves is no exception. Waves approaching a shoreline are modified into forms which are different from the ones that they had in deep water. Among the causes of these changes, the most important one is believed to be the change in water depth. Due to changes in depth the wave field undergoes reflection, diffraction, and breaking as well as refraction.

The waves coming in from deep water carry a fixed amount of energy. It is believed that almost all the energy is dissipated in the nearshore area, because the amount of energy reflected back to deep water is usually small. Wave refraction may result in energy concentration or dispersion depending upon the local geometry of the bottom. The concentration of wave energy can cause serious damage to ships and harbor facilities, especially when the wave height is large. Besides these practical considerations, wave refraction is very important from a theoretical point of view, because it is a fundamental phenomenon of wave propagation in a non-homogeneous medium.

According to linear wave theory, waves approaching a shoreline start "feeling the bottom" when the water depth becomes approximately less than one half of the wave length, thus the irregular bottom topography makes the wave speed vary along the crestline such that the waves in shallower water will proceed slower than those in deeper water. In general wave speed is a function of the density of the wave propagating medium. When waves cross the boundary between two different media, according to Snell's law, the ratio of the sine of the angle of incidence in medium 1, to the sine of the angle of the refracted wave in medium 2, is same as the ratio of the wave speed in medium 1 and to that in medium 2. In the case of water waves, the medium is generally assumed to be homogeneous; however the changing water depth is believed to be the major cause of wave refraction.

Researchers studying wave refraction developed a graphical method using this linear wave theory. The first practical procedure was given by Sverdrup and Munk (1944). Johnson et al. (1948) expanded this into a graphical wave front method by estimating the spreading of the adjacent wave orthogonals. In 1952, Arthur et al. reported a method for constructing the orthogonals directly without first drawing the wave fronts, thereby eliminating one of the graphical steps with a concommitant in the drafting errors associated with them. In using all of these methods, only

one frequency component of waves was considered, in an effort to better approximate natural wave fields a random sea had to be considered. Pierson et al. (1955) introduced a method to use a deep water spectrum as an input for refraction calculations. The spectrum was divided into a number of segments and, for each of these, an average frequency and wave height were determined. The refraction of each of these components was then calculated and they were added to make a shallow water spectrum.

The development of the digital computer resulted in rapid advance in wave refraction study. Many researchers have designed numerical models, for example, Rizzoli et al. (1966), Karlsson (1968), Orr and Herbich (1970), Kenyon (1971), and Goldsmith et al. (1974).

Aside from these practical advances in computational methods there has been theoretical progress in the study of wave refraction. Munk and Traylor (1947) introduced the wave refraction equation in an article on the method of ray tracing. In 1958 an important step forward was made by Keller. He employed an asymptotic approximation to the classical, linear theory of small amplitude surface waves to derive the ray equation. This simple ray theory reproduces the failures of the standard ray methods at caustics and shoreline. In both cases, the wave amplitude goes to infinity. In 1971, Chao applied a uniform asymptotic solution involving the Airy function for the caustics. He found

that the wave amplitude decreases exponentially with increasing distance from the caustic and there also exists a phase shift of $|\pi/2|$ across the caustic. The next year (1972), Chao and Pierson reported that they produced a caustic successfully in a wave tank, and showed the verification of Chao's theoretical works. In 1975, Shen and Keller introduced a uniform ray theory, which does not have singularities at caustics and shores, by taking the proper forms of Airy functions. Quite recently Meyer (1979) reviewed the theory of water wave refraction especially the ray theory. He also derived the simple and the uniform ray theory, and discussed various applicabilities of these theories. Not only the first order theory mentioned above but also higher order approximation is applied to this wave refraction study (Grosch and Comery, 1977). They found that the effect of the finite amplitude of the waves is to reduce the magnitude of refraction as compared to the linear theory.

All of the studies mentioned above consider the case in which there is no energy dissipation. Some earlier researchers (Putnam and Johnson, 1949) have shown that the dissipation of energy by bottom friction can bring about significant loss of wave energy with a possible reduction of wave height, particularly for high waves of long period which are propagated into a region of very gentle bottom slope. Bretschneider and Reid (1954) used Putnam and

Johnson's equations when considering refraction in order to calculate the wave height modification along a gentle sloping bottom. Their method requires the solution of an integral equation along the wave rays. For complex conditions this can be only carried out numerically.

Lukasik and Grosch (1963) considered the wave energy dissipation via the linearized Navier-Stokes equation, and derived the energy dissipation rate function from the Stokes' second order wave theory. This dissipation rate function can be used to calculate the energy along the wave rays. Eagleson (1962) considered the progressive and shallow water waves using the linearized viscous equations of motion. He also derived a dissipation rate function which can be used to calculate the energy dissipation along the rays.

Besides the energy dissipation mechanism due to the above mentioned bottom friction, there are also a number of non-linear phenomena, occurring in wave propagation, which can influence the wave field as the wave energy propagates from deep water towards the shoreline. Considerable amount of works on this subject have been done by many researchers: Hasselmann discussed the non-linear energy transfer among wave components in his series of papers (1962, 1963a, 1963b) by assuming that the initial surface displacement has a joint normal distribution. He found that most of the energy transfer is among pairs of almost identical wave numbers.

A simple analytical result for a narrow band spectrum has been obtained by Longuet-Higgins (1976) and applied by Fox (1976) to the mean JONSWAP spectrum. It was found that there was a non-negligible energy transfer among the components near the peak of the spectrum and on the forward face of spectrum.

When short gravity waves override the top of the longer gravity waves, the short waves borrow energy from the long waves at the trough of the long wave and repay it at the crest of the long wave. If, however, the short waves splash or break, or form parasitic capillaries, they lose energy which they borrowed from the long waves. Thus the presence of parasitic capillary waves results in a continual energy drain from the longer waves (Longuet-Higgins, 1963).

All of the non-linear dynamical processes described above were developed in terms of deep water waves. In order to apply them in refraction models, it is necessary to extend them so as to apply to waves of finite water depth. Furthermore, most of the non-linear interactions are found to be very weak because they are third or higher order mechanisms (McGoldrick, 1965, 1970). In addition, these interactions are still subject to a fundamental uncertainty as to how the variations in the Reynolds stress are generated in wind flow over waves (Phillips, 1977). For these reasons, wind effects are not included in the present model. However, the interaction of capillary and gravity

waves and wave reflection due to underwater geometry are considered, and discussed in detail.

The aim of this work is to provide a possible solution to some of these problems. The finite amplitude theory is extended in this study to include dissipation mechanisms. Energy dissipation is expected to change the magnitude of refraction because energy dissipation results in the decrease of the wave height. This fact seems to be very important because in finite amplitude wave theory, the wave height affects the path of the wave ray, while the path of the wave ray directly affects the amount of energy dissipation.

One part of the present research is devoted to the study of finite amplitude monochromatic waves with various energy dissipation mechanisms, in which various topographies are employed. This case is compared with the nondissipation case. The other part deals with the spectrum changes due to refraction, shoaling, and energy dissipation. Third order wave theory is used in this study, because the finite amplitude wave theory is expected to be a more realistic model than the linear theory for the nature of sea surface.

Stokes' third order wave equations and wave intensity function are derived in Chapter 2. A newly innovated power refraction theory for shallow water wave spectrum is introduced, and a theoretical discussion of wave reflection is also included in the same chapter. Chapter 3 contains the

numerical methods and a description of the observed data analysis. Results of numerical experiments and their discussions appear in the next chapter. The final chapter is reserved for the conclusions, and suggestions for further study.

Chapter 2

THEORETICAL BACKGROUND

There are six subsections in this chapter. The first considers the important assumptions involved in the wave theory, and the wave equations up to third order. The second section derives the ray equation and wave intensity function. The third section considers the spectral transformation theory. The fourth section considers a new theoretical approach; the formulation of the power refraction theory. The fifth discusses the various dissipation mechanisms, and the last section is reserved for wave reflection by the underwater topography.

2.1 Stokes' Third Order Wave Equations

Before going into the equations, several assumptions must be stated. The most generally used and accepted approximation is that fluid motion is assumed to be inviscid, incompressible and irrotational. This is a good approximation when waves enter a region of water which is previously at rest. With this approximation, we can eliminate the density differences from the water column, and ignore pre-existing vorticity.

Over a flat bottom, taking $+x$ to be the direction of wave propagation, and $+z$ to be vertically upward, and the wave velocity $\bar{u}$ to be positive gradient of the potential function, ϕ, wave motion, $\bar{u}(x,z,t)$, may be represented as the solution of the problem (Laitone, 1962):

$$\phi_{xx} + \phi_{zz} = 0 \quad : \quad \phi = \phi(x - ct,z), \tag{2.1}$$

$$\eta_t + \phi_x \eta_x = \phi_z = (-c + \phi_x)\, \eta_x \quad : \quad z = \eta \tag{2.2}$$

$$\phi_t + \tfrac{1}{2}(u^2 + \omega^2) + g\eta = -\frac{\Delta P}{\rho} = 0 \quad : \quad z = \eta \tag{2.3}$$

$$\phi_z = 0 \quad : \quad z = -h\,, \tag{2.4}$$

where η surface elevation, c phase velocity, P pressure, ρ water density, u and ω particle velocity in the x and z directions respectively, g gravity. Equation (2.1) represents the continuity equation, equation (2.2) is the kinematic boundary condition of the free surface, equation (2.3) is the Bernoulli equation for the constant pressure at the surface, and equation (2.4) is the boundary condition for a flat horizontal bottom. Equation (2.4) can be rewritten for variable water depth, $h(x)$, as

$$\phi_z + \phi_x h_x(x) = 0\,. \tag{2.4b}$$

The mathematical difficulty and nonlinear character of the finite amplitude wave arise from the free surface boundary conditions (2.2) and (2.3) since the free surface profile

η is in itself an unknown function of the independent variables.

A small-perturbation series expansion is introduced to obtain the higher order approximation, as follows

$$\eta(x - ct) = \sum_{n=1}^{\infty} \sigma^n \eta_n (x - ct), \tag{2.5}$$

$$c = c_o + \sum_{n=1}^{\infty} \sigma^n c_n , \tag{2.6}$$

$$\phi = \sum_{n=1}^{\infty} \sigma^n \phi_n (x - ct, z) , \tag{2.7}$$

$$F(x - ct, z) = \sum_{n=1}^{\infty} \sigma^n \sum_{m=1}^{\infty} \frac{\eta^m}{m!} \left(\frac{\partial^m F}{\partial z^m}\right)_{z=0} . \tag{2.8}$$

Using these equations, we get the solutions to the first order problem,

$$\eta_1 = b \sinh Q \cos \theta , \tag{2.9}$$

$$c_o = \frac{gh}{Q} \sqrt{\tanh Q} , \tag{2.9a}$$

where $Q = kh = 2\pi h/L$, $\theta = 2\pi(x - ct)/L$. By continuing in the same manner we get the second order solution,

$$\eta_2 = \eta_o + \frac{b^2 Q}{4h} \left(\frac{2 \cosh^3 Q + \cosh Q}{\sinh Q}\right) \cos 2\theta , \tag{2.10}$$

$$\eta_o = -\frac{1}{4}\frac{b^2 Q}{h}\tanh Q\,, \tag{2.11}$$

$$C_1 = 0\,. \tag{2.12}$$

This solution will be exactly the same as the second approximation of Stokes' (1880) first method if we let $\sigma = 1/\sinh(Q)$.

Taking the third order approximation for particular components like phase velocity and wave height, which will be used for calculating the ray tracing, does not invalidate the second approximation. In a manner similar to the second order approximation, the wave phase velocity is found to be

$$c = c_o(1 + \sigma^2\, c_2/c_o)$$

$$= \sqrt{(g/k)\tanh kh}\,\left[1 + \frac{(bk)^2}{16\sinh^4 kh} *\right.$$

$$\left.\{9 + 8\cosh^4 kh - 8\cosh^2 kh + O(bk)^4\}\right], \tag{2.13}$$

where b is the coefficient of the first term for Stokes' wave profile, and h is the constant water depth. The height of the wave to the third order is

$$H = 2b\left\{1 + \frac{3(bk)^2}{64}\left[\frac{1 + 8\cosh^6 kh}{\sinh^6 kh}\right] + O(bk)^4\right\}. \tag{2.14}$$

The parameter σ is chosen to be small, as

$$\sigma = \frac{1}{\sinh kh} \quad . \tag{2.15}$$

This solution is good only for constant depth; however, it will be applied to the case of variable depth with the assumptions that the depth change is very slow and the bottom is smooth enough, thus the water depth is locally almost constant. Fortunately the natural sea bed slopes are generally very small, and in most cases it is less than an order of 1/1000 (Shepard, 1963).

2.2 Standard Ray Theory

The refraction of the component wave will now be considered. Starting from Fermat's principle, according to which the ray is a path of minimum travel time, it can be shown that the expressions for the parametric representations of the ray, $x = x(t)$ and $y = y(t)$, satisfy the equations (Fig. 1),

$$\frac{dx}{dt} = c \cos \theta \, ,$$

$$\frac{dy}{dt} = c \sin \theta \, ,$$

$$\frac{d\theta}{dt} = - \frac{Dc}{Dn} \, , \tag{2.16}$$

where c is wave phase velocity, t is the travel time, θ the angle between the ray and the x-axis, and D/Dn denotes the differentiation with respect to arc length n along

the ray. The phase velocity is defined as

$$\frac{ds}{dt} = c \quad \Rightarrow \quad dt = \frac{1}{c}\, ds \ , \tag{2.17}$$

From the equations (2.16)and (2.17), we get

$$\frac{d\theta}{ds} = -\frac{1}{c}\frac{Dc}{Dn} \ , \tag{2.18}$$

which states that the curvature of the ray is equal to the logarithmic velocity gradient along the wave front, and that the ray bends toward the direction of lower velocity.

The variation of $\beta(=\ell/\ell_0)$ which is the ratio of ray separation between neighboring rays, in terms of the arc length along a ray is derived as

$$D\theta = (\frac{D\theta}{Dn}) \cdot \ell \ : \quad D\ell = D\theta \cdot Ds \ ,$$

the first equation above means that the changes of the rays propagating angle, $D\theta$, along the wave crest is equal to the product of the length along the wave crest, ℓ , and the rate of change of the angle along the crest, $\frac{D\theta}{Dn}$. The second equation above means that the expansion of the wave crest, $D\ell$, during the travel of distance, Ds, is the product of the angle change, $D\theta$, and the distance DS. Thus these two equations can be combined as,

$$\frac{1}{\ell} \cdot \frac{D\ell}{Ds} = \frac{D\theta}{Dn} \ , \tag{2.19}$$

therefore, the equation of ray separation is written

$$\frac{1}{\beta}\frac{D\beta}{Ds} = \frac{D\theta}{Dn} \cdot \qquad (2.20)$$

In words, the logarithmic change in the separation factor along the wave orthogonal is equal to the curvature of the wave front.

In order to apply these equations to a rectangular coordinate system, the differentials must be expressed in terms of x and y. A modified wave orthogonal separation equation has been derived by Munk and Arthur (1952). The following portion is primarily from their work.

To eliminate θ, the following differential operators are used:

$$\frac{D}{Ds} = \cos\theta \frac{\partial}{\partial x} + \sin\theta \frac{\partial}{\partial y}, \qquad (2.21a)$$

$$\frac{D}{Dn} = -\sin\theta \frac{\partial}{\partial x} + \cos\theta \frac{\partial}{\partial y} \cdot \qquad (2.21b)$$

By differentiating equation (2.21a) with respect to n, and equation (2.21b) with respect to s, then subtracting the latter from the former we get the following equations,

$$\frac{D}{Dn}\frac{D\theta}{Ds} - \frac{D}{Ds}\frac{D\theta}{Dn} = \left(\frac{\partial\theta}{\partial x}\right)^2 + \left(\frac{\partial\theta}{\partial y}\right)^2 = \left(\frac{D\theta}{Ds}\right)^2 + \left(\frac{D\theta}{Dn}\right)^2$$

$$= \frac{1}{c^2}\left(\frac{Dc}{Dn}\right)^2 + \frac{1}{\beta^2}\left(\frac{Dc}{Ds}\right)^2 . \qquad (2.22)$$

Now we differentiate equation (2.18) with respect to n and equation (2.20) with respect to s getting

$$\frac{D}{Dn}\frac{D\theta}{Ds} - \frac{D}{Ds}\frac{D\theta}{Dn} = \frac{-1}{c}\frac{D^2c}{Dn^2} - \frac{1}{\beta}\frac{D^2\beta}{Ds^2} + \frac{1}{c^2}\left(\frac{Dc}{Dn}\right)^2 + \frac{1}{\beta^2}\left(\frac{D\beta}{Ds}\right)^2 . \tag{2.23}$$

By substracting equation (2.22) from equation (2.23) we get

$$\frac{1}{\beta}\frac{D^2\beta}{Ds^2} + \frac{1}{c}\frac{D^2c}{Dn^2} = 0 . \tag{2.24}$$

We can modify the equation (2.24), making it only a function of β and θ and s. From equation (2.20) and (2.21b), we get the following equations

$$\frac{1}{c}\frac{D^2c}{Dn^2} = \frac{1}{c}\left[\sin^2\theta\,\frac{\partial^2c}{\partial x^2} - \sin 2\theta\,\frac{\partial^2c}{\partial x\partial y} + \cos^2\theta\,\frac{\partial^2c}{\partial y^2}\right] - \frac{Dc}{Ds}\frac{D\theta}{Dn}$$

$$= q + p\,\frac{1}{\beta}\frac{D\beta}{Ds} ,$$

where

$$p = -\frac{1}{c}\left[\cos\theta\,\frac{\partial c}{\partial x} + \sin\theta\,\frac{\partial c}{\partial y}\right] ,$$

$$q = \frac{1}{c}\left[\sin^2\theta\,\frac{\partial^2c}{\partial x^2} - \sin 2\theta\,\frac{\partial^2c}{\partial x\partial y} + \cos^2\theta\,\frac{\partial^2c}{\partial y^2}\right] .$$

Therefore, equation (2.24) becomes

$$\frac{D^2\beta}{Ds^2} + p\frac{D\beta}{Ds} + q\beta = 0 \ . \qquad (2.25)$$

This equation will be used to calculate the wave separation by the finite difference method. The numerical steps and approximation equations will be discussed in Chapter 3.

2.3 Spectrum Transformation Theory in Shallow Water

Consider an arbitrary area A bounded by a closed contour s containing the total energy EdA. Also consider an element of s such as ds having a unit normal vector $\bar{n}$ and a group velocity through Ds of $\overline{Cg}$. The area A has within it energy sources and/or sinks of strength Q per unit area. The expression of conservation of energy per unit area A is

$$\frac{\partial}{\partial t}\int EdA + \oint E\,\overline{Cg}\cdot\bar{n}ds + \int QdA = 0 \ . \qquad (2.26)$$

The first term of equation (2.26) denotes the time rate of change of total energy, the second term means that the loss or gain of energy across the boundary, and the last term states that the creation or dissipation of energy in the s. Using Green's theorem, equation (2.26) can be written as

$$\iint [\frac{\partial E}{\partial t} + \nabla \cdot (E \overline{Cg}) + Q] \, dA = 0 , \tag{2.27}$$

since the area A is arbitrary the integrand must be zero everywhere. Therefore

$$\frac{\partial E}{\partial t} + \nabla \cdot (E \overline{Cg}) = - Q . \tag{2.28}$$

If the energy dissipation Q is zero, the equation (2.28) becomes

$$\frac{\partial E}{\partial t} + \nabla \cdot E \overline{Cg} = 0 . \tag{2.29}$$

In order to consider this energy equation in wave number and/or frequency space, we must show that the wave energy density per unit area of wave number space is invariant following the wave group when there is no loss or gain of wave energy. The following derivation is from Phillips (1977). Consider a group of waves whose wave numbers lie in the element of area $\tilde{A}$ of the wave number plane, specified by the vectors $\bar{k}$, $\bar{k} + \delta\bar{k}'$, $\bar{k} + \delta\bar{k}''$ thus $\bar{\partial}\tilde{A}$

$$\delta\tilde{A} = | \delta\bar{k}' \times \delta\bar{k}'' | \tag{2.30}$$

An equation to specify the changes in $\delta\tilde{A}$ can be derived from the kinematical law of the conservation of waves as follows,

$$\frac{\partial \bar{k}}{\partial t} + \nabla n = 0 , \tag{2.31}$$

where n is a wave frequency. For the incremental wave-number $\delta\bar{k}'$

$$\frac{\partial}{\partial t}\,\delta\bar{k}' + \nabla\delta n = 0\,, \tag{2.32}$$

where δn is the correponding increment in wave frequency. In the absence of convection effects $\delta n = \overline{Cg}\,.\,\delta\bar{k}'$, the equation (2.32) becomes

$$\frac{\partial}{\partial t}\,\delta\bar{k}' + \nabla(\overline{Cg}\cdot\delta\bar{k}') = 0\,. \tag{2.33}$$

From this and the corresponding equation for $\delta\bar{k}''$, it follows immediately that

$$\begin{aligned}&\frac{\partial}{\partial t}\{\delta\bar{k}'\times\delta\bar{k}''\} + \overline{Cg}\cdot\nabla(\delta\bar{k}'\times\delta\bar{k}'')\\ &+ (\delta\bar{k}'\times\delta\bar{k}'')\,\nabla\cdot\overline{Cg} = 0\,.\end{aligned} \tag{2.34}$$

This equation can be written in terms of A,

$$\frac{\partial}{\partial t}\,\delta\tilde{A} + \nabla\cdot(Cg\,\delta\tilde{A}) = 0\,. \tag{2.35}$$

For a continuous spectrum, the energy contained in this set of wave numbers is $E(k)\,\delta\tilde{A}$, so in the absence of currents, the energy balance becomes

$$\frac{\partial}{\partial t}\{E(k)\,\delta\tilde{A}\} + \nabla\cdot\{E(k)\,\overline{Cg}\,\delta\tilde{A}\} = 0. \tag{2.36}$$

We combine equation (2.35) and (2.36) to get the following relationship.

$$\frac{\partial}{\partial t} E(k) + \overline{Cg} \cdot \nabla E(k) = 0 . \qquad (2.37)$$

Thus, the spectral energy density is conserved following a wave group, even if the properties of the medium vary and refraction effects are significant. We can generalize equation (2.37) with energy dissipation function Q.

$$\frac{\partial}{\partial t} E(k) + \overline{Cg} \cdot \nabla E(k) = - Q(k) . \qquad (2.38)$$

Now, we have two energy transport equations (2.28) and (2.38); the former is in physical space, and the latter is in wave number space. By assuming there is no every flow between the different wave numbers, the equation (2.28) can be applied for wave energy dissipation in physical space, then, transferred to wave number space.

2.4 Power Refraction Theory

This approach is a new method, introduced for the first time in this study. For simplicity, let us consider a wave field which has only two wave components, and corresponding wave numbers, k_1 and k_2, with propagation direction θ. In terms of wave length, the first wave (subscript 1) is longer than the second (subscript 2). These wave components do not change their propagation directions unless the water

depth is shallow enough for the wave components to feel the bottom.

Assume these wave components are very close to each other in wave number space. At a certain depth, one of the component waves starts "feeling the bottom" and begins deviating from the other (Fig. 2a).

In the standard ray tracing method for water wave refraction, there are two choices; the first is to assume that there exists only one component wave by taking an average of k_1 and k_2 (Sverdrup and Munk, 1944; Johnson et al., 1948; Arthur et al., 1952; etc.). The second is tracing the two components separately, then adding these two separate wave fields (Pierson et al., 1955; Rizzoli et al., 1966; Karlsson, 1968; Orr and Herbich, 1970; Kenyon, 1971; etc.).

The power refraction method presented here is completely different from the ones mentioned above. At a given point, suppose the first component of the waves starts feeling the bottom and changes direction by $\Delta\theta$. In figures 2b, P_1 and P_2 are the power vectors of the component waves k_1 and k_2, respectively; the directions are those of their group velocities and also those of the phase velocities. The power is assumed to be conserved, thus

$$|P_t| = |P_1| + |P_2| \ . \qquad (2.41)$$

If we assume that one of the components, k_1, feels bottom, then the direction of new power flow is determined as

$$\theta_p^{n+1} = \tan^{-1} \left\{ \frac{|P_1| \sin(\theta_p^n + \Delta\theta_1) + |P_2| \sin(\theta_p^n)}{|P_1| \cos(\theta_p^n + \Delta\theta_1) + |P_2| \cos(\theta_p^n)} \right\}, \qquad (2.42)$$

where the $\Delta\theta_1$ is the angle of refraction due to the change in water depth and the superscript n denotes the calculation step. For finding $\Delta\theta_1$, the following equation, which can be derived easily from equations (2.18) and (2.21b), can be used:

$$\frac{d\theta}{ds} = \frac{1}{c} \left\{ \sin\theta \frac{\partial c}{\partial x} - \cos\theta \frac{\partial c}{\partial y} \right\}. \qquad (2.43)$$

This equation can be solved numerically for a given water depth and frequency (see Chapter 3 for details).

The two component waves have different instantaneous directions of propagation, but they are assumed to merge together to propagate in the direction of θ_p^{n+1}. This is a valid approximation if the components are very close to each other. In this way, a many-component wave field can be simplified, and we can trace the dominant wave power transmission line.

Its generalization is immediate, supposing there are i components in a given wave field. For simplicity, the smaller subscripts, i.e. 1, 2, etc., denote the longer

wavelength waves, thus the wave length decreases with an increasing subscript. The power in scalar units is

$$P_t = \sum_{n=1}^{i} P_n , \quad n = 1,2,\ldots,j-1,j,j+1,\ldots i-1,i \tag{2.44}$$

and the direction of the power, P_t, being transmitted is, when the longer waves are feeling bottom (from 1 to the j-1 components),

$$\theta_P^{n+1} = \tan^{-1} \left\{ \frac{P_1 \sin \theta_1^n + P_2 \sin \theta_2^n \ldots (P_j + P_{j+1} \ldots P_i) \sin \theta_P^n}{P_1 \cos \theta_1^n + P_2 \cos \theta_2^n \ldots (P_j + P_{j+1} \ldots P_i) \cos \theta_P^n} \right\}, \tag{2.45}$$

where $\theta_1, \theta_2, \ldots \theta_{j-1}$ are the instantaneous directions of the component waves, $k_1, k_2, \ldots, k_{j-1}$, which are undergoing refraction. The components $k_j, k_{j+1}, \ldots k_i$ are not feeling bottom at that given water depth, therefore, they must propagate to the same direction as the previous step. At once, this wave group chooses a power transmitting direction by equation (2.45), all the components of the wave group are assumed to propagate in this direction. In other words, all the components of a wave field participate in determining the direction of the power transmission. However, each component's contribution to the direction-determination is different from the others. The contribution

of each individual component wave to the determination of the direction of the wave group increases with increasing power of its own, but the wave group must propagate in the chosen direction after the decision.

Following the wave propagation, this wave group will propagate a distance, DS , and after that, all the components of the group will "vote" again to determine which way to go. Because the component waves refract instantaneously with the standard wave equation, the change of the water depth affects all the bottom-feeling components.

If energy dissipation exists for these wave components, then, this dissipation will directly affect the "voting" of direction determination. If the energy distribution among the wave components is changed, it will also influence the direction of wave power transmission.

2.5 Energy Dissipation Mechanisms

This section consists of three subsections. The first discusses the dissipation mechanisms due to bottom friction, and three different dissipation rate functions are used. In the second subsection, capillary waves are considered as one of the dissipation mechanisms which drain wave energy from the gravity waves. The last subsection deals with white capping which can be a dominant mechanism in a favorable condition.

2.5.1 Bottom Friction

The wave energy dissipation due to bottom friction has been discussed by many researchers (Putnam and Johns, 1949; Bretschneider and Reid, 1954; Ippen, 1966; Hasselmann and Collins, 1968; Long, 1973; Shemdin et al., 1978; and Iwagaki and Tsuchiya, 1966). Putnam and Johnson (1949) set up a model for energy dissipation due to bottom friction and Bretschneider and Reid (1954) applied this model, ending up with the integral equations which were solved by a graphical method. Recently Grosskopf (1980) reviewed this method and found that the model is questionable when the wave spectrum is broad or multipeaked or when the bathymetry is irregular.

Hasselmann and Collins (1968) developed a quasi-linear theory in which the effect of the entire wave spectrum was taken into account when calculating wave energy dissipation for a given spectral component. In 1972, Collins used a much simplified formula from this quasi-linear model to calculate the energy dissipation due to bottom friction as well as the energy generation due to wind. The nonlinear bottom scattering effect was investigated by Long (1973). It turned out that to apply this model to wave energy dissipation, the detailed directional wave spectrum was required. For the present study, two laminar damping equations as well as Putnam and Johnson's model are applied.

A. Third order version of Putnam and Johnson's model.

In this model it is assumed that the friction coefficient does not vary with the wave velocity, and that the sea bottom is a plane surface of constant slope.

The tangential stress, τ, on unit area at any instant is given by

$$\tau = C_f \rho U_b^2 , \tag{2.51}$$

where C_f is the friction coefficient, ρ fluid density, and U_b water velocity at the bottom boundary, calculated from inviscid theory. The instantaneous rate at which energy dissipated per unit area is

$$\tau U_b = C_f \rho U_b^3 , \tag{2.52}$$

then the temporal average rate of energy dissipation per unit area is

$$D = \frac{1}{T}\int_0^T \tau U_b \, dt , \tag{2.53}$$

in which T is a wave period. Applying the third order wave theory and carrying out the integration, we have the dissipation rate function to third order,

$$D_f = - C_f \rho \{\frac{4}{3\pi} \alpha^3 + \frac{3}{4} \alpha^2 \beta + \frac{14}{5\pi} \alpha\beta^2\} , \qquad (2.54)$$

where

$$\alpha = \sigma H / \sinh kh ,$$

$$\beta = \frac{3}{4} \sigma k H^2 / \sinh^4 (kh) ,$$

and σ is wave frequency. Here H is a wave height, k wave number, and h water depth. This model is different from the other two models which will be described in following sections in the way that the dissipation function is directly proportional to the cube of wave height. If β equals zero, this equation goes back to the linear energy dissipation rate function which was derived by Putnam and Johnson (1949).

B. Lukasik and Grosch's model

This model (1963) was derived from the Stokes' second order wave theory which represents the wave profile by a sum of trigonometric functions. They used the linearized Navier-Stokes equation, and to second order, found that,

$$D_f = \frac{DE}{Dt} = - \frac{1}{2} \mu c^2 (\frac{b}{h})^2 \beta \sum_{n=1}^{3} n^{\frac{1}{2}} A_n^2 , \qquad (2.55)$$

where b is the coefficient of the first term in the Stokes expansion, h water depth, μ the dynamic fluid viscosity, c phase velocity of the component wave, and $\beta = \sqrt{\rho/2\nu}$,

ν is a kinematic fluid viscosity, and the expansion coefficients are:

$$A_1 = 1 ,$$

$$A_2 = 3\, bL^2 / (16\, \pi^2\, h^3) ,$$

and $$A_3 = 27(bL^2)^2 / (1024\ \pi^4\, h^6) .$$

C. Eagleson's model

The shearing stress exerted on a smooth horizontal bottom by progressive, shallow water waves is considered in this model (1962), using the linearized viscous equations of motion. The average rate of the dissipation of wave energy is written as,

$$D_f = \frac{DE_L}{Dt} = -\frac{k}{2\pi}\int_0^d\int_0^L \mu\left[\left(\frac{\partial v}{\partial x}\,\frac{\partial u}{\partial y}\right)^2 - 4\left(\frac{\partial u}{\partial x}\,\frac{\partial v}{\partial y} - \frac{\partial v}{\partial x}\,\frac{\partial u}{\partial y}\right)\right] dx\, dy \qquad (2.56)$$

where μ is the dynamic viscosity of water. Then for shallow waters, a boundary layer will form at the bottom, making $\partial u/\partial y$ very large in this area while the gradient $\partial v/\partial x$ is still quite small. Because the gradients $\partial u/\partial x$, and $\partial v/\partial y$, are small for long waves, the first term, which represents the contribution of the bottom resistance,

will predominate. Then he wrote the dissipation rate function for the case of $\beta/k>>1$,

$$D_f = -\frac{\mu}{2}\beta\left(\frac{f}{\sigma}\right)^2 \left(1 + \frac{2k}{\beta}\sinh 2kh\right) , \qquad (2.57)$$

where μ is a dynamic fluid viscosity, $\beta = \sqrt{\sigma/2\nu}$ in which ν is a kinematic fluid viscosity and H wave height,

$$\frac{f}{\sigma} = kcH \,/\, 2 \sinh kh .$$

For the present study, the second term was neglected because the second and higher order portion represent the internal dissipation. Thus the equation reduces as

$$D_f = -\frac{\mu\beta}{2}\left(\frac{f}{\sigma}\right)^2 . \qquad (2.58)$$

2.5.2 Capillary Waves

In this section the energy balance of capillary waves is considered and the energy transfer rate from gravity wave to capillary waves is estimated.

According to Longuet-Higgins (1963), as the steepness of the short gravity wave increases the crest becomes sharper; the local curvature increases and sooner or later, before the surface slope becomes discontinuous, the influence of surface tension becomes locally important. This gives rise to a travelling local disturbance on the primary

gravity wave and because the group velocity of capillary waves is greater than the phase velocity, this produces a train of standing capillaries ahead of the distrubance on the forward face of the gravity wave. These capillary waves extract energy from the short primary waves to be dissipated by molecular viscosity. When dissipation is taken into account, the energy balance equation for the capillary waves takes the form (Phillips, 1977),

$$\frac{\partial}{\partial s}\left[E_c \ (Cg - U) \right] - S\frac{\partial U}{\partial s} = - 4\nu \ k_c^2 \ E_c \ , \qquad (2.59)$$

where s represents the distance along the surface from the primary wave crest, S is the radiation stress, U is the velocity of the water near the crest of the primary wave, k capillary wave-number, ν kinematic viscosity, γ surface tension per unit density. S can be taken to be the radiation stress for pure capiallary waves in deep water, $S = (3/2)E_c$. With the capillary wave number $k_c = U^2/\gamma$, the equation (2.59) reduces to

$$\frac{1}{E_c}\frac{\partial E_c}{\partial s} = \frac{2}{U}\left[\frac{\partial U}{\partial s} - \frac{4\nu}{\gamma^2} U^4\right] . \qquad (2.60)$$

The left hand side of the equation (2.60) is the rate of energy change along the wave surface with respect to the energy itself; while in the right hand side, the first term indicates the source term, the energy coming from the

gravity wave, and the second term is the "sink" or "dissipation" term. If the first term of the right hand side of equation (2.60) is the same as the second term, then the energy of the capillary wave is constant along the surface of the gravity wave the capillary is riding.

From equation (2.60), it is possible to evaluate the total gain of energy for the capillary waves from the gravity wave by direct integration by neglecting the second term for a moment. Thus we get for a gravity wave length,

$$E_c(s) = \frac{E_{co}}{U^2(0)} U^2(s) , \qquad (2.61)$$

where the subscript c denotes the capillary wave, and $s = 0$ at the crest of the gravity wave. For this equation, if E_c can be evaluated, then the rate of energy dissipation for the gravity wave due to this mechanism also can be evaluated.

Let's assume that the capillary wave exists in all of the wave fields in which we have an interest, and the capillary wave is at its maximum steepness. Now we can evaluate the maximum energy for the capillary wave without considering waves breaking, or bursting over the water surface. Therefore, the energy of a capillary wave per unit area is

$$E_c = \frac{1}{2} \rho \gamma k_c^2 a_c^2 = \rho \gamma \overline{(\nabla \zeta)^2} , \qquad (2.62)$$

where overbar denotes the local average of the capillary wave surface. According to Crapper (1957), the maximum capillary wave steepness is 0.73, thus the energy of the capillary wave must be less than or equal to the energy with this maximum steepness. By taking maximum possilbe steepness, the energy of a capillary wave at the gravity wave crest will be at a maximum ($=E_{cmax}$). Now the capillary wave energy along the gravity wave surface is

$$E_c = E_{cmax} \frac{U^2(s)}{U^2(0)} \quad .$$

Therefore, the energy dissipation of gravity wave due to this capillary wave is

$$\begin{aligned} \frac{dE_g}{dx} &= - \frac{2E_{co}}{U^2(0)} < U \frac{\partial U}{\partial x} > \\ &= - \frac{2E_{co}}{U^2(0)} \left[\frac{1}{L} \int_0^L U \frac{\partial U}{\partial x} \, dx \right] , \end{aligned} \tag{2.63}$$

but, $\frac{\partial U}{\partial x}$ must be positive because the first term of equation (2.60) is considered only when it is a source term for capillary waves. Thus the equation becomes

$$\begin{aligned} \frac{dE_g}{dx} &= - \frac{2E_{co}}{U^2(0)} \frac{1}{L} \int_0^{L/2} U \frac{\partial U}{\partial x} \, dx \\ &= - \frac{E_{cmax}}{L} \left(\frac{4 \, kH \, \cosh kh}{1 - H^2 k^2 \cosh^2 kh} \right) . \end{aligned} \tag{2.64}$$

This equation can be compared with the equations (2.54), (2.55) and (2.58) of the previous section.

Returning to the dissipation term in equation (2.60), we will estimate energy dissipation of a capillary wave along the gravity wave surface. Because the capillary wave number is a function of U^2, as the water velocity increases the wave length will decrease rapidly and eventually become so small that it will dissipate by the viscosity effect. The energy equation for a capillary wave assuming no source function, will be

$$E_c(s) = E_{co} \exp \{ - \frac{8\nu}{\gamma^2} \int_0^s U^3 \, ds \} \qquad (2.65)$$

As we can see in this equation, the energy dissipates exponentially when the water velocity and/or integration distance increases. This means that the energy supplied by the gravity wave (source for capillary waves, which is in turn a sink for gravity waves) disappears almost completely during one cycle of the gravity wave.

Equation (2.64) is plotted in Figure 13, with the disspation rate due to bottom friction. The figure shows that the effect of a capillary wave on gravity wave energy dissipation is much lower in low frequency waves than that given by bottom friction, although the maximum possible energy for the capillary wave is used. The effect of a capillary wave on gravity wave energy dissipation seems to

be much smaller than the values which are plotted in Figure 13. The capillary wave effect gradually increases when the frequency gets smaller. In waves with periods less than one second, the capillary wave effect is greater than that given by bottom friction. For the present study, the main frequency of gravity wave is smaller than 0.3 HZ, therefore the capillary wave effect is very small, thus it is not included in the model.

2.5.3 White Capping

In any case, what we clearly know is that the wave amplitude does not become infinite. To be physically reasonable, we have to find the way to limit the wave height. Resonant interactions and nonlinear interactions are very weak because they are third order mechanism (Hasselmann, 1962, 1963; and McGoldrick, 1965, 1970). Therefore the size of waves must be limited by another process and the obvious candidate is wave breaking. Though white capping in deep water and wave breaking on the shore are among the most important causes of energy loss of gravity waves, it is extremely difficulty to analyze them.

The wave undergoing white capping and/or breaking was modelled by Longuet-Higgins and Cokelet (1976). They pointed out that wave breaking occurs when two crests of the wave pattern run together or when a wave moves into a region

where the energy density is locally high or when waves riding over the crest of a longer one have an energy excess as a result of the radiation stress effect.

The probability distribution of breaking wave heights has been examined by Nath and Ramsey (1976), using the JONSWAP spectrum.

For the present study, the direct computation of energy dissipation due to white capping was not included, because the present model does not include wind which is the main cause of white capping. All the non-linear theories for energy dissipation or transfer existing at the time of this study, are for deep water cases, and most of all, the magnitude of energy dissipation due to this mechanism is small (McGoldrick, 1965, 1970). However, under specific circumstances such as intensive ray convergence, this white capping seems to appear and play an important role for energy dissipation. The theoretical investigations for these mechanisms are not sufficiently developed in the quantitative sense to be included in a numerical model.

2.6 Underwater Reflection

The wave reflection by smooth underwater topography has been a topic of interest to many researchers (Kajiura, 1961; Shen and Keller, 1975; and Meyer, 1975, 1979). Although the present study deals with wave refraction

explicitly, wave reflection is closely related to wave refraction in both theoretical and practical ways. As Meyer (1979) pointed out, wave reflection due to underwater topography can be solved by the wave refraction equation and the same results arrived at by long wave approximation. The present section is not intended to describe the whole wave reflection theory; instead the reflection theory due to Meyer (1979) will be reviewed briefly, then the reflection coefficient will be estimated. In that way we can compare the magnitude of this effect with others such as dissipation.

According to Meyer (1979), the equation for wave reflection is

$$\frac{d^2f}{d\xi^2} + 2\,\phi(\xi)\,\frac{df}{d\xi} + \varepsilon^{-2} f = 0 , \qquad (2.66)$$

where f is wave function, ξ is an intrinsic distance, ϕ is a modulation function and ε is wave length scale. By a long wave approximation, the following Riccatic equation

$$\frac{da}{d\xi} = 2ia/\varepsilon + (a^2 - 1)\,\phi , \qquad (2.67)$$

is obtained (see Meyer, 1979; and Kajiura, 1961) where a is a local reflection coefficient.

This equation is not easy to solve unless a is very small in which case it may be treated as a constant. Under this consideration, we get the following equation by direct integration of equation (2.67),

$$a(\xi)\ e^{-2i\xi/\varepsilon} = \int_{-\infty}^{\xi} [\{a(s)\}^2 - 1]\ e^{-2is/\varepsilon}\ \phi ds\ . \qquad (2.68)$$

When ξ goes to infinity, this equation becomes

$$a_+ = \int_{-\infty}^{\infty} (a^2 - 1)\phi\ e^{-2i\xi/\varepsilon}\ d\xi\ . \qquad (2.69)$$

Only considering the magnitude of a_+, we get the reflection coefficient

$$R = |a_+| = \left| \int_{-\infty}^{\infty} (a^2 - 1)\ \phi\ e^{-2i\xi/\varepsilon}\ d\xi \right|\ . \qquad (2.70)$$

This integral equation (2.70) has the awkward property that the integrand is not small but fluctuates so rapidly that almost all of its contributions to the integral cancel one another. Thus the whole integral is much smaller than $|a|^2$. Meyer modified this equation to avoid this problem. He solved equation (2.66) near the turning point by Langer's approximation method, which shows the function to be locally approximatable in terms of Hankel functions. On the other hand, equation (2.70) can be approximated by a stationary

phase method away from the turning point. Then matching these two solutions, he got

$$Re^{2m/\varepsilon} \Rightarrow \left| 2 \cos \frac{\pi}{2+\nu} \right| \text{ as } \varepsilon \rightarrow 0 , \tag{2.71}$$

where $m = - m(\xi)$ and $\nu = (1/\mu) - 2$, and $(\xi - \xi_o)\, \phi \rightarrow \nu\mu/2$, where ξ goes to ξ_o. Here ξ_o is a turning point. Therefore, the reflection coefficient R is

$$R = |a_+| \sim \left| 2 \cos \frac{\pi}{2+\nu} \right| e^{-2m/\varepsilon} . \tag{2.72}$$

Figure 14 is a plot of $2m/\varepsilon$ versus wave frequency at the maximum sloping point of the topography type (5) of Figure 15. As we can see in this figure, $2m/\varepsilon$ is very large in magnitude in the frequency range of the present study ($\sim O(10^{-1})$). Thus the reflection coefficient R, which is proportional to the negative exponential of $2m/\varepsilon$, is an extremely small number because the front cosine function is an order of 1 or less. This is the reason why wave reflection is not included in this model. However, this reflection coefficient does not represent reflection from the beach. Beyond the wave breaking point, wave theory is limited, therefore the present model is not intended to be applicable for wave reflection from the beach.

Chapter 3

NUMERICAL METHODS AND FIELD DATA ANALYSIS

3.1 Numerical Methods

The numerical models used in this study are of two kinds. The first is a standard ray tracing method using third order Stokes' phase velocity, and the second is a modified method which traces the main wave power transmission direction. For both cases, the energy dissipation equation is solved using a Runge-Kutta method (see Appendix B).

3.1.1 Coordinate System and Velocity Gradients

The basic equation for the ray tracing is derived from equations (2.18) and (2.21b). It is,

$$\frac{d\theta}{ds} = \frac{1}{C} \left\{ \sin\theta \frac{\partial C}{\partial x} - \cos\theta \frac{\partial C}{\partial y} \right\}. \qquad (3.1)$$

The wave speed $C(x,y)$ is defined on a locally orthogonal grid by $C(i\Delta x, j\Delta y) = C_{i,j}$, with i and j integers (see Fig. 3). The derivatives in equation (3.1) are approximated

$$\frac{\partial C}{\partial x} \simeq \frac{1}{2\Delta x} (C_{i+1,j} - C_{i-1,j}) , \qquad (3.2a)$$

$$\frac{\partial C}{\partial y} \simeq \frac{1}{2\Delta y} (C_{i,j+1} - C_{i,j-1}) . \qquad (3.2b)$$

by second order centered differences. Thus the semi-discrete form of equation (3.1) is

$$(\frac{d\theta}{ds})_{i,j} = \frac{1}{2C_{i,j}} \{ \frac{\sin \theta_{i,j}}{\Delta x} (C_{i+1,j} - C_{i-1,j}) - \frac{\cos \theta_{i,j}}{\Delta y} (C_{i,j+1} - C_{i,j-1}) \} , \qquad (3.3)$$

with $\theta_{i,j}$ the direction of wave propagation at $(i\Delta x, j\Delta y)$. Now for sufficiently small Δs,

$$\Delta x \simeq \Delta s \cos \theta_{i,j} ,$$

$$\Delta y \simeq \Delta s \sin \theta_{i,j} , \qquad (3.4)$$

so that

$$\Delta\theta_{i,j} \simeq \frac{1}{2C_{i,j}} [(C_{i+1,j} - C_{i-1,j}) \tan \theta_{i,j} - (C_{i,j+1} - C_{i,j-1}) \cot \theta_{i,j}] . \qquad (3.5)$$

If $\theta^{k}_{i,j}$ is the direction of wave propagation at the end of the k'th step, then the new direction of wave propagation $\theta^{k+1}_{i,j}$, is

$$\theta_{i,j}^{k+1} = \theta_{i,j}^{k} + \Delta\theta_{i,j}^{k} \quad . \tag{3.6}$$

The wave propagates a distance Δs in the direction $\theta_{i,j}^{k+1}$ to the point $(x_{i,j} + \Delta x, y_{i,j} + \Delta y)$. The gris is now moved so that it is centered at this point and the calculation is repeated.

The second derivatives of the wave phase speed are needed for the calculation of the wave intensity function which is the inverse of the square root of the refraction coefficient. These second derivatives are approximated by centered differences

$$\frac{\partial^2 C}{\partial x^2} \simeq \frac{1}{(\Delta x)^2} \{ C_{i+1,j} + C_{i-1,j} - 2C_{i,j} \} ,$$

$$\frac{\partial^2 C}{\partial y^2} \simeq \frac{1}{(\Delta y)^2} \{ C_{i,j+1} + C_{i,j-1} - 2C_{i,j} \} ,$$

and

$$\frac{\partial^2 C}{\partial x \partial y} \simeq \frac{1}{4\Delta x \Delta y} \{ C_{i+1,j+1} - C_{i-1,j+1} + C_{i-1,j-1} - C_{i+1,j-1} \} . \tag{3.7}$$

3.1.2 Wave Intensity Function

The second order differential equation (2.25) for the wave intensity function is

$$\frac{d^2\beta}{ds^2} + p \frac{d\beta}{ds} + q\beta = 0 . \tag{3.8}$$

It is approximate by second order centered differences. We, again, approximate the gradients as,

$$\frac{d\beta}{ds} \simeq \frac{1}{2\Delta s} (\beta^{k+1} - \beta^{k-1}) ,$$

$$\frac{d^2\beta}{ds^2} \simeq \frac{1}{(\Delta s)^2} \{\beta^{k+1} + \beta^{k-1} - 2\beta^k\} . \qquad (3.9)$$

By substituting the gradients into the equation (3.8), and solving for β^{k+1}, we get

$$\beta^{k+1} = \frac{(p\Delta s - 2)\ \beta^{k-1} + (4 - 2q(\Delta s)^2)\ \beta^k}{p\Delta s + 2} , \qquad (3.10)$$

where

$$p \simeq \frac{1}{C_{i,j}} \left[\frac{\cos \theta_{i,j}}{\Delta x} (C_{i+1,j} - C_{i-1,j}) + \frac{\sin \theta_{i,j}}{\Delta y} (C_{i,j+1} - C_{i,j-1})\right] ,$$

and

$$q \cong \frac{1}{C_{i,j}} \left\{\frac{\sin^2 \theta_{i,j}}{(\Delta x)^2} [C_{i+1,j} + C_{i-1,j} - 2C_{i,j}] - \frac{\sin 2\theta_{i,j}}{4\Delta x \Delta y} * [C_{i+1,\ j+1} - C_{i-1,j+1} + C_{i-1,j-1} - C_{i+1,j-1}] + \frac{\cos^2 \theta_{i,j}}{(\Delta y)^2} * [C_{i,j+1} + C_{i,j-1} - 2C_{i,j}]\right\} .$$

This recursion relation, equation (3.10), is applied at each

step using the previous values of β^k and β^{k-1}, where k-1 denotes current calculation step.

3.1.3 Third Order Wave Speed

In the third order Stokes' wave theory, the phase speed is written as equation (2.13). Squaring this equation and neglecting the higher order terms, we get

$$C^2 = \frac{g}{k} \tanh (kh) \{1 + \frac{(bk)^2}{8 \sinh^4 kh} [9 + 8 \cosh^4 kh - 8 \cosh^2 kh]\}. \quad (3.11)$$

To find this speed for a given wave frequency and water depth, we need more equations. Though two variables are known, one more variable, b, where b is the first term for Stokes' wave profile, is still unknown. Equation (2.14) is used to find b. By neglecting the higher order terms, equation (2.14) is

$$H = 2b + \frac{3}{64} (2b) (bk)^2 [\frac{1 + 8 \cosh^6 kh}{\sinh^6 kh}]. \quad (3.12)$$

Multiplying by k we get

$$Hk = 2 bk + \frac{3}{256} (2 bk)^3 [\frac{1 + 8 \cosh^6 kh}{\sinh^6 kh}]. \quad (3.13)$$

Then rewriting this equation we get

$$Hk = \alpha + \alpha^3 R , \quad (3.14a)$$

where

$$\alpha = 2\ bk\ ,$$

and
$$R = \frac{3}{256}\ \left[\frac{1 + 8\ \cosh^6 kh}{\sinh^6 kh}\right]. \qquad (3.14b)$$

Here we can rewrite equation (3.11), as

$$C = \frac{g}{\omega_o}\ \{\tanh kh\}\ [1 + \alpha^2 S], \qquad (3.15a)$$

where ω_o is the wave frequency, and

$$S = \frac{1}{32}\ \{9 + 8\ \cosh^4 kh - 8\ \cosh^2 kh\}\ /\ \sinh^4 kh\ . \qquad (3.15b)$$

Assuming the wave frequency to be invariant, we get the dispersion relation, to third order,

$$\omega_o^2 = [gk\ \tanh\ (kh)]\ (1 + \alpha^2 S)\ . \qquad (3.16)$$

The solution of equation (3.14) is straight forward (Abramowitz and Stegun, 1970),

$$\alpha = A + B\ , \qquad (3.17a)$$

where

$$A = \{\frac{1}{2}\ (\frac{kH}{R}) + [\frac{1}{4}(\frac{kH}{R})^2 + \frac{1}{27\ R^3}]^{1/2}\}^{1/3}\ , \qquad (3.17b)$$

$$B = \{\frac{1}{2}\ (\frac{kH}{R}) - [\frac{1}{4}(\frac{kH}{R})^2 + \frac{1}{27\ R^3}]^{1/2}\}^{1/3}\ . \qquad (3.17c)$$

Now, assuming that $\alpha = 0$, equation (3.16) is solved for k, then with this k, R is computed from equation (3.14b) and A and B are computed from equation (3.17b) and (3.17c) by substituting R into them. Then α can be found by equation (3.17a), and the value of S computed from equation (3.15b), equation (3.16) can be solved for k again with this α and S. With this new value of k, a new value of R is computed, etc. This procedure is continued until k converges to the desired accuracy (Grosch and Comery, 1977).

3.1.4 Evaluation of Energy Dissipation

Wave energy dissipation is calculated from equation (2.28), rewriting in terms of power, $P(\omega)$,

$$\frac{d}{ds} P(\omega) = - Q \ , \qquad (3.18)$$

where Q is the dissipation rate function. This equation is solved by a fourth order Runge-Kutta method. The detailed description of this method is given in Appendix B. Three different dissipation rate functions are applied. The wave energy is obtained by dividing $P(\omega)$ by $Cg(\omega)$. For the non-dissipative case, Q is set to zero, thus the subroutine to calculate the energy dissipation is replaced by the constant wave power, in order to be consistant with the wave theory used.

3.1.5 Calculation for Power Refraction Model

The numerical calculation for this method starts by applying the deep water spectrum. The deep water spectrum as an input for the present calculation is from the reference spectrum of Figure 6a. It is assumed that all the components of the wave field which have that deep water spectrum propagate in an identical direction. This angle is set to be the wave strarting angle. The deep water spectrum is used to get the discrete frequencies and corresponding energy density in that frequency band. Thus the wave heights of the component wave, $H_o(\omega)$, are calculated by

$$H_o(\omega) \simeq \sqrt{E_o(\omega)\ \Delta\omega}\ , \tag{3.19}$$

where $E_o(\omega)$ is the spectral energy density at frequency ω, and $\Delta\omega$ is the frequency band whose center is ω. These wave heights are assumed to be the deep water wave heights of the component waves. After calculating the group velocity, $Cg_o(\omega)$, the deep water wave power, $P_o(\omega)$, is calculated by

$$P_o(\omega)\ \Delta\omega \simeq E_o(\omega)\ \Delta\omega \cdot Cg_o(\omega), \tag{3.20}$$

where subscript o denotes deep water, or initial condition.

With these $P(\omega)$ and the initial wave propagation angles, for a given depth a new wave propagation angle, θ_p^{n+1}, is determined by equation (2.45). With this new angle, the wave group is allowed to propagate a distance, ds, which is a numerical calculation step. For finding the instantaneous direction of the bottom-feeling components, θ_1^n, θ_2^n, ..., θ_{j-1}^n in equation (2.45), equation (3.5) is used. When the wave group moves to a new point, the new water depth and new wave height are calculated. Thus, a new direction is calculated with these new values.

3.1.6 Wave Height Evaluation

If there exists energy dissipation, the new values of power, $P(\omega)$, must be calculated at each calculation step. Equation (3.18) is used for this new power distribution. This new power distribution is expected to affect the determination of the new propagation direction of the wave group. Wave spectral energy distribution will also be directly affected, because the spectral energy for the frequency is determined by dividing $P(\omega)$ by $Cg(\omega)$. This energy, $E(\omega)$, replaces the one that was calculated in a previous step. In this way, the energy spectrum for the wave field can be evaluated at any calculation step.

Since the present study considers wave energy dissipation, the wave height must be evaluated at each calculation step. The formula used to calculate the wave height, H, is

$$H = H_o \, K_r \, K_s \, K_p \, , \tag{3.21}$$

where H_o is deep water wave height, and K_r is refraction coefficient, K_s shoaling coefficient, and K_p is the energy dissipation coefficient (Ippen, 1966).

For the present model, each coefficient is evaluated by the following:

$$K_r = \sqrt{\ell_o/\ell} = 1/\sqrt{\beta} \, , \tag{3.22}$$

where β is the wave intensity function which can be evaluated by equation (3.10),

$$K_s = \sqrt{Cg_o/C_g} = \sqrt{k/2 \; k_o \; n} \, , \tag{3.23}$$

where k is wave number, and $n = \frac{1}{2} \left(1 + \frac{2kh}{\sinh 2kh}\right)$,

$$K_p = \sqrt{P\ell/P_o\ell_o} \, , \tag{3.24}$$

where P is wave power, and ℓ is the distance between the adjacent rays. At each calculation step, this wave height, H, is to evaluate the energy dissipation because the dissipation rate functions, are functions of wave height.

3.2 Field Data Analysis

This section is devoted to the method to analyze the sea surface elevation data. The first subsection discusses the general description of data and the method of the

spectrum analysis. The second deals with the frequency and spectrum transformation. This subsection is needed because the data used is from a moving sensor and must be transformed to the fixed coordinate system.

3.2.1 About the Data

The wave height data used for the present study was provided by the Langley Research Center (Hampton, Virginia), NASA. The method of data aquisition and transformation of the analog signal into digital data can be found elsewhere (Morris, 1979). According to Morris, the maximum sustained wind speed was about 31 m/sec, due to tropical storm Amy, passing through the sampling area two days before the data gathering. The surface winds in the test area where from the northwest at 2.5 to 5 m/sec, perpendicular to the dominant swell direction. This swell direction was also the direction of data sampling (Fig. 4). The sampling interval of the data was 0.02 second. The aircraft velocity was 84 m/sec and so the digitization interval of 0.02 seconds corresponds to a spatial interval of 1.68 m.

These data were passed thru a high pass filter to remove low frequency energy (less than 0.15 Hertz in apparent frequency) due to aircraft vertical motion (Linnette, 1961). Rolling and pitching motions of aircraft were assumed to have a negligible effect on the data record with an aircraft of this size (NASA C-54).

The autocorrelation is estimated via the direct calculation method (Bendat and Piersol, 1971) with

$$C_r \equiv C(r\Delta t) = \frac{1}{N-r} \sum_{n=1}^{N-r} \eta_r \, \eta_{n-r} \, , \; r = 0,1,2 \; \ldots \; m \qquad (3.25)$$

where $\eta_r = \eta(r\Delta t)$ is the surface elevation, r is lag number, m is the maximum lag number and N number of total data points. The deep water data (the first 12 minute sample) was used to calculate the autocorrelation taking the maximum time lag as 8 seconds (Fig. 5) because this time lag gives us an acceptable decrease in the magnitude of the autocorrelation (about 0.03). The integral time scale is also estimated for the autocorrelation calculated above by (Monin and Yaglom, 1979),

$$T = \int_0^\infty C(\tau)\, d\tau \qquad (3.26)$$

$$\simeq \Delta t \sum_{r=0}^{m} C(r\Delta t), \; r = 0,1,2, \; \ldots \; m.$$

where Δt is the time interval for sampling of data.

The total data is grouped as follows. The first group is from the first 12 minutes of sampling. This group is assumed to be a deep water reference and its spectrum is called the reference spectrum, because the water depth of this sampling area is deep enough (over 1,000 m which is much larger than the wavelength of interest for the

present study). The second group is from the next 6 minutes of sampling. The third is from the next 6 minutes, and the last group is the last 4.727 minutes. This grouping is an arbitrary division, considering water depth along the sampling line. The groups and their respective names which will be used in this study are:

Group I: Deep Water Reference Group (Segments 1 to 4)

Group II: Transitional Group (Segments 5 and 6)

Group III: Shoaling Group (Segments 7 and 8)

Group IV: Nearshore Group (Segments 9 and 10).

In order to obtain raw spectral estimates, the fast Fourier transformation (FFT) procedure was used. Each segment is used to get a separate spectrum. The data of each segment is divided into M sections, with N data points. The number of data points of each section must be a power of 2 for the spectrum analysis program used, so that a certain amount of data is lost during this process. The confidence bands are estimated for each spectrum. The method used for this estimate is from Hinich and Clay (1968). Because the spectra used for the present study were passed through the Hanning smoothing device, the variance of the spectrum is

$$\text{Var } (V_k) \simeq \frac{3}{8M} S^2(f_k) , \qquad (3.27)$$

where V_k is the real spectrum, and $S(f_k)$ is the spectrum estimated from the present method, and M is the number of segment. Thus, an 80% confidence band was esfimated by

assuming that the sea surface has a normal distribution. The FFT program used is from Dr. Grosch (Old Dominion University, Department of Oceanography, Norfolk, Va.).

3.2.2 Spectrum Transformation

The data from moving sensors are required to be transformed to get the true frequency from the apparent frequency. Assuming the true wave frequency is invariant, the wave speed may be written as

$$C = \omega_o/k = \omega/k \ , \tag{3.28}$$

where ω is radian frequency, and k is wave number. Since the data are sampled from an aircraft, the frequency is shifted by the Doppler effect; the true frequency is

$$\omega = kV \cos \phi - \omega_a \ , \tag{3.29}$$

where ω_a is apparent frequency, V is the aircraft velocity, and ϕ is the angle between the directions of wave propagation and aircract flight. This angle gives the correction for the error due to the angular deviation from actual wave propagation direction. For the present study we do not have true wave propagation direction, therefore a series of tests for the spectrum response has been tried by changing the angle, ϕ , up to 30 degrees. Here we apply the dispersion relation to find the wave number

for a given water depth and frequency of the wave component. The dispersion relation used for this calculation is from equation (3.16),

$$\omega^2 = gk \tanh (k\bar{h}) \, [1. + \alpha^2 S], \qquad (3.30)$$

where g is gravity, and $\bar{h}$ is the mean water depth, through which the given wave is propagating. The wave height for this calculation is estimated by equation (3.19) using the apparent frequency and spectrum.

Now substituting equation (3.30) into equation (3.29) we get

$$\omega_a = kV \cos \phi - \sqrt{gk \tanh (kh) \, (1+\alpha^2 S)} \, . \qquad (3.31)$$

By a similar interation method to that described in section (3.1.3), the wave number k is found, then by equation (3.30) wave frequency is calculated.

The spectral transform is based on the fact that the apparent energy within the apparent wave frequency interval $\Delta\omega_a$ is equal to the true energy within the corresponding true frequency interval $\Delta\omega$.

$$S_a(\omega_a) \, \Delta\omega_a \simeq S(\omega) \, \Delta\omega \, , \qquad (3.32)$$

Because the data used for the spectrum calculation is not a continuous function in the time domain, but a discrete

function, the true spectrum is calculated using the apparent spectrum and the frequency interval of this spectrum as

$$S(\omega) \approx \frac{\Delta\omega_a}{\Delta\omega} \; S_a(\omega_a) \; . \qquad (3.33)$$

This spectrum $S(\omega)$ is plotted in Figure 6a to 6g for the case of $\phi = 0^o$. In Figure 21a to 21g, the effects of the choice of ϕ are illustrated. The results shown in these figures show that we can not discuss the spectral shape in more detail than this band because a certain angle of measurement error might exist. But fortunately, the variation due to this possible angular measurement error is not significant compared with the 80% confidence band plotted on the same figures in the range of angle $\phi \leqslant 30$ degrees. However, if the angle ϕ is large, i.e. 60 degrees, then the difference would be very significant, because the cosine function of equation (3.31) drops much faster than in lower angle $(\phi \leqslant 30^o)$.

Chapter 4

RESULTS AND DISCUSSION

4.1 General View

The wave theory used for the present study is the third order Stokes' theory. Before going into the presentation of the calculation results, it will be more understandable to first consider their assumptions and involving limitations. For the third order Stokes' theory, the perturbation parameter, σ, must be less than 1 for the theory to converge (equation (2.15)). This requires that h/L be larger than 0.1402. This means that the applicable zone for longer waves exists much further from a shore than for shorter waves. This is a limitation that one can easily violate. However, the applicability of this theory can be somewhat extended by following condition; the series can converge even though $1/\sinh Q$ is close to unity if b is small enough, because the proportional constant of the series in Stokes' wave theory is also a function of b. Furthermore, this theory requires that equation (2.14) converges in order to have the height of water surface bounded. Therefore, the equation can be expanded and rearranged, and wave height, H, is

$$H = 2b \left[1 + \frac{27}{64} \left(\frac{b}{h}\right)^2 \left(\frac{L}{2\pi h}\right)^4 \ldots\right], \qquad (4.1)$$

where b is the coefficient of the first term in the Stokes expansion, h water depth, and L wavelength. Thus the second term in the bracket must be less than unity (Laitone, 1962).

The other condition for the series convergence is due to subcritical speed,

$$\left(\frac{h}{L}\right)^2 > \frac{3\sqrt{6}}{16\pi^2} \left(\frac{b}{h}\right) . \qquad (4.2)$$

This condition is the most critical one. Once this is satisfied then the wave height is bounded because the condition for wave height boundedness is within this condition (equation 4.1).

Since the linear theory is used for a comparative purpose, the limitation of the theory will be discussed briefly. By way of deriving the solution of the first order wave theory, only the first term of the Taylor series expansion was retained. Thus, the ratios between neglected terms and retained term in the boundary condition (equation (2.2)) for this linearized equation, such as, $\phi_x \eta_x / \eta_t$, will give some criteria for the validity of the theory (see Perigrine (1972) for detail). Those calculations show that Hk must be less than unity, tanh (kh), and cotanh (kh).

If the water depth is deep enough, these conditions will be reduced to $Hk<<1$. This means that the wave steepness must be small. If water depth, h, is shallower, these conditions become $H<<h$. Therefore, linear wave theory is invalid before the wave goes to breaker point when we assume the wave breaks at $H_b/h_b = 0.78$ (McCowan, 1894).

In spite of these limitations, the third order Stokes' wave theory seems to be the best one for the present wave refraction study. The reasons are as follows: Because the wave refraction starts in relatively deep water ($\sim h/L_o = 1/2$) and continues until breaking, the finite amplitude theory is the only one to cover this wide range of area. Secondly, it incorporates the energy dissipation model developed by Lukasik and Grosch (1963).

The choice of the criterion, $H_b/h_b = 0.78$, is from the theoretical work of McCowan (1894), which is a universally used rule of thumb for engineers and sedimentologists. The theoretical maximum wave height-to-depth ratio has been a topic of many reserchers (Packham, 1952; Davies, 1952; Laitone, 1960; Lenau, 1966; Divoky et al., 1969, etc.). Except Packham who reported H_b/h_b as 1.03, most theoretical values are in the range of 0.73 to 0.89. This wave height-to-depth ratio has been also extensively studied by experimental method. Experimental results have shown that the H_b/h_b is in the range of 0.6 to 1.56 (Collins and Weir, 1969; Galvin, 1969; and Weggel, 1972). Thus the choice

of 0.78 for H_b/h_b seems to be reasonable also for the present study. Wave breaking occurs in deep water also when the wave steepness is high. The breaking criterion over the entire range of water depths is given the Miche's formula (1944, see Galvin, 1972),

$$\frac{H_b}{L_b} = 0.142 \tanh (2\pi h_b/L_b), \qquad (4.3)$$

where the subscript b denotes the condition at breaking point. When the water depth is shallower, the hyperbolic function can be approximated by $2\pi h_b/L_b$. Thus, the wave breaking criterion becomes $H_b/h_b = 0.89$, and, when the depth goes to infinity, $H_b/L_b = 0.14$. Thus the deep water wave steepness must be less than this value, otherwise the wave will break. Therefore, no attempt was made to consider a wave steepness higher than this value for the entire phase of this study. The computation is designed to stop when the wave rays meet these wave breaking criteria.

The results of the present model calculations along the bottoms of constant slopes are summarized in Figures 7 to 12. The angles of ray incidence are measured counter-clockwise from the normal line to the beach.

The differences in refraction coefficients ($K_r = \sqrt{\ell_o/\ell}$) between the calues using third and first order wave theory are plotted in Figure 7. The peak difference in K_r reaches

over 10 percent for angles slightly greater than 45 degrees. It also shows that the third order effect (the differences in K_r) increases as the wave steepness increases, because the wave phase speed is also a function of wave height in third order wave theory. The definition of the refraction coefficient can give a crude estimate for the existing maximum difference in the refraction coefficients. Thus, at the wave breaking depth,

$$\Delta K_r = \sqrt{\ell_o/\ell_3} - \sqrt{\ell_o/\ell_1}$$

$$= \sqrt{\ell_o}\ (1/\sqrt{\ell_3} - 1/\sqrt{\ell_1})\ ,$$

when the initial angles go to zero, ℓ_3 and ℓ_1 both approach ℓ_o. The differences go to zero. On the other hand, if the initial angle goes to $\pi/2$, then ℓ_3 and ℓ_1 go to infinity, also, $1/\sqrt{\ell_3}$ and $1/\sqrt{\ell_1}$ go to zero respectively. Therefore, there must exist a maximum of K_r at some angle within the range 0 to 90 degrees in incidence angle.

Figure 8 shows an exactly identical case to Figure 7, except energy dissipation is included. The general shape is very close, but the magnitudes of the differences between the third and first order refraction coefficients are considerably reduced. This is because the energy dissipation reflects the decrease in wave height, and this decreases wave height influences to the third order effect on the

wave refraction. Figure 9, a combination of Figures 7 and 8, shows the pure effect of energy dissipation on wave refraction. The peak of the features is considerably shifted to the higher angles. This is because great increases in wave traveling distances due to the larger angle of incidence reduce the wave height greatly. Then, the wave ray with energy dissipation proceeds much closer to the shore without breaking. The energy dissipation reduces the refraction coefficient as much as 3 percent at a higher wave steepness.

The striking phenomenon of the third order effect in water wave refraction is the difference in the wave propagating direction near the wave breaking point beyond which the wave theory is not applicable (Fig. 10). For a fixed initial wave angle, the final wave propagation angle increases as wave steepness increases, because the two effects are additive, i.e. higher wave breaks in deeper water; so the distance within which the wave can be refracted is reduced, and, also, a larger wave height reduces the amount of wave refraction. At a fixed wave steepness, the final propagation angle generally increases, but not monotonically. At larger incident angles, such as 70 or 80 degrees, the final ray proceeding angles decrease instead of increase, because the divergence of wave rays results in a great decrease in wave height and the waves proceed to the shallower places due to this amplitude

decrease, thus, the wave is more subjected to be refracted. For the energy dissipation case, the final angle decreases considerably due to amplitude decreases by the similar way mentioned above. Figure 10 shows the same, but much amplified tendency for the final angles to increase at larger angles of incidence.

Figures 11a, 11b, and 11c are contours of the water depth at the wave breaking point, as a function of wave steepness and frequency for a constant slope bottom (slope = 0.0008). The broken line contour represents the case in which energy dissipation is accounted for. At a fixed wave steepness the breaking depth decreases as the wave frequency increases as expected, and, for a fixed frequency as the steepness increases, the wave breaking depth increases. The effect of energy dissipation reduces the wave breaking depth, because the energy dissipation reflects a wave height decrease. In the case of an oblique incident angle (Fig. 11b), the dissipation effect is much amplified, again as expected. The contour lines become steeper than those in normal incident angles. This implies that for a given frequency and wave steepness, waves with oblique angle of incidence break in much shallower places than those with normal incidence. In effect the increases in travel distance due to oblique incident angles result in an increase of energy dissipation. Figure 11c shows the 60 degree incident angle case. The higher steepness waves are better

afftected by ray divergence. The contour lines of this angle become steeper than those found in the previous cases.

The refraction coefficients are also decreasing as the bottom slope increases (Fig. 12). The broken lines are the cases for energy dissipation. As we see in the previous figures (Figs. 7 to 11), a higher wave steepness reduces the amount of wave refraction. The case in which the wave steepness is 0.0, corresponds to the first order case. Bottom topographies steeper than 0.0024 shown in Figure 12 have not been considered for the two following reasons: (1) the natural continental shelf slope greater than this value is not common; and (2) because Stokes wave theory is used for the present study, the water depth change per a wave length ($\sim O(10^2 m)$) must not be of comparable magnitude with wave steepness.

4.2 Ray Trajectories

This section shows several typical examples of wave trajectories when they propagate over an area of special topographies. These topographies have very gentle slopes and no singulaties on their surfaces, so that the model can avoid unnecessary difficulties. The choices of the bottom types and the wave parameters are arbitrary, but they are chosen by considering the effect of the parameters which were discussed in the previous section.

4.2.1 Valley

This topography is designed to be symmetrical with respect to $x = x_o$. The water depth, h, is

$$h = h_o(1 + \gamma[\tanh^2 \frac{x - x_o}{W} - 1]), \qquad (4.4)$$

where h_o is the water depth at $x \to \pm \infty$, W is constant which determines the width of the valley, and γ is a dimensionless constant. If γ is positive, the topography is a ridge, and if negative, it becomes a valley (Fig. 15).

Figure 16a shows seven trajectories which have different initial propagation angles. The general behavior of the ray is as expected; bending away from the normal to the contour lines when the ray moves into deeper water, and bending towards the normal when moving from deeper to shallow water. The rays whose initial angles are greater than 38 degrees are refracted back to the shallower area, while the rays less than 37 degrees initial angle crossed the valley. This implies that there exists an initial angle (critical angle) which makes the ray propagate along the axis of the valley without changing direction. Also the divergence of the wave rays increases very rapidly as the initial angle goes closer to the critical angle. Figure 16b shows the case of no energy dissipation. As expected, the effect of refraction was reduced. The fact is the most noticeable when we compare the wave ray of

initial angle 36 degrees of the both figures (Figs. 16a and 16b). This striking feature being a purely third order effect, can not be identified when we use only the linear wave theory.

4.2.2 Slope from Shallow to Deep Water

This bottom type is designed to have a gentle slope between two constant depth planes. The water depth h is

$$h = h_o(1 - \gamma[\tanh \frac{x - x_o}{W} - 1]), \qquad (4.5)$$

The same values for x_o and W as in the cases of ridge/valley are used for these topographies. As we seen in equation (4.5), water depth starts from shallow water and gradually increases to deep water for the given wave. By comparing Figures 17a, 17b, and 17c, one can find marked differences along these trajectories. The rays of Figure 17c are the most strongly refracted, because the first order theory has been used for this trajectory calculation. The dissipation effect on the ray trajectories is also distinct. The rays whose initial propagating angles are 31 and 32 degrees to the positive x-axis show the most different shapes in Figure 17a and Figure 17b. The energy divergence is most severe when the initial angle of the ray gets closer to the critical angle (the initial angle which makes

the wave ray run parallel to the y-axis). If the initial angle, θ_o, is 0 degrees, the energy of the wave will not diverge. On the other hand if θ_o is 90 degrees, the wave energy will not diverge either. This implies that the maximum energy divergence occurs at the critical angle, and after that, the divergence rate reduces gradually. The maximum angle of turning in Figures 17a and 17b is different from that of Figure 17c, which is for the linear theory.

4.2.3 Hollow and Mount

The topographies of this section have rotational symmetry about the point $x = x_o$ and $y = y_o$. Their contour lines are concentric circles. The water depth, h, is

$$h = h_o \left(1+ \gamma \left(\tanh \frac{R}{S} - 1\right)\right) , \qquad (4.5b)$$

where $R = \sqrt{(x - x_o)^2 + (y - y_o)^2}$, and h_o is the water depth at $R \to \infty$, S is the constant for dimension of the topography, and γ is a dimensionless constant (if $\gamma>0$, mount and if $\gamma<0$, hollow).

R_o is chosen for the topographic effect to be 1 percent of the maximum effect point. Thus R_o becomes 3S. This R_o is considered as the radius of the topographies (Fig. 18).

Figure 19a shows the typical trajectories over the hollow described above. The wave rays are intensively converged on the area of the upper right of the topography. The rays whose initial y-coordinate is greater than $R_o/4$ converge, but the rays whose y-coordinate is less than $R_o/4$ diverge. Therefore, behind the topography the energy level is less than the average. This topography is symmetric about x-axis, thus, similar phenomena may exist on the negative side of the x-axis. Figure 18b is the case for energy dissipation. The trajectories show a similar pattern with Figure 19a, but in the area of ray convergence we can notice that some differences exist. The ray convergence area shows considerable differences from those of the third orders'. In all cases, the effect of this topography is negligible when Y_o is greater than R_o.

Figures 20a through 20c are the typical trajectories for wave rays to cross over mount. Similarly as considered for the hollow, the rays whose initial y-coordinate is greater than R_o run almost parallel to x-axis, and the ray on the x-axis also propagates without any bending. As shown in Figure 20c, the rays whose Y_o is greater than $R_o/5$ diverge when crossing the mount. Thus there exist rays which converge and possibly makes caustic behind the mount. These rays are those of which Y_o is less than $R_o/5$.

Tables 1a, 1b, and 1c show the angles of ray propagation after passing the hollow with their corresponding parameters. Because the rays started with a 0 degree angle with respect to x-axis, the angles listed in the table represent directly the effects of refraction. As the wave height increases, the effect of wave refraction decreases because the third order effect gets greater. If the wave length increases for those given conditions, the wave refracts more. Tables 2a, 2b, and 2c shows the same procedures for a mount. A similar tendency was shown in these tables as in Table 1s. However, the differences in final ray propagation angles between first and third order theories, with and without energy dissipation, are much smaller. This is because the distance that the rays can refract is much shorter in this bottom type than those in the cases of the hollow (Fig. 18).

4.3 Caustics

When a wave propagates over a non-uniform depth area, the phase function of the wave will continually change. When we assume the wave frequency to be invariant, the gradient of the phase function becomes a wave number. The equation for the water wave refraction can also be expressed explicitly as a function of wave number. Thus the finding of the wave number along the wave trajectory will be the fundamental question of water wave. Therefore, the

instantaneous direction of the wave number will be the same as the direction of wave propagation.

The tangent to the ray of a wave is

$$\frac{dy}{dx} = \tan\theta = \frac{S_y}{S_x} \quad , \tag{4.7}$$

where θ is the instantaneous direction of wave propagation, and S_x and S_y are components of the phase function to x and y direction respectively. The followings are some numerical examples showing the striking caustic behavior over the topography parallel to the y-axis (see Fig. 15). Because the contour lines are prallel to the y-axis, $\partial k/\partial y = 0$, where k is the wave number. Therefore, $\partial S/\partial y$ must be a constant, say β (see Meyer, 1979), also $S_x^2 = k^2 - \beta^2$. Now the tangent line to the wave ray can be written as (choose + sign)

$$\frac{dy}{dx} = \tan\theta = \frac{\beta}{\sqrt{k^2 - \beta^2}} \quad . \tag{4.8}$$

If we consider the wave runs from shallow to deeper water, then wave number decreases continuously, but, for a given frequency, at some depth the wave number will become a deep water wave number (or asymptotically approaches k_∞). When the water depth goes to infinity, the wave number approaches ω_o^2/g (see equation (3.16)), because α goes to 0, and tanh kh goes to 1. Now at a given point (x_o, y_o), the

slope is

$$\left(\frac{dy}{dx}\right)_o = \frac{\beta}{(k_o^2 - \beta^2)^{\frac{1}{2}}} = \tan \theta_o \ . \qquad (4.9)$$

Thus when β goes to k_o, θ_o approaches 90^o and as β goes to 0, θ_o goes to 0^o. In this case, because k_o is greater than k_∞, there can be two possible cases depending on the magnitude of β.

(1) If β is smaller than k_∞, there is no singularity for equation (4.8) because dy/dx is always real for all k. Therefore, after a certain depth, the wave will propagate with the angle θ_∞ with k_∞.

(2) If β is greater than k_∞, when the wave propagates to deeper water, the wave number k will approach k_∞, thus the wave number k will have the same magnitude at some depth that β has. At this depth the equation (4.8) goes to infinity, and the angle of propagation should be 90^o. Beyond the depth the equation (4.8) becomes imaginary. This line which has that depth is called caustic. The wave cannot cross that line, instead refracting back to shallow water. At the caustic line $x = x_c$, the dispersion relation will be

$$\omega_o^2/g = k_c \tanh k_c h_c \ . \qquad (4.10)$$

Thus solving for h_c, we can find water depth for the caustic as

$$\frac{h_c}{L_o} = \frac{1}{k_c L_o} \tanh^{-1}(\omega_o^2/gk_c) \ . \qquad (4.11)$$

As pointed out before, k_c must be the same as β at $x = x_c$, if k_c exists. Now let's look at the angles to see whether the ray with that initial angle will have a caustic or not. By solving equation (4.9) for β, we get

$$\beta = k_o \sin \theta_o \ . \qquad (4.12)$$

If β is greater than k_∞, then the caustic may exist. Therefore the critical angle for caustic existence is

$$\theta_{cr} > \sin^{-1} \frac{|k_\infty|}{|k_o|} \ . \qquad (4.13)$$

Let's take two examples to compare this analytic result with the model.

1. Valley

As initial conditions, k_o and ω_o are 0.0365 and 0.453 respectively. The initial angle of propagation is chosen to be 41 degrees, then β, k_∞, and caustic depth are as follows,

$$\beta = k_o \sin \theta_o = 0.0239 = k_c \ ,$$

$$k_\infty \Rightarrow \omega_o^2/g = 0.0209 \ ,$$

$$\therefore \ h_c/L_o = \frac{1}{\beta L_o} \tanh^{-1} (k_\infty/\beta) = 0.328 \ .$$

The model calculation shows 0.359 for h_c/L_o, which is very close to the numerical results. The critical angle by equation (4.12) shows $\theta_{cr} > 35.01^o$, but the water depth of the topography does not go to infinity. Because the maximum depth for caustic existence is $(1/2)L_o$ for this valley, k_c can be found from equation (4.11). We get $k_c = 0.0219$, therefore, $\theta_{cr} > \sin^{-1}(k_c/k_o) = 36.92^o$.

Figures 16a and 16b show the ray whose initial angle θ_o is 38 degrees turned back, but the ray of 37 degrees crossing the valley. Thus the analytic value shows very good agreement with the calculated values from the present model, although the model calculations use the third order theory.

2. Slope from Shallow to Deep Water (Slope S to D)

Similarly, picking up k_o and ω_o as 0.036466, and 0.4061056 respectively, and an initial angle of propagation of 35 degrees; then β, k_∞, and caustic depth are

$$\beta = k_o \sin \theta_o = 0.020916 = k_c ,$$

$$k_\infty \Rightarrow \omega_o^2/g = 0.01682875 ,$$

$$\therefore \quad h_c/L_c = 0.30840 .$$

The model shows $h_c/L_o = 0.3127$ in Figure 17a. The critical angle is found in a similar way as in the valley case. The analytic solution shows $\theta_{cr} > 31^o$ for the ray to turn back

to shallow water at $h/L_o = 1/2$. Figure 17c shows exact agreement for this case.

4.4 Power Refractions

As described in Chapter 2, the tracing of a dominant power transmitting line is an analog to the ray tracing of the standard ray theory. For a comparison, the spectral energy density, E, is normalized by dividing the maximum value of the reference spectrum, E_{omax}.

The trajectory of the power refraction cases is a function of the shape of the spectrum (see equation (2.45)). The entire shape of the spectrum affects the direction of the wave group. These power refraction trajectories seem to be directly related to the energy dissipation. In order to examine the applicability of this power refraction model, three kinds of calculations are conducted. The first one is the spectrum transformation over the topographies in Figure 15. The second one is from comparing the present model with Hasselmann and Collins' model (1968). Then the third one is due to the spectral calculation for the measured data.

Figures 22 and 23 are the trajectories from standard ray theory for a peak component of the deep water spectrum, and from power refraction theory for the whole components of the spectrum. The trajectories show remarkably close shapes.

Figure 24 shows the spectrum transformation due to water depth decrease. The reference spectrum (Fig. 6) is supplied as a deep water spectrum (initial values) for this calculation. Equation (2.55) is used for the dissipation rate function. The low frequency components diminish very fast as expected. As the water depth decreases, the spectrum reduces gradually and gets a different shape from the deep water spectrum. The frequency range of the energy dissipation extends fairly wide.

Figure 25 is for the case of bottom topography ridge. It shows the similar shape as the case of Figure 24. Most energy losses are from the components around the peak frequency. The corresponding positions of spectrum calculation are marked on the trajectory of Figure 23.

We can not expect the shift of the spectral peak to any other frequencies, unless the energy dissipation is very strong. On both Figures 24 and 25, the spectrum "e" show the tendency of the shift of energy peak. We can see this phenomenon more clearly at next example.

Figure 26 shows the spectral transformation for constant water depth (100m). The spectrum (B) is from Hasselmann and Collins' model (1968), which considers a spectral dissipation due to turbulent bottom friction. The initial distribution of energy at $x = 0$ was chosen to correspond to a 40-knot Pierson-Moskowitz spectrum (1964) with a

spreading factor proportional to $\cos^4 \chi$. The spectrum (A) is due to the present power refraction model with the same initial spectrum for the same depth, using Putnam and Johnson's (1949) dissipation rate function (this is the case of $\beta = 0$, for equation (2.54)). In both spectra, the drag coefficient, C_f, used is 0.015. The two spectra are remarkably similar in their shapes. The shifting of the frequency of the maximum energy is also similar. The amount of the energy at the spectral peak shows a slight difference (about 10%) between them.

Excepting the use of a different dissipation rate function, the same conditions are applied to the calculation of Figure 27's spectra. Equation (2.55) is employed for the calculation of spectra in this figure. The spectra obtained by using these two different equations show considerable differences. At present, a better, wave applicable formula for the wave energy dissipation is "sought" after, and remains as an active area of study. Furthermore, the present model has the same problem as Hasselmann and Collins' model, in case of using Putnam and Johnson's dissipation rate function (this problem can be avoided by using one of the other two dissipation models). That is a choice of the drag coefficient because both of the models are using the quadratic frictional law. The value of $C_f = 0.015$ used by Hasselmann and Collins for spectrum (B) is the same value which was reported through the laboratory measurement

by Johnson (1965) and field estimate by Bretschneider and Reid (1954). However, there are some uncertainties in choosing this coefficient. In 1967, Iwagaki and Kakinuma calculated this coefficient from the data of both significant and mean wave height, and the transformation data of wave spectra at five different Japanese coastal stations. They obtained much higher values (0.027 to 0.18) than that of Bretschneider and Reid. More recently, another field measurement at 100 Cm from sea bottom shows the wide variation of C_{100}, $3.5 * 10^{-3}$ to $5.4 * 10^{-2}$ (Ludwick, 1975). As this coefficient was measured in the tidal entrance of the Chesapeake Bay, and might show a wider variation than the value on the continental shelf, the choice of drag coefficient for the calculation of wave energy dissipation is at present uncertain.

The constants between the observed and the simulated spectra are given in the next six figures (Figs. 28a through 28f). In the general view, the observed spectra are wider than the predicted ones. The observed spectrum widens when the water depth becomes shallower, however, the model spectrum does not become broader than the reference spectrum. This seems to be because the present model does not include any inter-componental energy flow of the wave field, also the local wind and current effects. When the water depth gets shallower, the mechanisms which are not included in the present model, such as local wind and/or currents, may

have important role for the spectral energy redistribution. The other possible error source is due to the use of the mean water depth for the true frequency calculation (see equation (3.30)). This discontinuity in water depth used for these transformations may cause the abrupt change or broadening of the observed spectra.

It is interesting that the observed spectrum is between the two calculated spectra (Figs. 28d through 28f) using two different dissipation rate functions. The significant disagreement occurs in the spectra of the regions in which the water depth is very shallow. It is probably because the dissipation rate function of model 1 (equation (2.54)) gives a strong energy damping for shallower water, while model 2 (equation (2.55)) gives less dissipation. The comparison of the relative dissipation rates of these functions gives evidence lending support to this discrepancy. At the low frequency range (less than 0.1 HZ) the relative energy dissipation rate of model 1 is greater than of the model 2 by more than 1 order of magnitude (see Fig. 13).

Nevertheless, simulated and observed spectra (Figs. 28a through 28e) show reasonable agreement in the magnitudes of their peaks. However, no agreement occurs in spectra (Fig. 28f) obtained from nearshore sampling. This nonagreement may be due to the inclusions of extranary data. Because segment 10's data is inclusive of the swash zone,

some of the above data may have been obtained beyond the wave breaking point.

The discrepancy between the observed and the simulated spectra (refer to Figs. 28a through 28g) may be explained by a "distortion" in the wave spectra obtained (refer to Figs. 21a through 21g) when observed and expected angles differ. In the data collecting process of the present study, the dominant swell direction in deep water was assumed to be identical to the sampling direction. This does not mean that the wave remains the same direction in shallow water as in deep water, but that the aircraft used to obtain the data is assumed to fly at an almost constant angle with respect to the normal to the shoreline, and as the wave refracts, going nearshore, the angle of deviation from the aircraft direction may be different by more than the 30 degrees, which was assumed to be the maximum possible error. Furthermore, if various wave components having different directions of propagation exist in deep water, then, the measurement error may increase at an even greater rate.

This disagreement does not disappear even though we use the PNJ method for spectrum transformation for this data segment. Morris (1979) reported similar discrepancies between the observed and the simulated spectra for the data segment 10 by using the PNJ method. This is similar to spectra produced by the present power refraction model. Therefore, the advantages of the power refraction model as

compared with the PNJ method can be summarized as follows: (1) it is easy to use, and (2) less calculation is required. It costs less, because it needs only one sweep of calculation, while the PNJ method requires multiple times of sweep depending upon the frequency components considered. (3) It is physically more reasonable because the power refraction model considers the whole shape of the spectrum.

Chapter 5

CONCLUSIONS AND FURTHER SUGGESTIONS

Two different kinds of models have been formulated for the present study. The first model is utilized in a parametric study over constant sloping bottoms. Ray trajectories, obtained for using this model, are tested for several topographies. The second model is a power refraction model, which provides a new approach for a spectral transformation in shallow water.

Within the limits of Stokes' wave theory, the results obtained from the parametric study yield the following conclusion. The ab initio hypothesis (i.e. different wave trajectories can be obtained with linear and third order wave theory, both with and without energy dissipation) is verified.

Using the first and the third order wave theory, an approximate 10% difference in the refraction coefficient was obtained for a bottom of constant slope, thus showing that the energy and trajectories of those waves are not identical. Energy dissipation, also, introduces considerable differences in wave refraction coefficients. The differences due to energy dissipation go up to approximately

3% for a wave steepness of 0.1, with an initial angle of about 60 degrees. The maximum effect of energy dissipation on wave refraction was found to be at about 60 degrees of incident angle. For a fixed wave steepness, the wave refraction coefficient decreases as the sea floor gets steeper.

The final wave propagation angles, obtained by using the two wave theories and energy dissipation, show large differences. These angle differences increase gradually with an increase of wave steepness and, in general, with an increase in the initial wave incidence angles. But at a high wave steepness and large incident angles, the differences are reduced because of a strong decrease in energy and ray divergence.

The wave refraction phenomenon also has an effect on the wave breaking depth. The depth decreases as wave frequency increases, and increases as the wave steepness increases. If energy dissipation is taken into account waves break in shallower depth than if it is neglected. Large incident angles also reduce the depth of wave breaking, due to severe energy dissipation and ray divergence.

In summary, the third order theory best applies for the cases of large wave heights and large wave incident angles. Further, energy dissipation must be considered when the wave approaches at large oblique angles.

Contemporary field data on the scale of the present numerical model is lacking. Wave directional frequency spectra on a similar scale as the continental shelf's width, and wave number spectra need to be incorporated into this finite wave refraction model. A better approximation for a specific area should take into account both the local wind and current effects.

Based on the results and discussions of Chapter 4, the following conclusion can be drawn for the power refraction model. The model gives a reasonable result for relatively deeper water, however, it does not reproduce the realities encountered by the irregular ocean floor region in which the water depth is very shallow. More studies on the wave energy dissipation rate function are necessary to better predict the wave field of this shallow water region.

Table 1a. Final ray proceeding angle after crossing the Hollow(h_{max}/L_o=1/2, R_o= 99% influence of topography).

H_o/h_o	y_o	3rd order no diss.(deg)	3rd order w/ diss. (deg)	1st order (deg)
1/8	$R_o/1$	4.8464	4.8713	5.0515
	$R_o/2$	29.2691	29.4298	30.2268
	$R_o/3$	38.9618	39.0901	39.5106
	$R_o/4$	40.3307	40.4156	40.6744
	$R_o/5$	38.4337	38.5018	38.7277
1/4	$R_o/1$	4.3955	4.4628	
	$R_o/2$	27.6509	28.0563	
	$R_o/3$	37.6712	38.0724	
	$R_o/4$	39.4074	39.7020	
	$R_o/5$	37.6342	37.8769	
1/2	$R_o/1$	3.6161	3.7053	
	$R_o/2$	24.5028	25.2449	
	$R_o/3$	34.4041	35.4117	
	$R_o/4$	36.6467	37.5449	
	$R_o/5$	35.2079	35.9784	

Table 1b. Final ray proceeding angle after crossing the Hollow(h_{max}/L_o=1/3, R_o=99% influence of topography).

H_o/h_o	y_o	3rd order no diss.(deg)	3rd order w/ diss.(deg)	1st order (deg)
1/8	R_o/1	4.9973	5.0338	5.4107
	R_o/2	30.7068	30.9523	32.3612
	R_o/3	42.2613	42.5011	43.5616
	R_o/4	45.8025	46.0723	46.6865
	R_o/5	45.9083	47.0496	46.4819
1/4	R_o/1	4.5206	4.5078	
	R_o/2	28.8205	29.2733	
	R_o/3	40.3469	40.9712	
	R_o/4	44.2438	44.9285	
	R_o/5	44.5691	45.1622	
1/2	R_o/1	4.1684	4.1990	
	R_o/2	26.5119	27.0456	
	R_o/3	37.0143	38.2127	
	R_o/4	40.9510	42.3271	
	R_o/5	41.5145	42.7917	

Table 1c. Final ray proceeding angle after crossing the Hollow(h_{max}/L_o=1/4, R_o=99% influence of topography).

H_o/h_o	y_o	3rd order no diss.(deg)	3rd order w/ diss.(deg)	1st order (deg)
1/8	$R_o/1$	5.0155	5.0452	5.5402
	$R_o/2$	31.0002	31.2642	34.0859
	$R_o/3$	42.9598	43.3731	44.8711
	$R_o/4$	47.3621	47.7016	48.5823
	$R_o/5$	47.8070	48.2119	48.8787
1/4	$R_o/1$	4.7359	4.7670	
	$R_o/2$	29.4936	29.8484	
	$R_o/3$	40.9737	41.7391	
	$R_o/4$	45.2059	46.6888	
	$R_o/5$	46.2597	46.9348	
1/2	$R_o/1$	4.5845	4.6055	
	$R_o/2$	28.3434	28.6266	
	$R_o/3$	38.5233	39.5047	
	$R_o/4$	42.2097	43.7205	
	$R_o/5$	43.0670	44.5484	

Table 2a. Final ray proceeding angle after crossing the Mount (h_{max}/L_o=1/2, R_o=99% influence of topography).

H_o/h_{min}	Y_o	3rd order no diss.(deg)	3rd order w/ diss.(deg)	1st order (deg)
1/8	$R_o/1$	-0.0269	-0.0269	-0.0270
	$R_o/2$	-0.7568	-0.7568	-0.7560
	$R_o/3$	-4.5724	-4.5725	-4.5728
	$R_o/4$	-13.5448	-13.5478	-13.5705
	$R_o/5$	-24.5290	-24.5428	-24.6203
1/4	$R_o/1$	-0.0272	-0.0271	
	$R_o/2$	-0.7605	-0.7603	
	$R_o/3$	-4.5693	-4.5697	
	$R_o/4$	-13.4671	-13.4787	
	$R_o/5$	-24.2617	-24.3134	
1/2	$R_o/1$	-0.0280	-0.0280	
	$R_o/2$	-0.7750	-0.7745	
	$R_o/3$	-4.5620	-4.5628	
	$R_o/4$	-13.1897	-13.2295	
	$R_o/5$	-23.3044	-23.4812	

Table 2b. Final ray proceeding angle after crossing the Mount(h_{max}/L_o=1/3, R_o=99% influence of topography).

H_o/h_{min}	Yo	3rd order no diss.(deg)	3rd order w/ diss.(deg)	1st order (deg)
1/8	$R_o/1$	-0.1954	-0.1955	-0.1960
	$R_o/2$	-4.1887	-4.1888	-4.1905
	$R_o/3$	-16.8180	-16.8207	-16.8456
	$R_o/4$	-35.8522	-35.8656	-35.9579
	$R_o/5$	-49.0650	-49.1051	-49.3270
1/4	$R_o/1$	-0.1954	-0.1953	
	$R_o/2$	-4.1815	-4.1822	
	$R_o/3$	-16.7507	-16.7588	
	$R_o/4$	-35.5498	-35.6002	
	$R_o/5$	-48.2901	-48.4333	
1/2	$R_o/1$	-0.1950	-0.1950	
	$R_o/2$	-4.1560	-4.1560	
	$R_o/3$	-16.5220	-16.5220	
	$R_o/4$	-34.5971	-34.5971	
	$R_o/5$	-45.9854	-45.9854	

Table 2c. Final ray proceeding angle after crossing the Mount (h_{max}/L_o=1/4, R_o=99% influence of topography).

H_o/h_{min}	Y_o	3rd order no diss.(deg)	3rd order w/ diss.(deg)	1st order (deg)
1/8	R_o/1	-0.4537	-0.4540	-0.4537
	R_o/2	-8.8558	-8.8564	-8.8627
	R_o/3	-30.5955	-30.5981	-30.6455
	R_o/4	-55.0139	-55.0199	-55.2291
	R_o/5	-63.4392	-63.4593	-64.0055
1/4	R_o/1	-0.4528	-0.4531	
	R_o/2	-8.8360	-8.8373	
	R_o/3	-30.4478	-30.4641	
	R_o/4	-54.4165	-54.4745	
	R_o/5	-62.0963	-62.1596	
1/2	R_o/1	-0.4500	-0.4498	
	R_o/2	-8.7574	-8.7613	
	R_o/3	-29.8802	-29.9331	
	R_o/4	-51.9920	-52.1919	
	R_o/5	-56.5429	-56.7063	

Table C1. Ray position due to different increment per a step for a bottom of constant slope(θ_o=30°; bottom slope =0.001; d/L_o=0.1, H_o/L_o=0.03 at L_o=100m).

Δs(m)	y (x 10^5 m)
250	0.487100*
500	0.487060
750	0.487008
1000	0.486964
1250	0.486963
1500	0.486930
2500	0.486763

*The last two digits are those interpolated from the adjacent values.

Table C2. The first and the second derivatives of the wave speed with respect to x for each bottom slope and water depth (H_o/L_o=0.03 at L_o=100m).

Bottom slope	h/L_o	dc/dx	d^2c/dx^2
0.001	0.2	0.149976×10^{-3}	0.212935×10^{-7}
	0.1	0.347995×10^{-3}	0.212481×10^{-7}
0.002	0.2	0.299684×10^{-3}	0.428108×10^{-7}
	0.1	0.689973×10^{-3}	0.126951×10^{-6}
0.005	0.2	0.749505×10^{-3}	0.338289×10^{-6}
	0.1	0.166925×10^{-2}	0.920266×10^{-6}
0.001*	0.2	0.139026×10^{-3}	
	0.1	0.338927×10^{-3}	
0.002*	0.2	0.278053×10^{-3}	
	0.1	0.677855×10^{-3}	

* is due to the analytic derivation of dc/dx using linear wave equation as,

$$\frac{\partial c}{\partial x} = -\frac{gkA \sinh(2kh)}{\omega_o \cosh^2(kh)(2kh + \sinh(2kh))},$$

where A is a bottom slope.

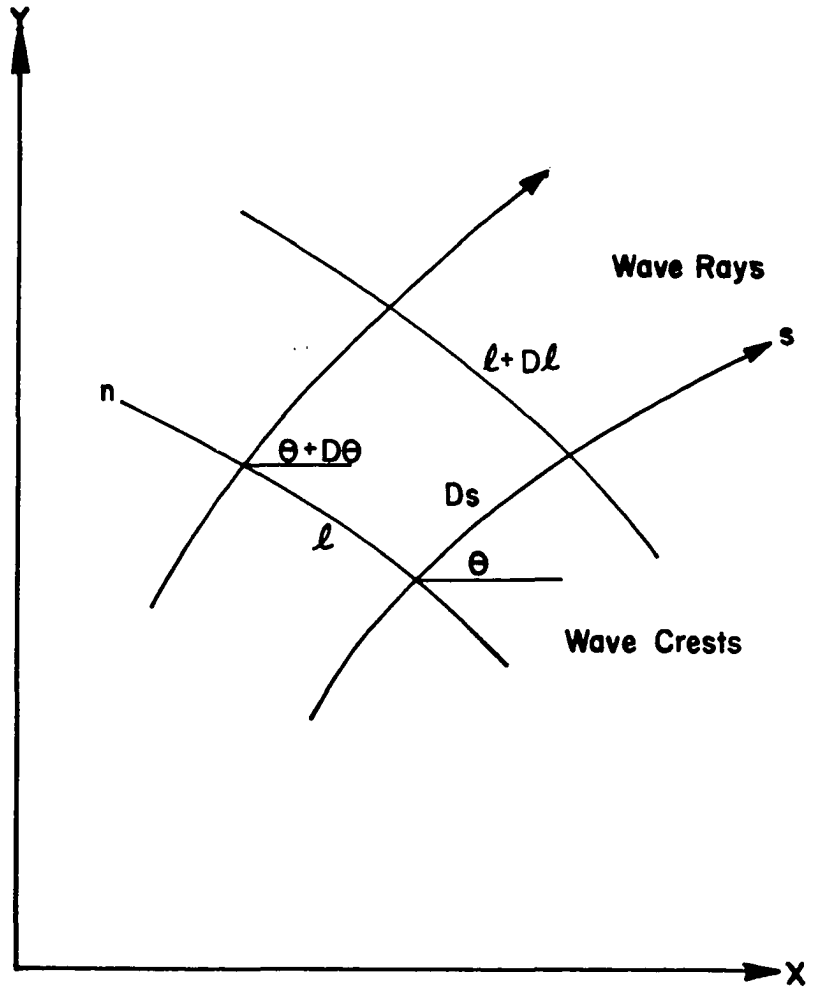

Fig. 1. Definition of terms and coordinate system.

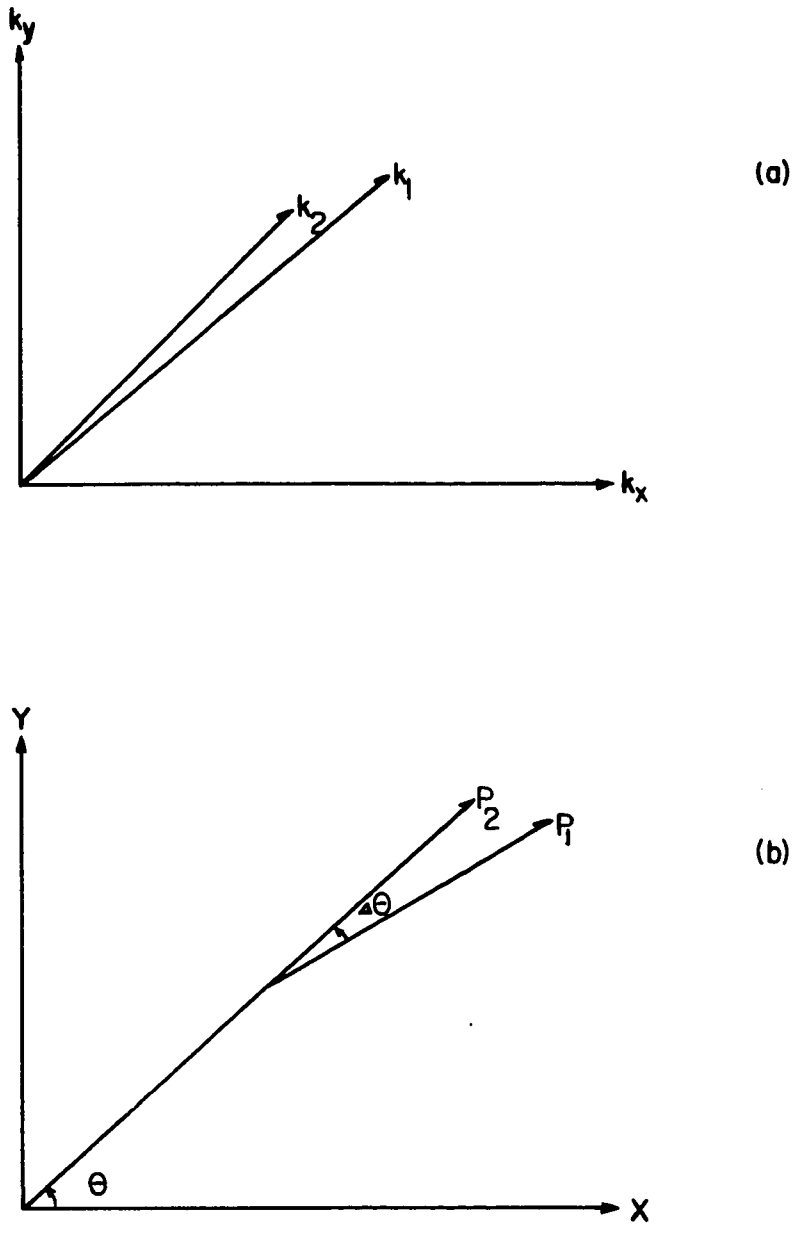

Fig. 2. Wave numbers and power vectors of a two component wave group.

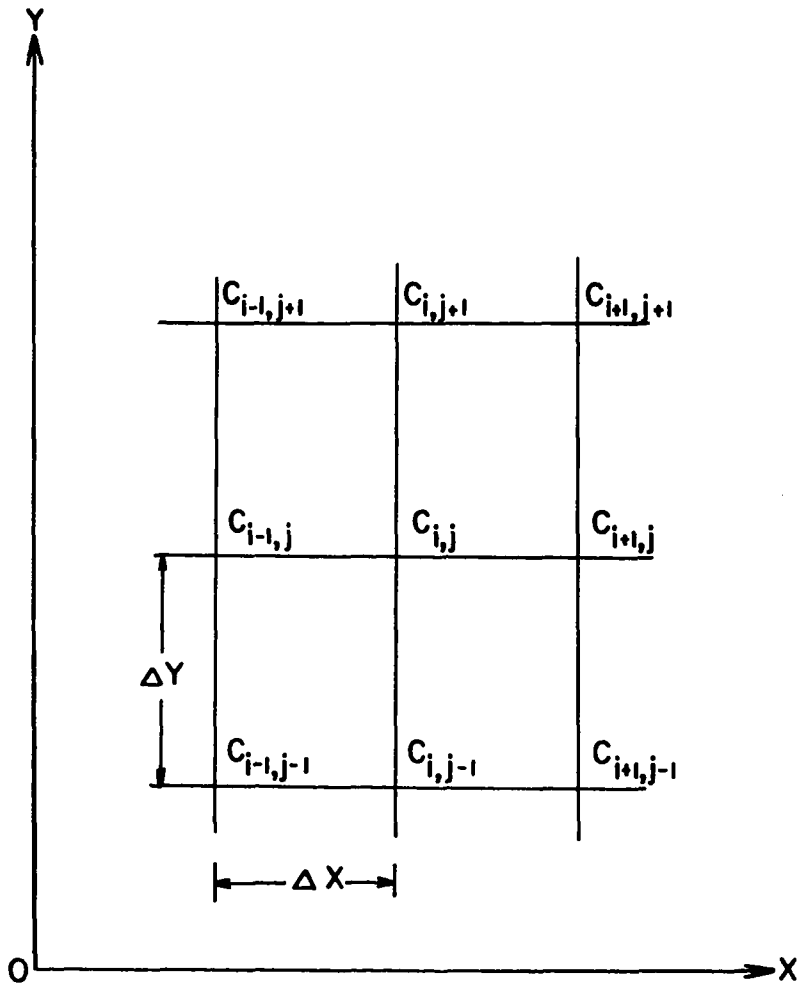

Fig. 3. Numerical scheme for wave ray trajectories.

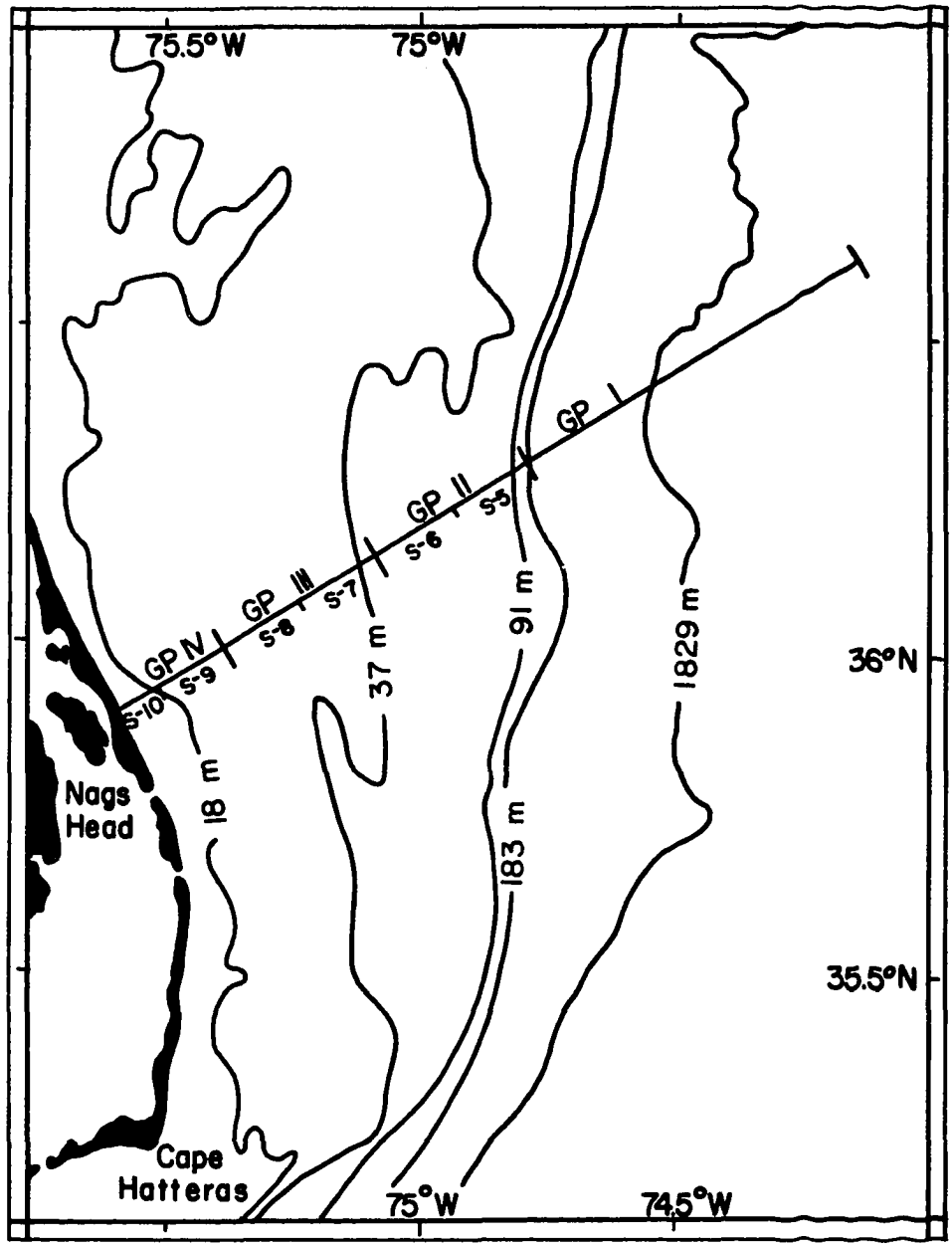

Fig. 4. Location of data sampling and grouping of data.

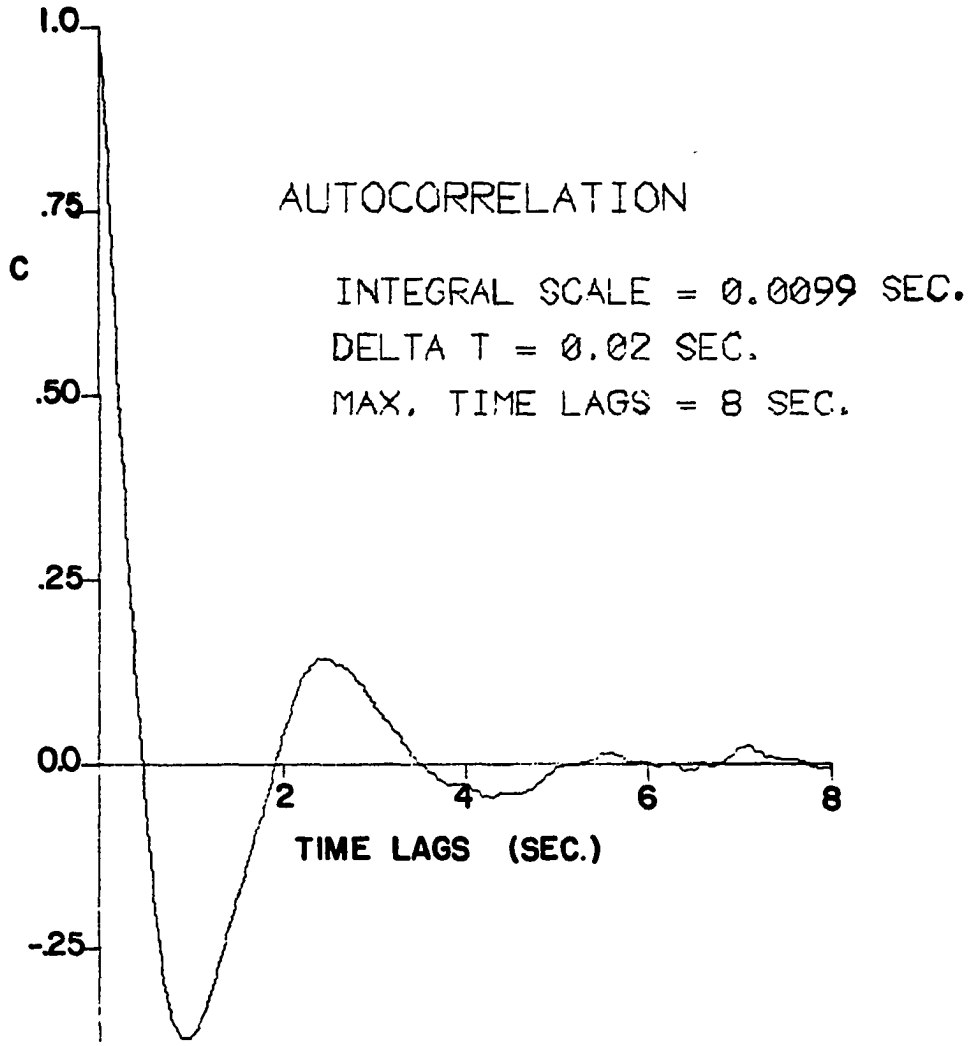

Fig. 5. Autocorrelation of water surface elevation.

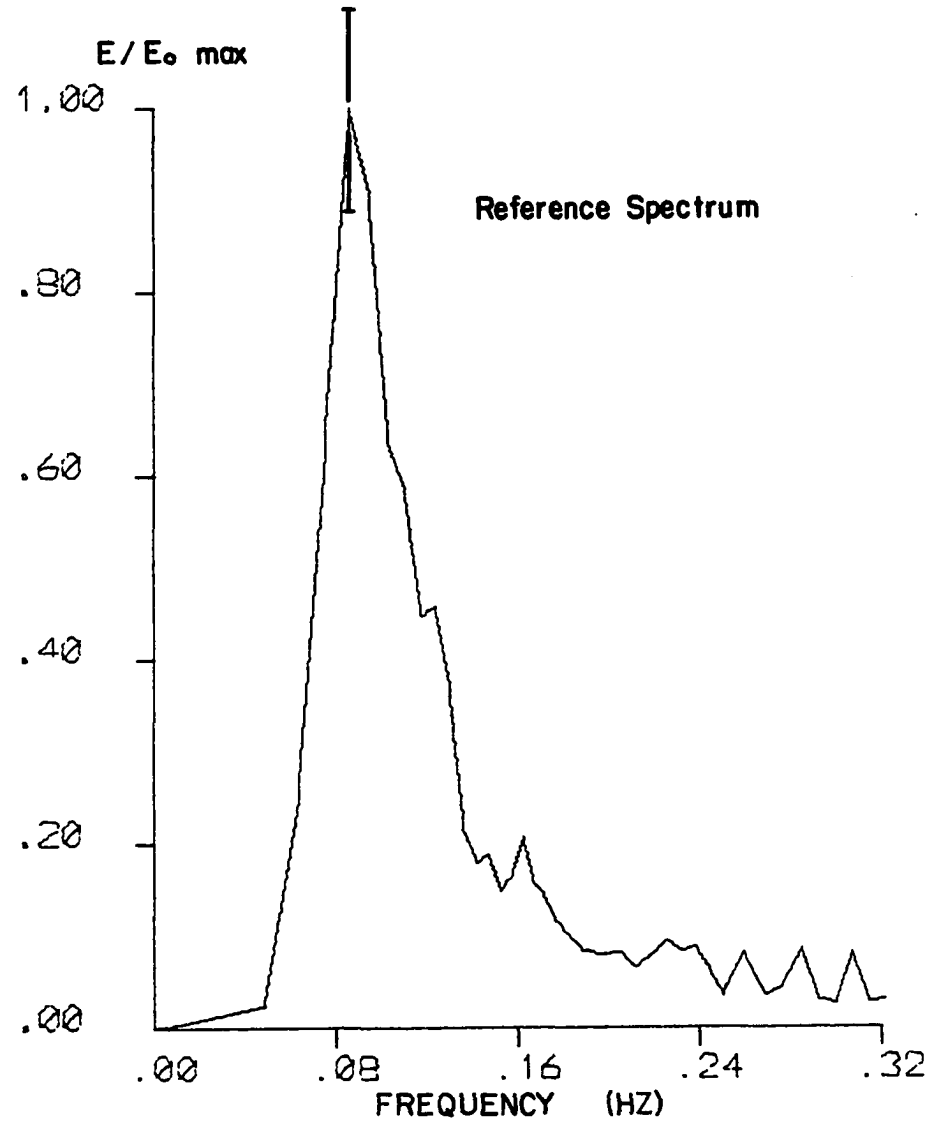

Fig. 6a. Reference spectrum from the first 12 minutes of data. (Vertical bar denotes 80% confidence band.)

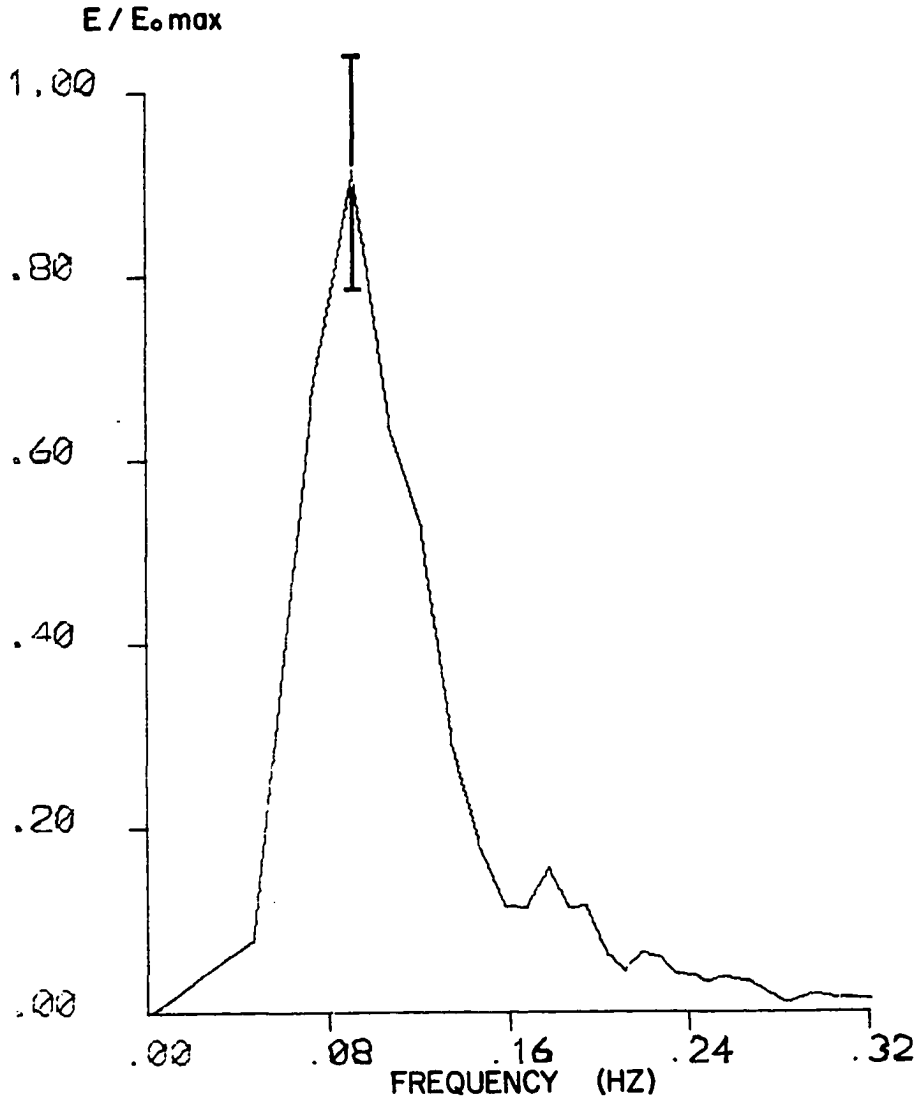

Fig. 6b. Spectrum from data segment 5. (Vertical bar denotes 80% confidence band.)

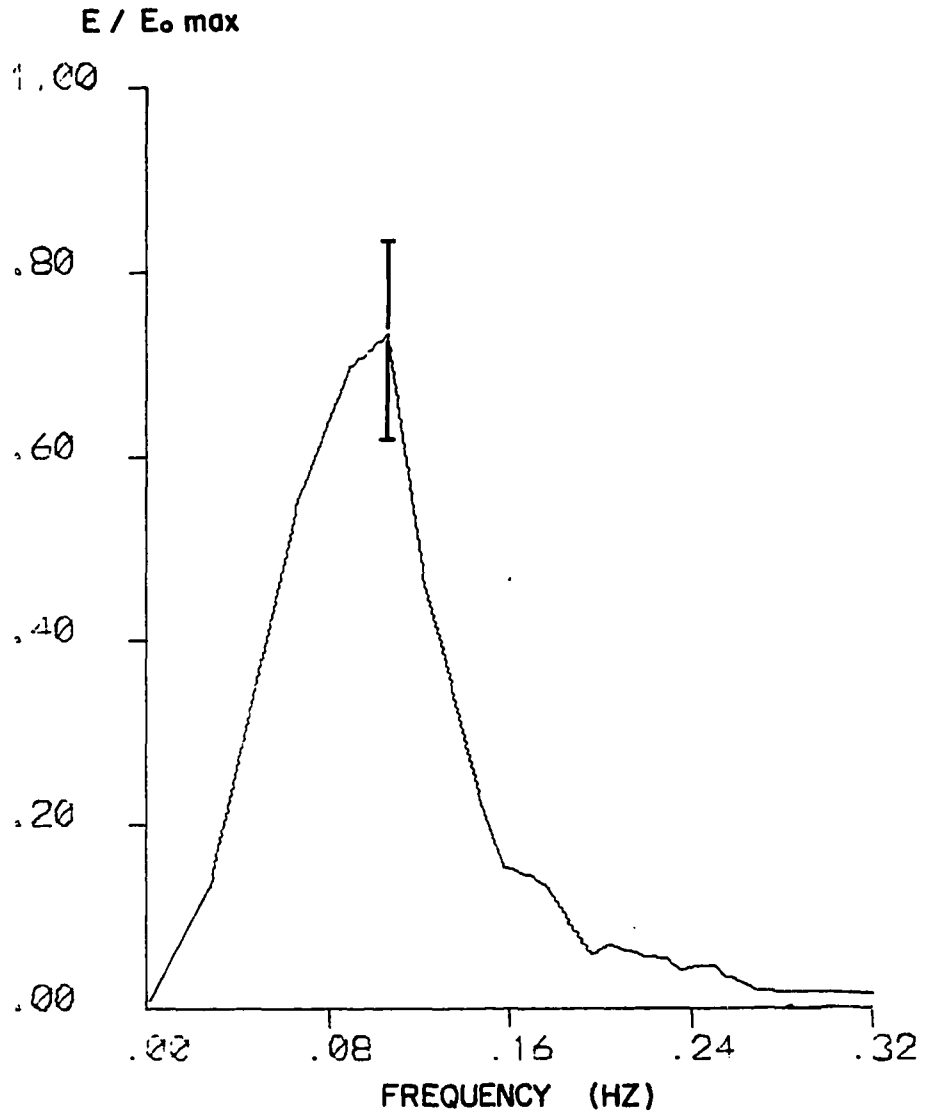

Fig. 6c. Spectrum from data segment 6. (Vertical bar denotes 80% confidence band.)

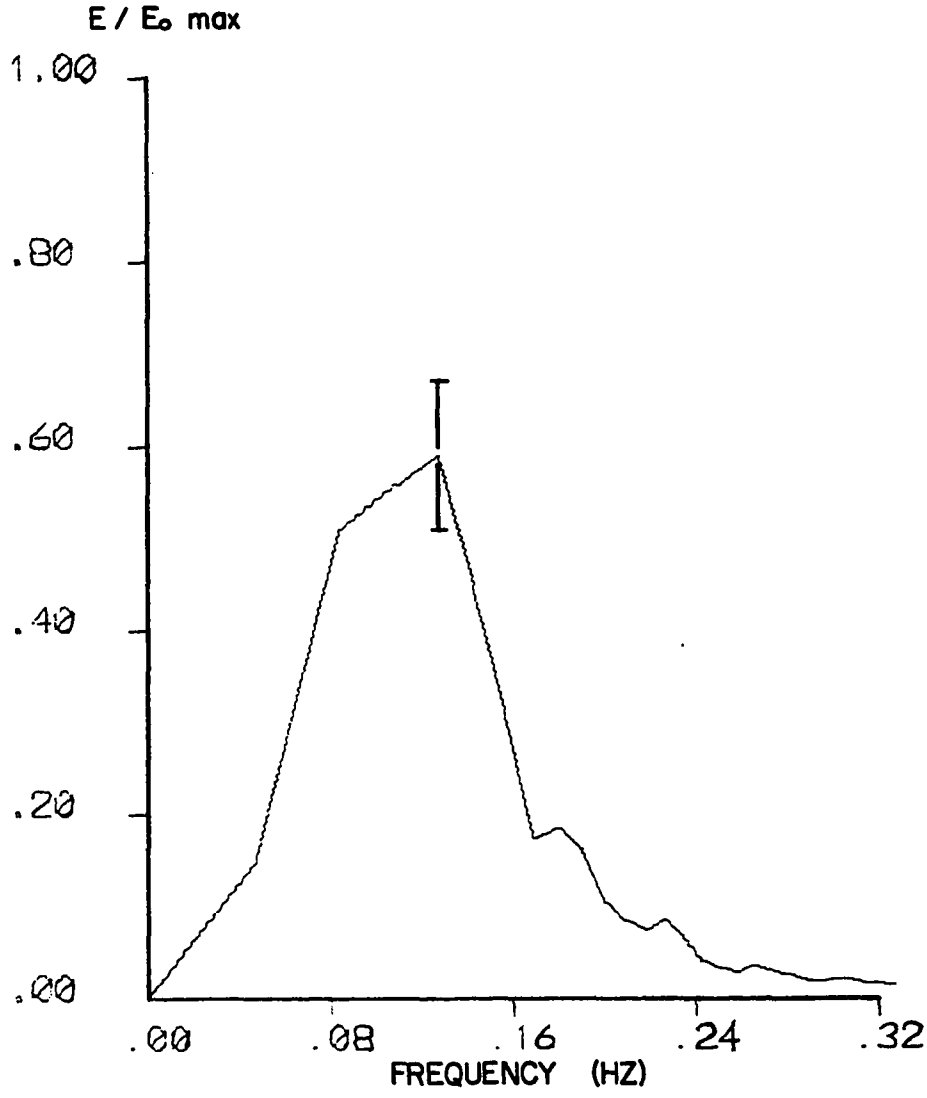

Fig. 6d. Spectrum from data segment 7. (Vertical bar denotes 80% confidence band.)

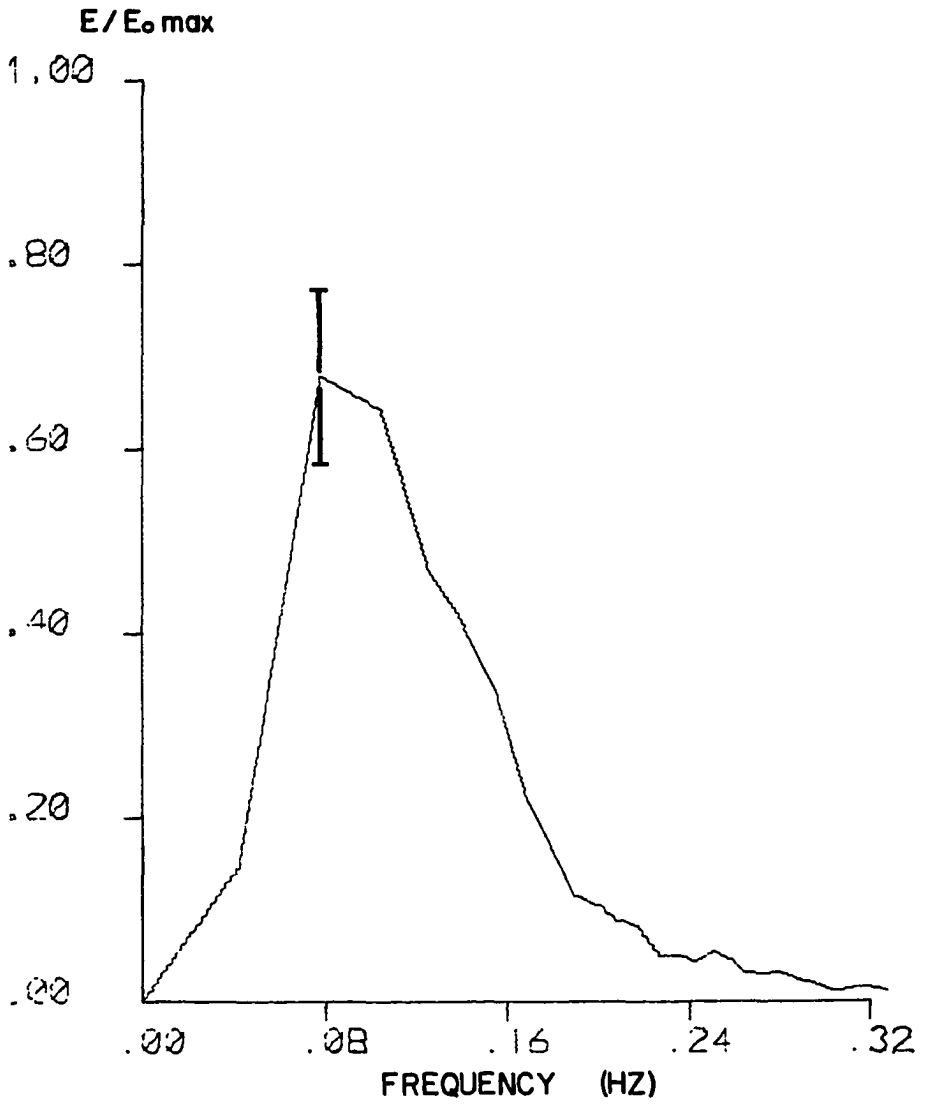

Fig. 6e. Spectrum from data segment 8. (Vertical bar denotes 80% confidence band.)

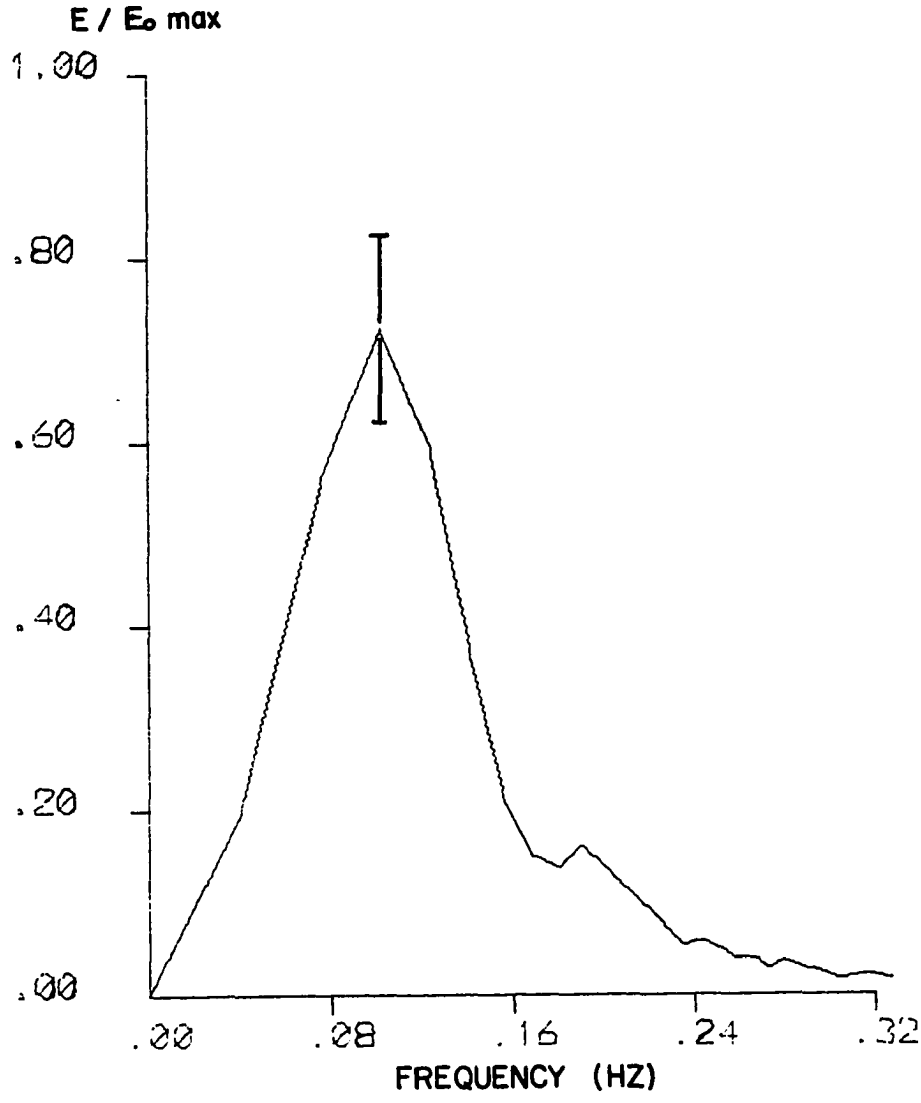

Fig. 6f. Spectrum from data segment 9. (Vertical bar denotes 80% confidence band.)

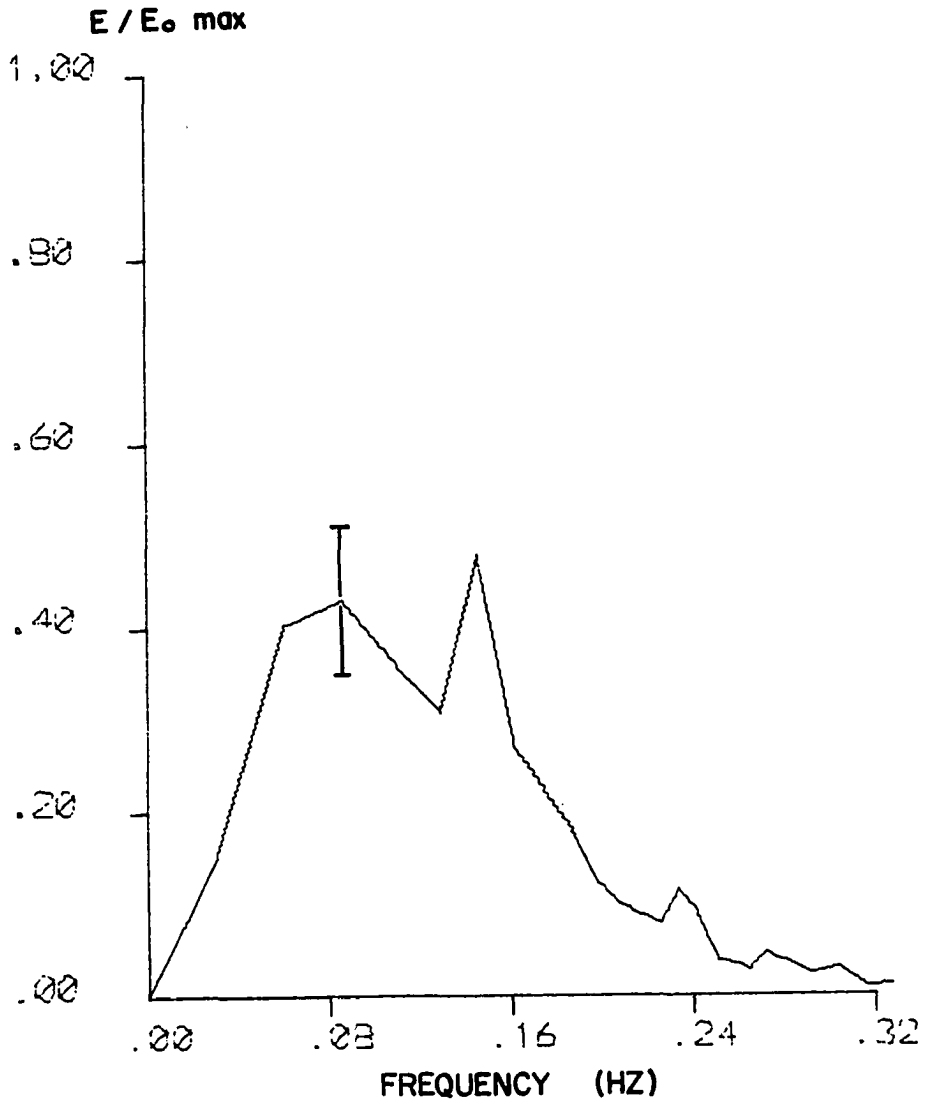

Fig. 6g. Spectrum from data segment 10. (Vertical bar denotes 80% confidence band.)

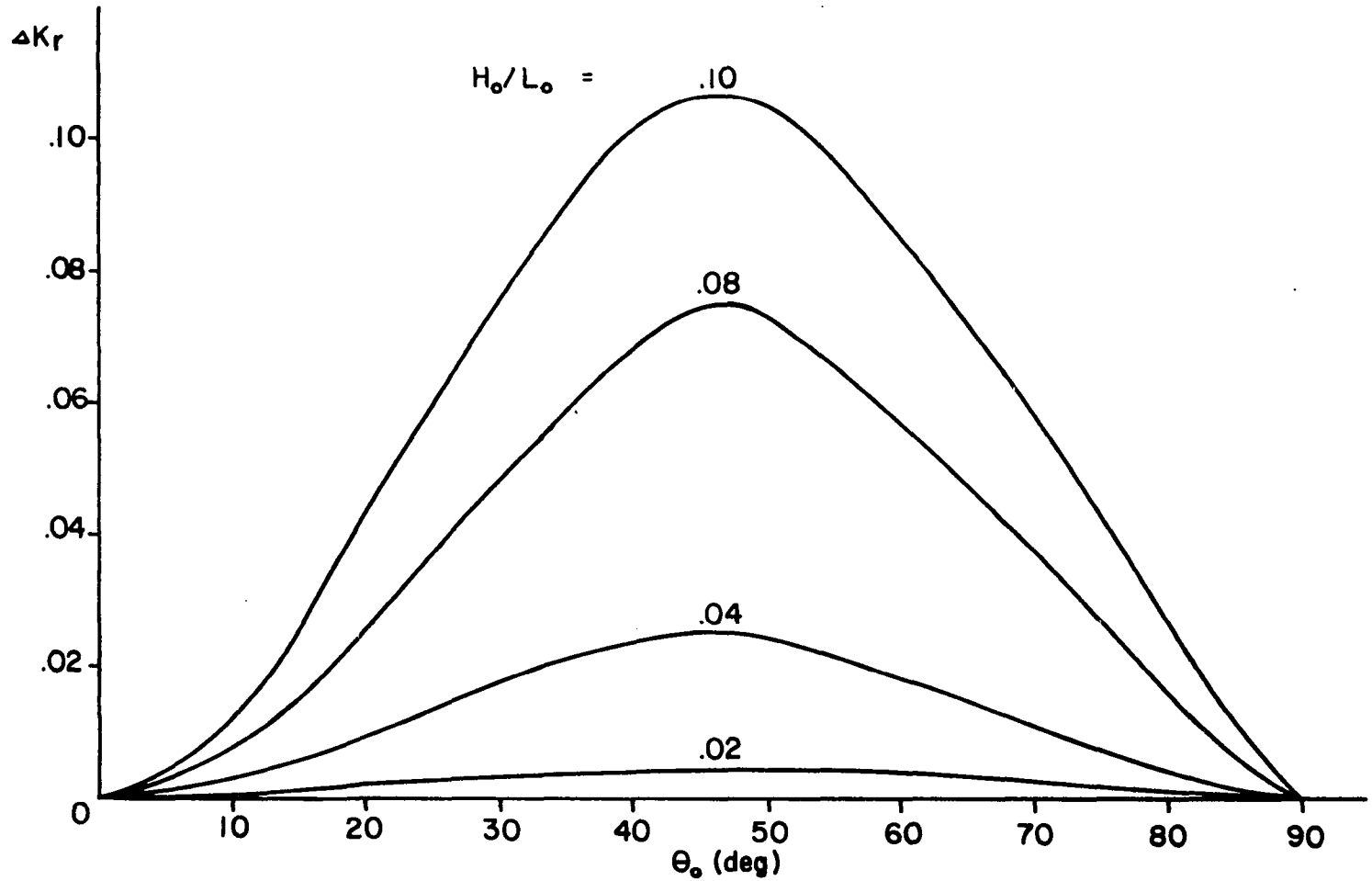

Fig. 7. Differences between refraction coefficients(ΔK_r) obtained near the wave breaking point for the third order wave theory without energy dissipation and the first order wave theory.

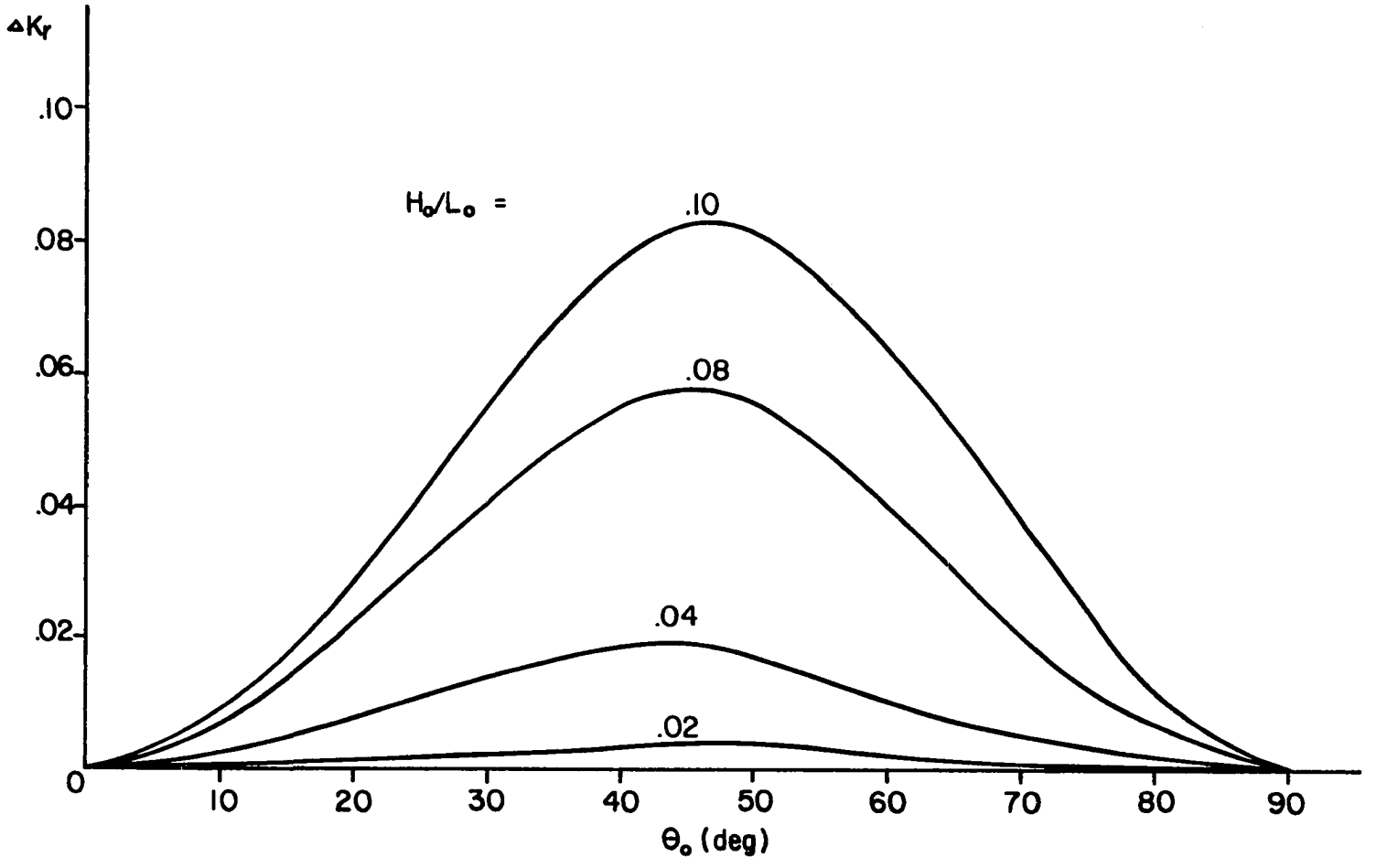

Fig. 8. Differences between refraction coefficients(ΔK_r) obtained near the wave breaking point for the third order wave theory with energy dissipation and the first order wave theory.

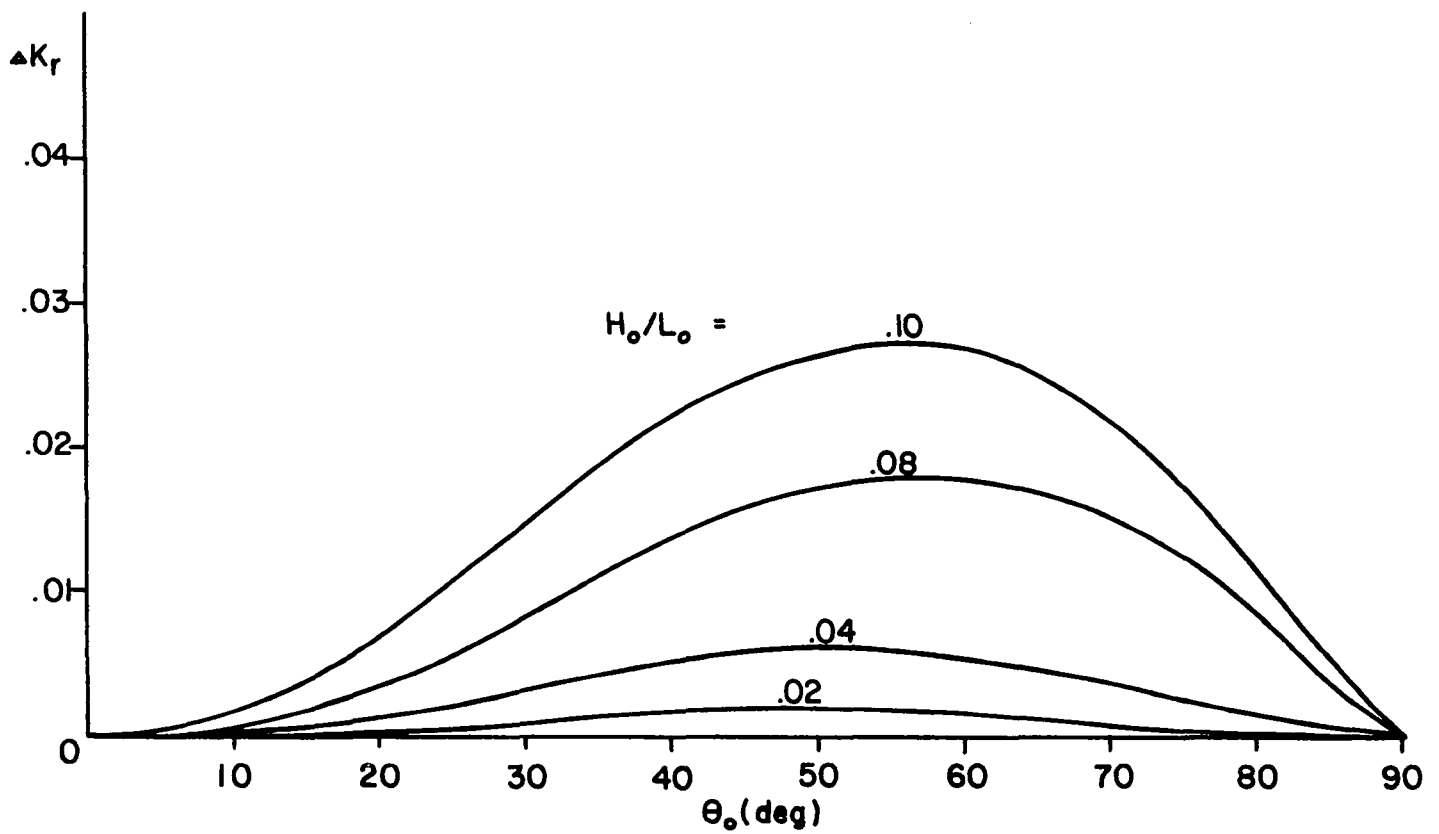

Fig. 9. Differences between refraction coefficients(ΔK_r) obtained near the wave breaking point for the third order wave theory with and without energy dissipation.

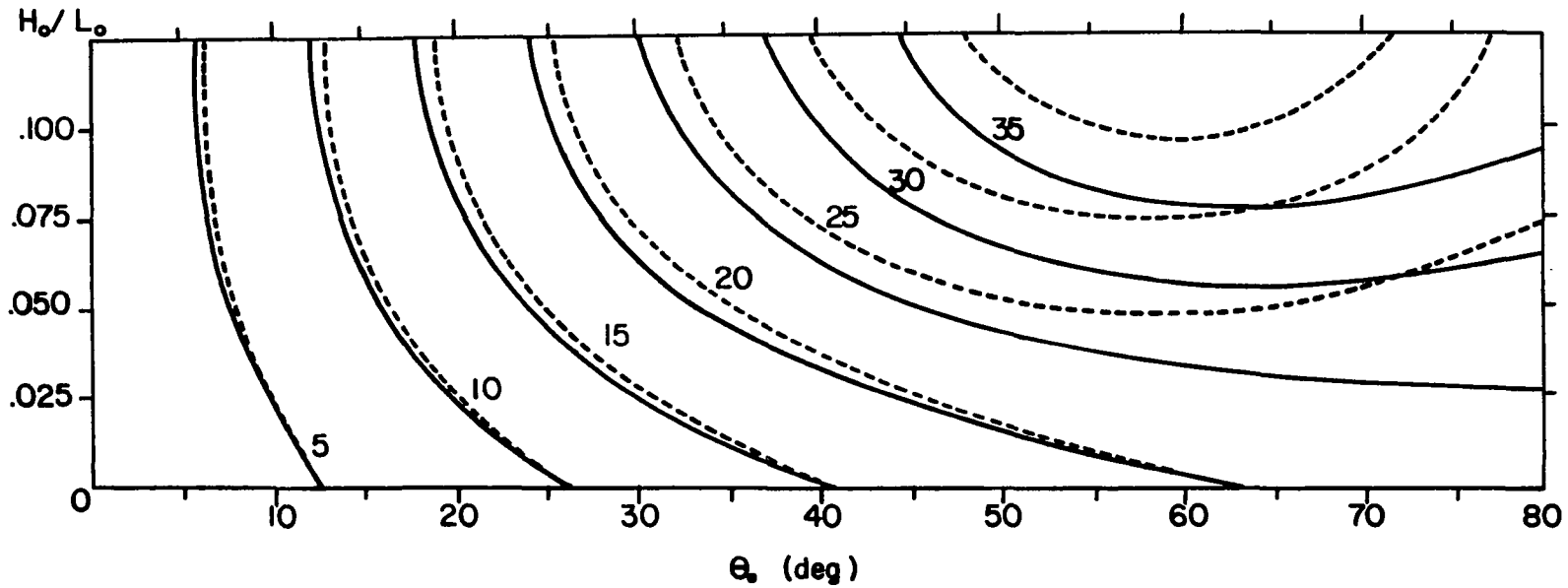

Fig. 10. Contours of wave propagation angles in degrees near the wave breaking point as a function of wave steepness and initial angle(bottom slope=0.0008). (Broken lines represent the case in which energy dissipation has been accounted for.)

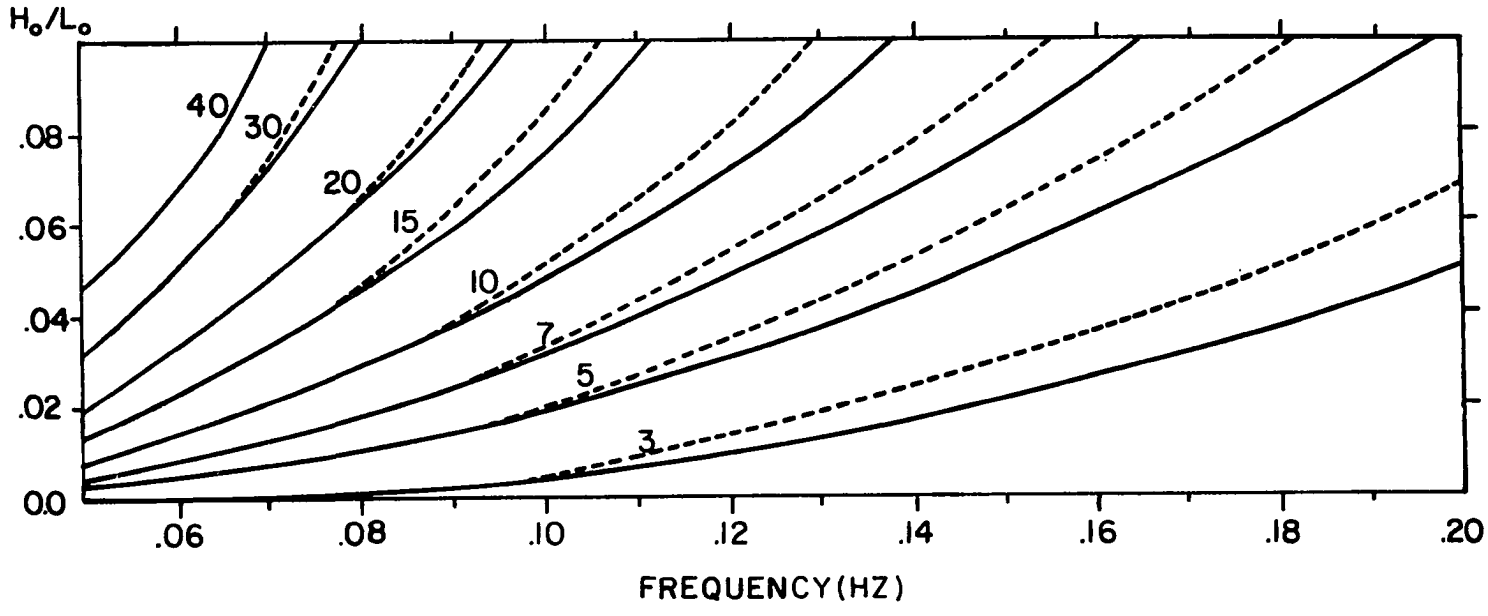

Fig. 11a. Contours of wave breaking water depths in meters as a function of wave steepness and frequency($\theta = 0^o$). (Broken lines represent the case in which energy dissipation has been accounted for.)

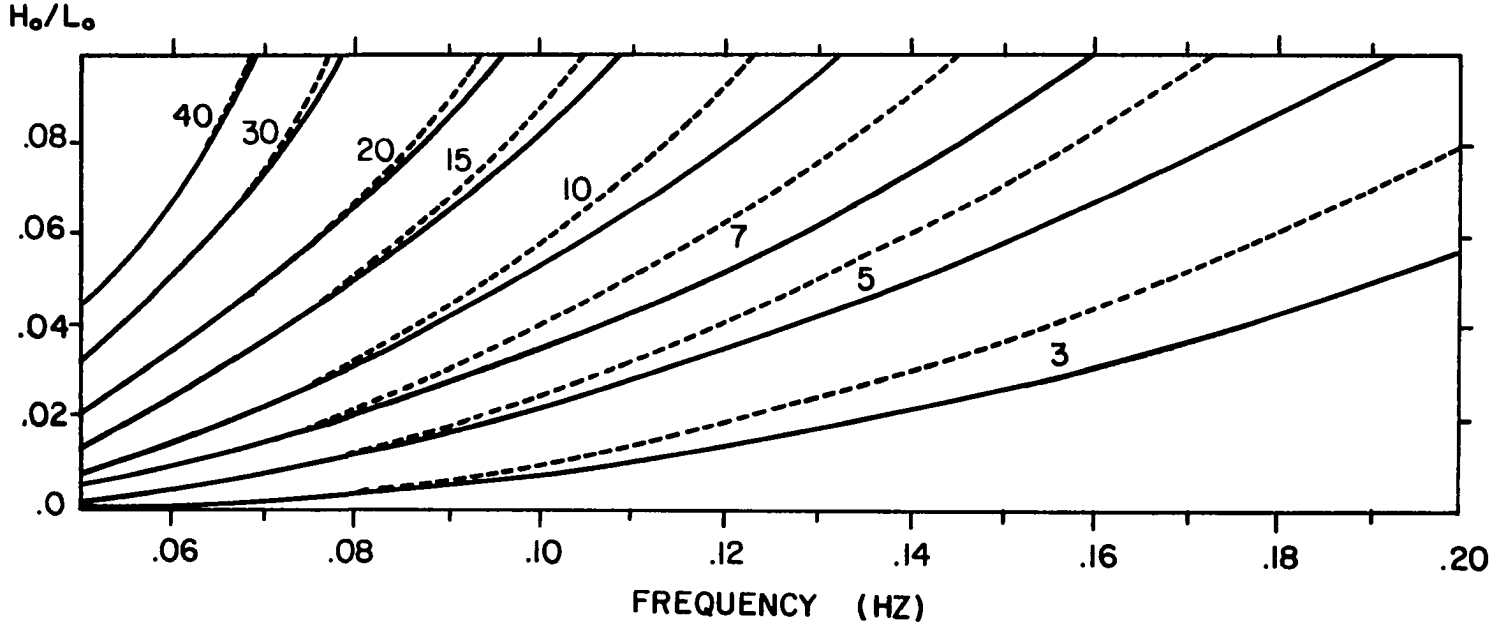

Fig. 11b. Contours of wave breaking water depths in meters as a function of wave steepness and frequency($\theta = 30^{o}$). (Broken lines represent the case in which energy dissipation has been accounted for.)

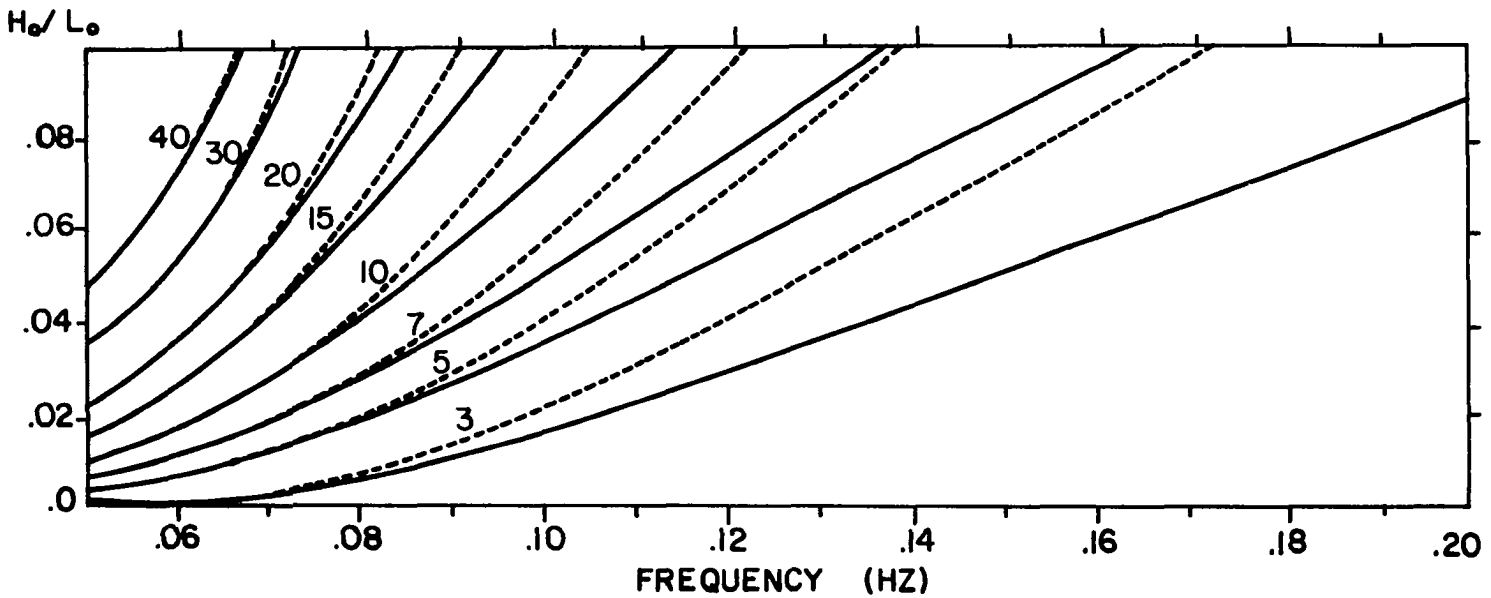

Fig. 11c. Contours of wave breaking water depths in meters as a function of wave steepness and frequency($\theta = 60^{o}$). (Broken lines represent the case in which energy dissipation has been accounted for.)

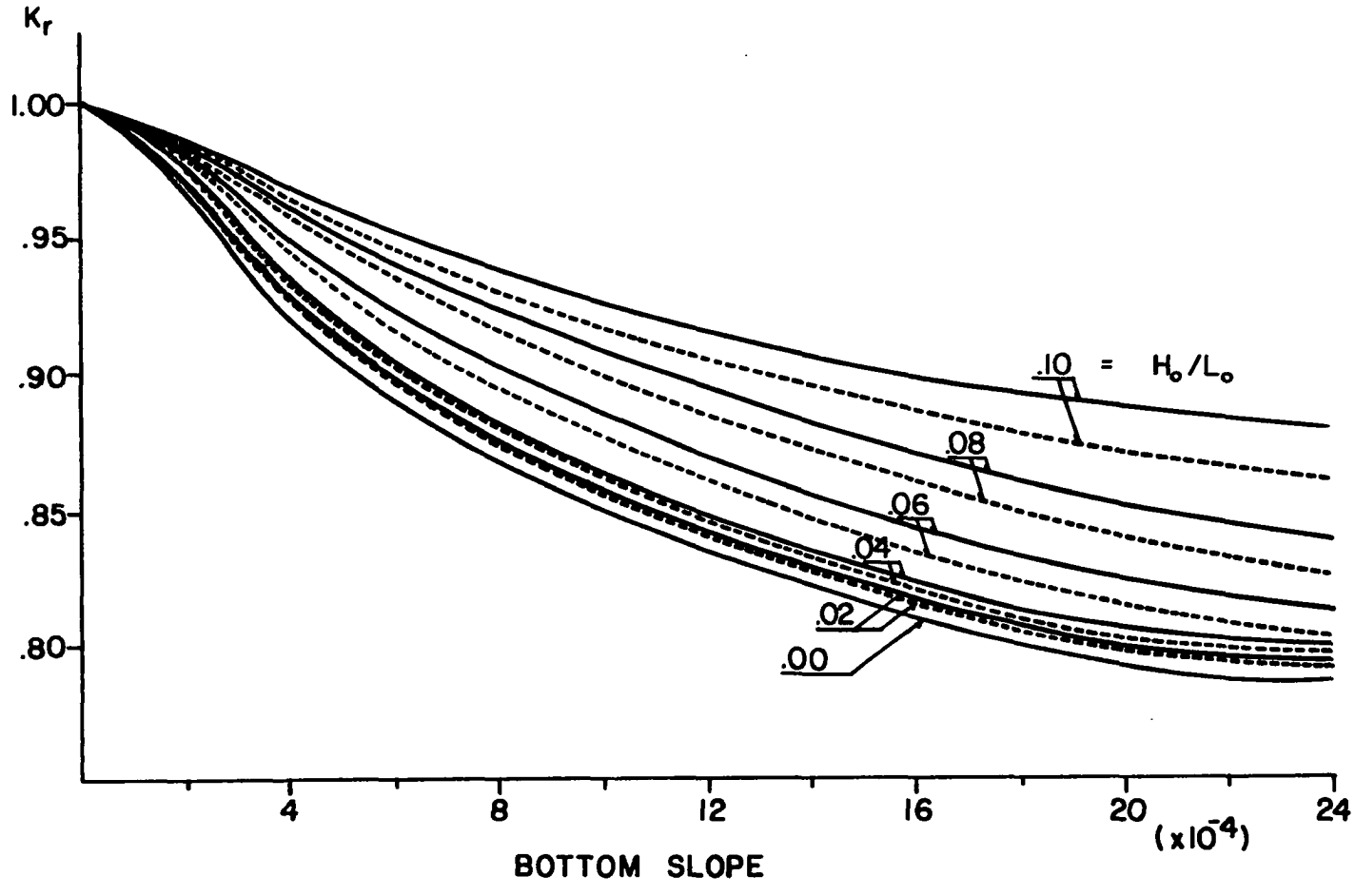

Fig. 12. Refraction coefficients near the wave breaking point as a function of bottom slope. (Broken lines represent the case in which energy dissipation has been accounted for.)

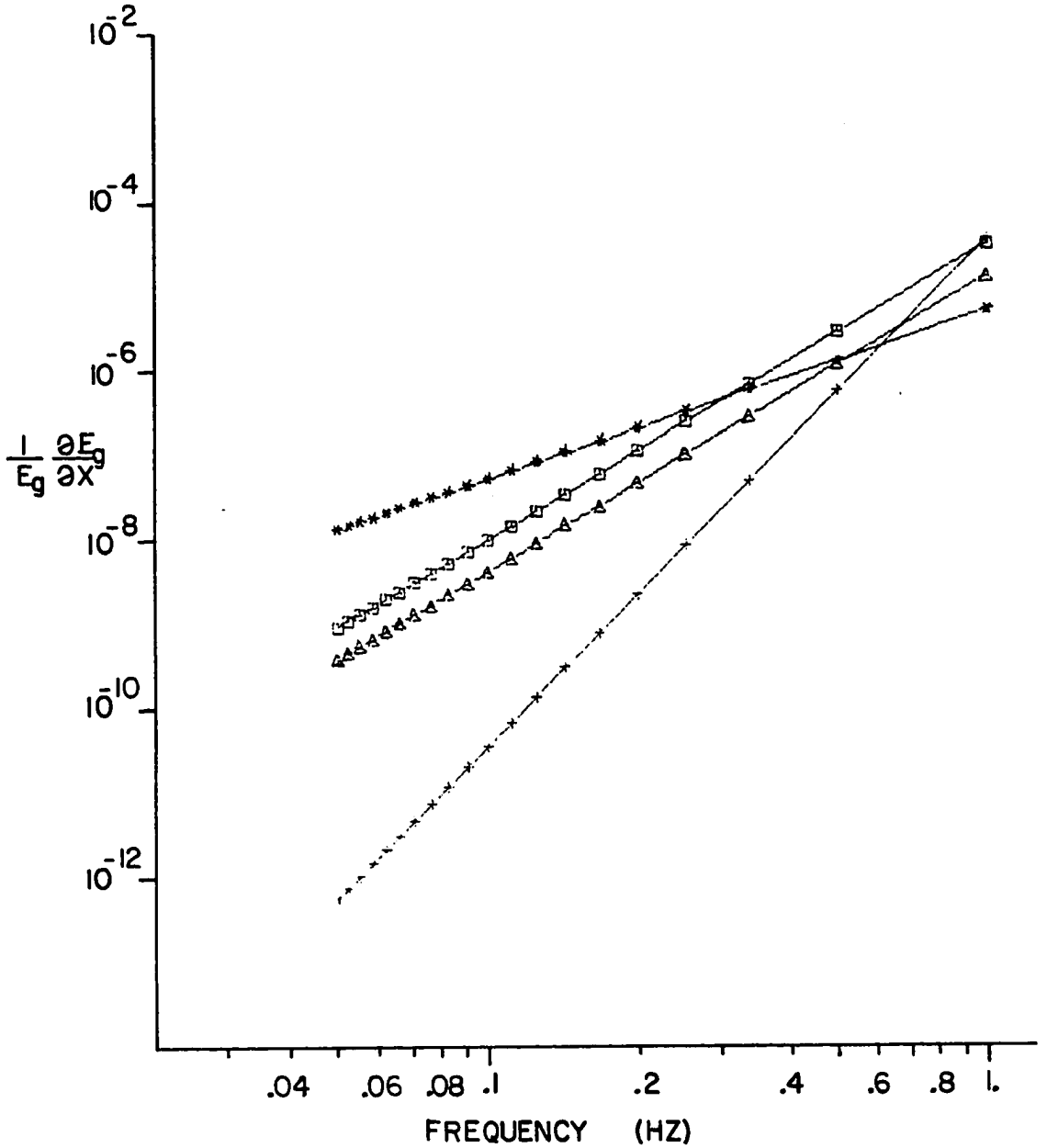

Fig. 13. Relative energy dissipation rate versus frequency due to capillary waves(+) and due to bottom friction by the following models: The third order version of Putnam and Johnson(*); Lukasik and Grosch(□); Eagleson(△).

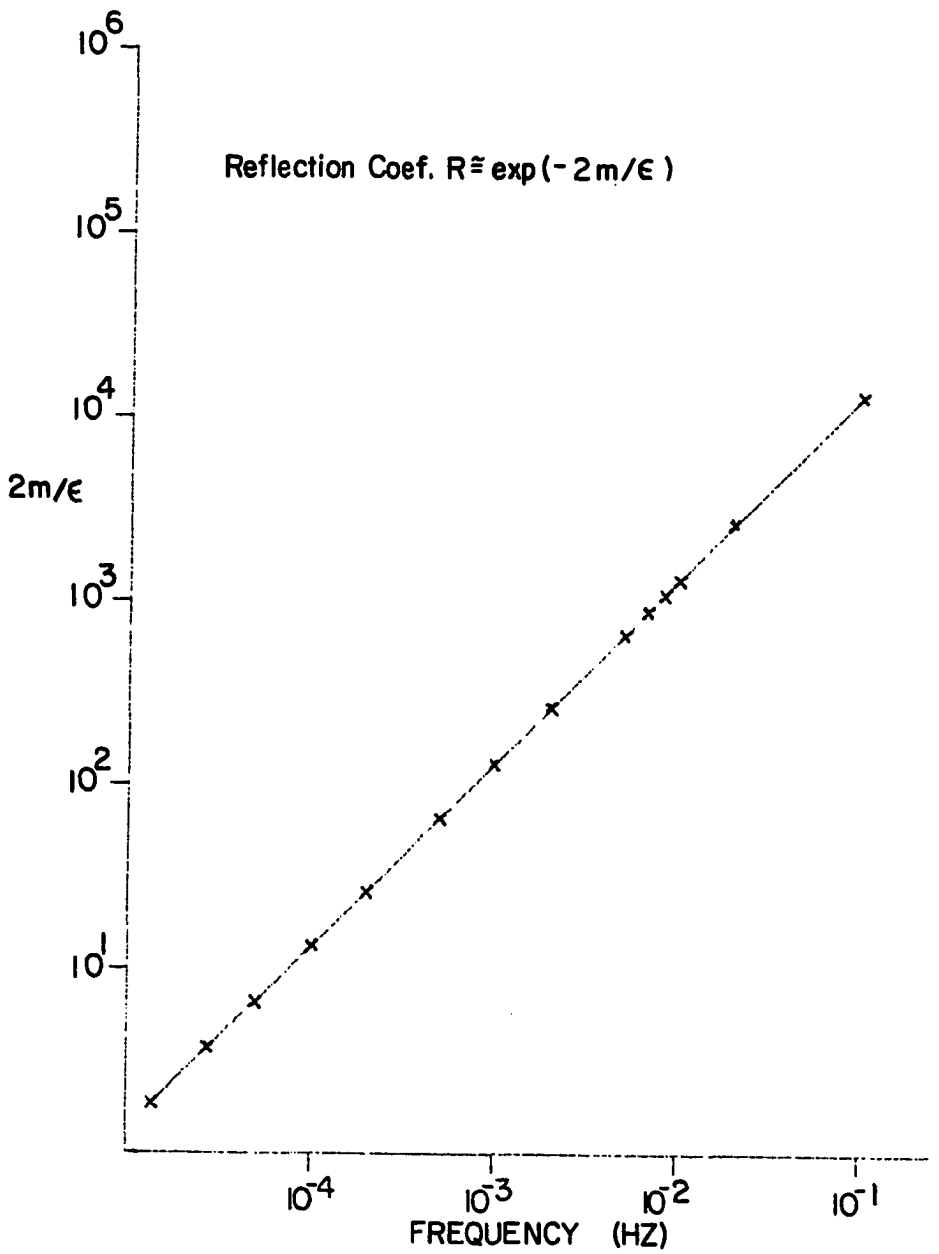

Fig. 14. Negative log. of reflection coefficient versus frequency at the maximum slope of the topography type 'Slope D to S'(see Fig. 15).

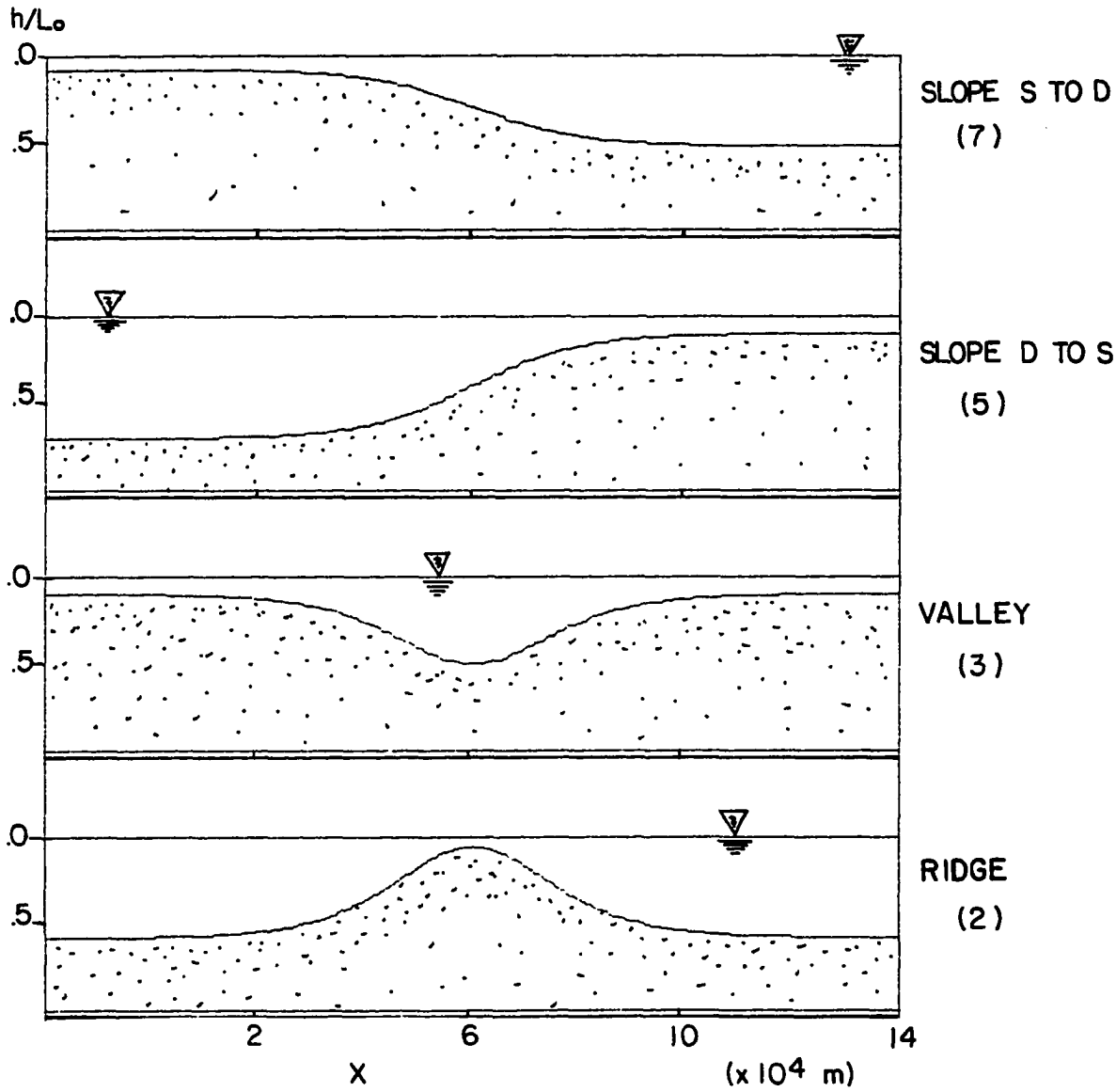

Fig. 15. Bottom topographies.

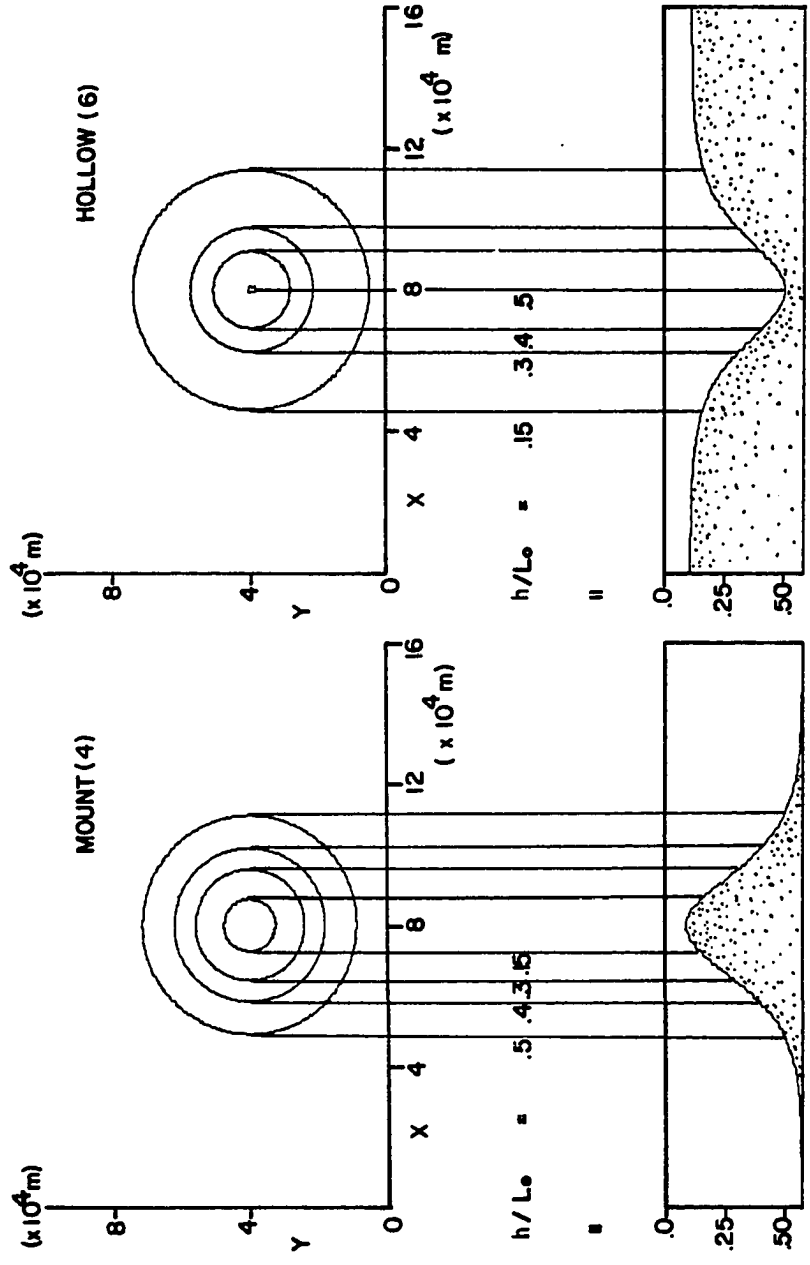

Fig. 18. Bottom topographies, Mount and Hollow.

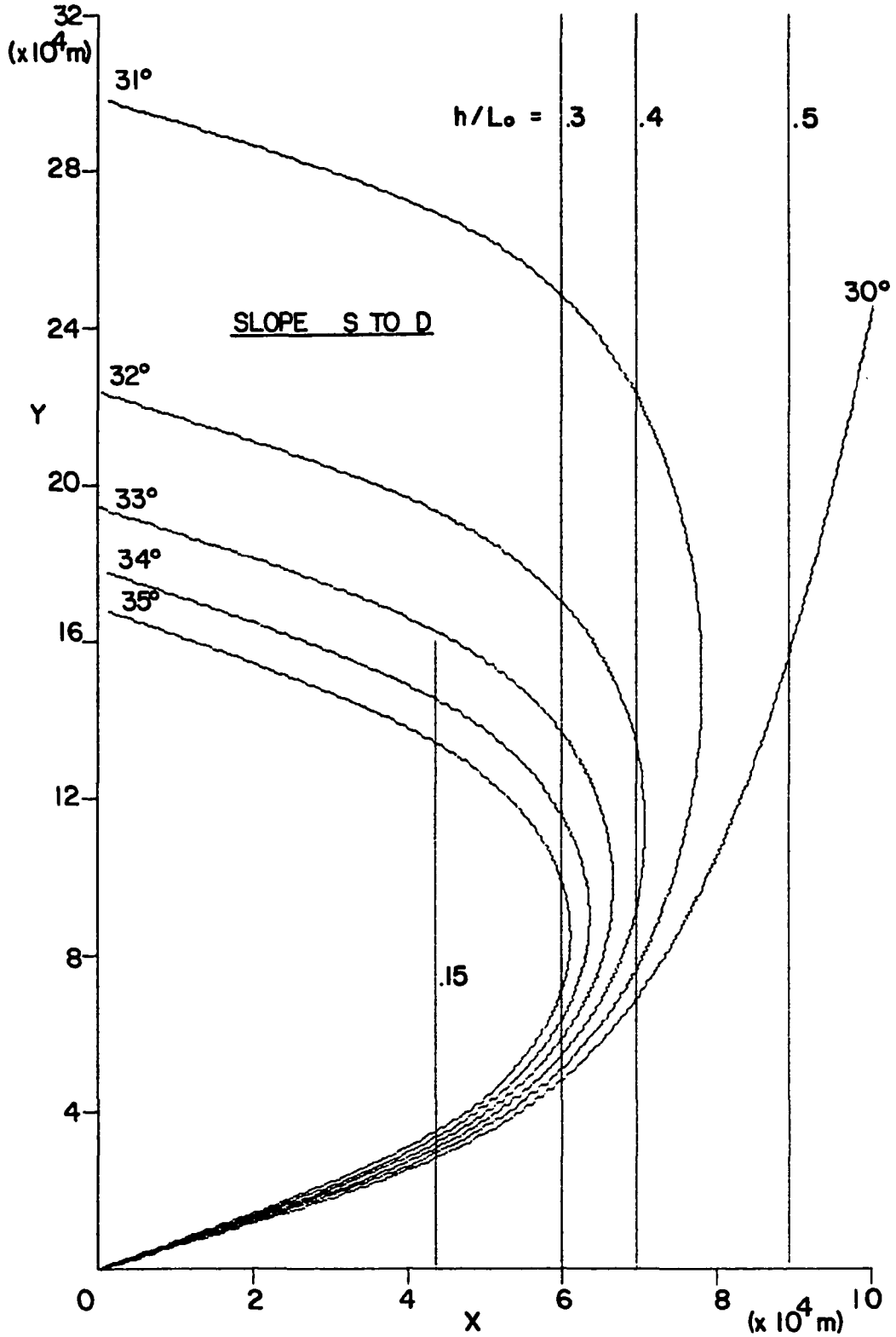

Fig. 17c. Ray trajectories using first order wave theory (h_o/L_o = 9/17.23, H_o/L_o = 4/172.3).

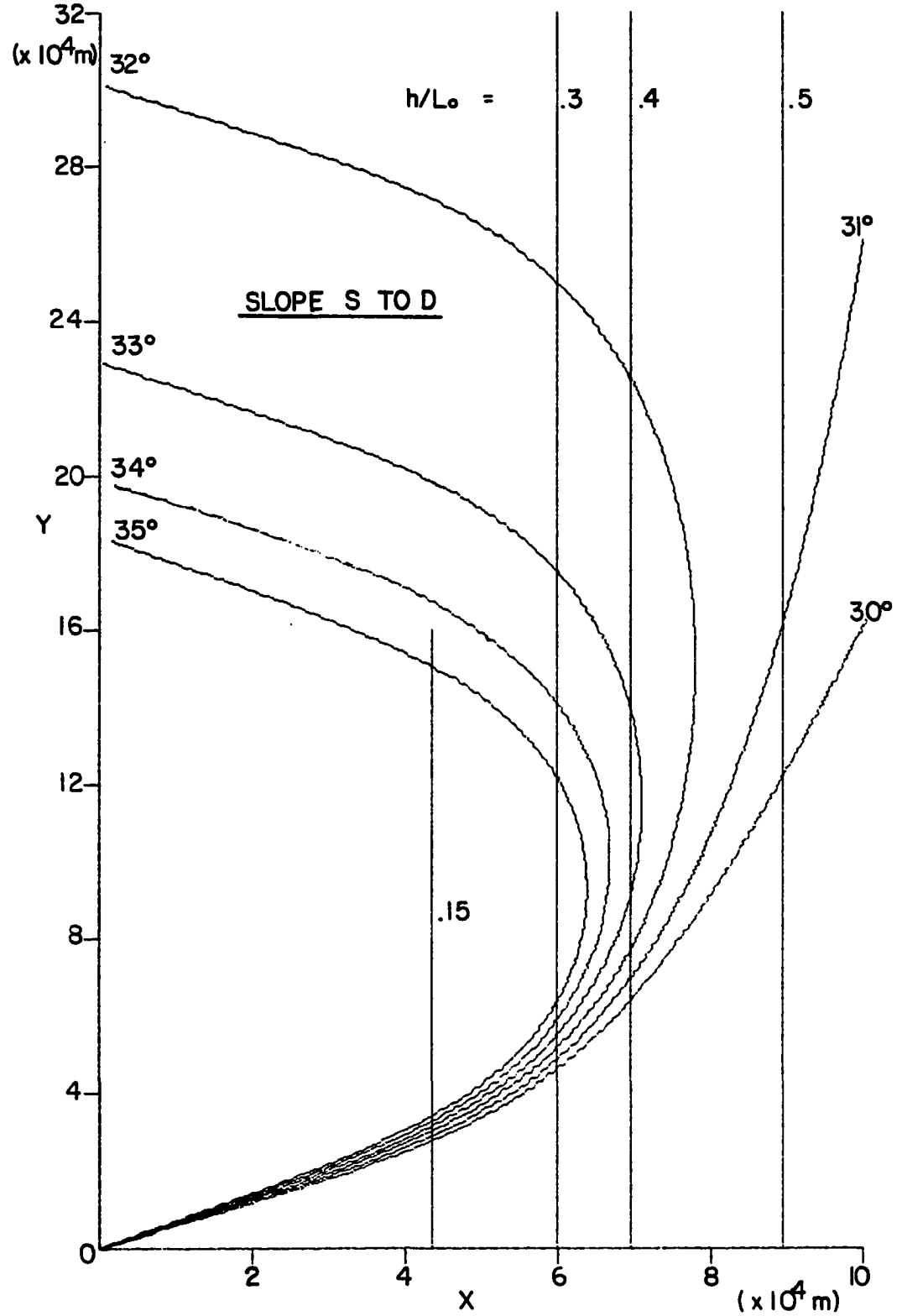

Fig. 17b. Ray trajectories using third order wave theory with energy dissipation (h_o/L_o = 9/17.23, H_o/L_o = 4/172.3).

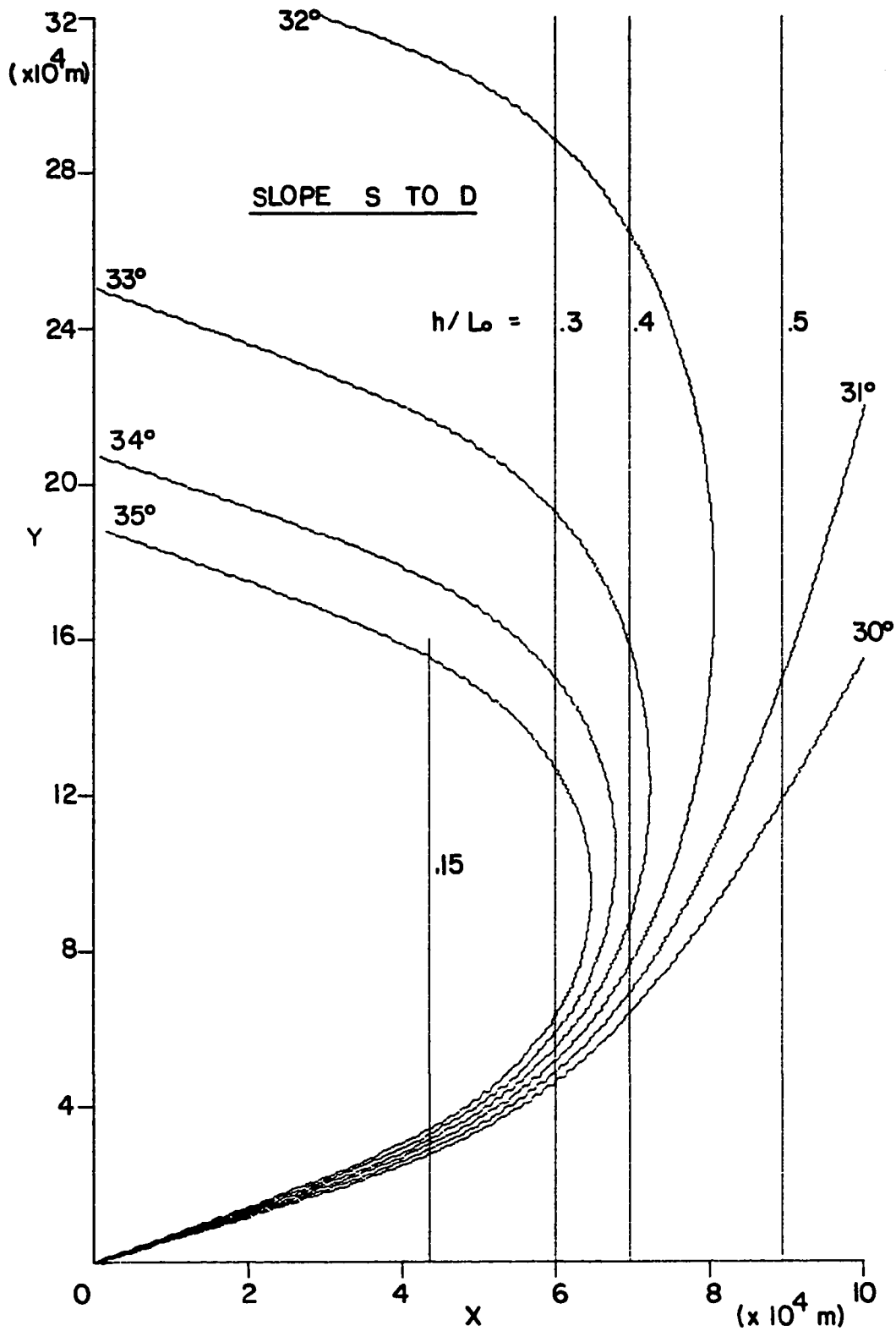

Fig. 17a. Ray trajectories using third order wave theory without energy dissipation (h_o/L_o = 9/17.23, H_o/L_o = 4/172.3).

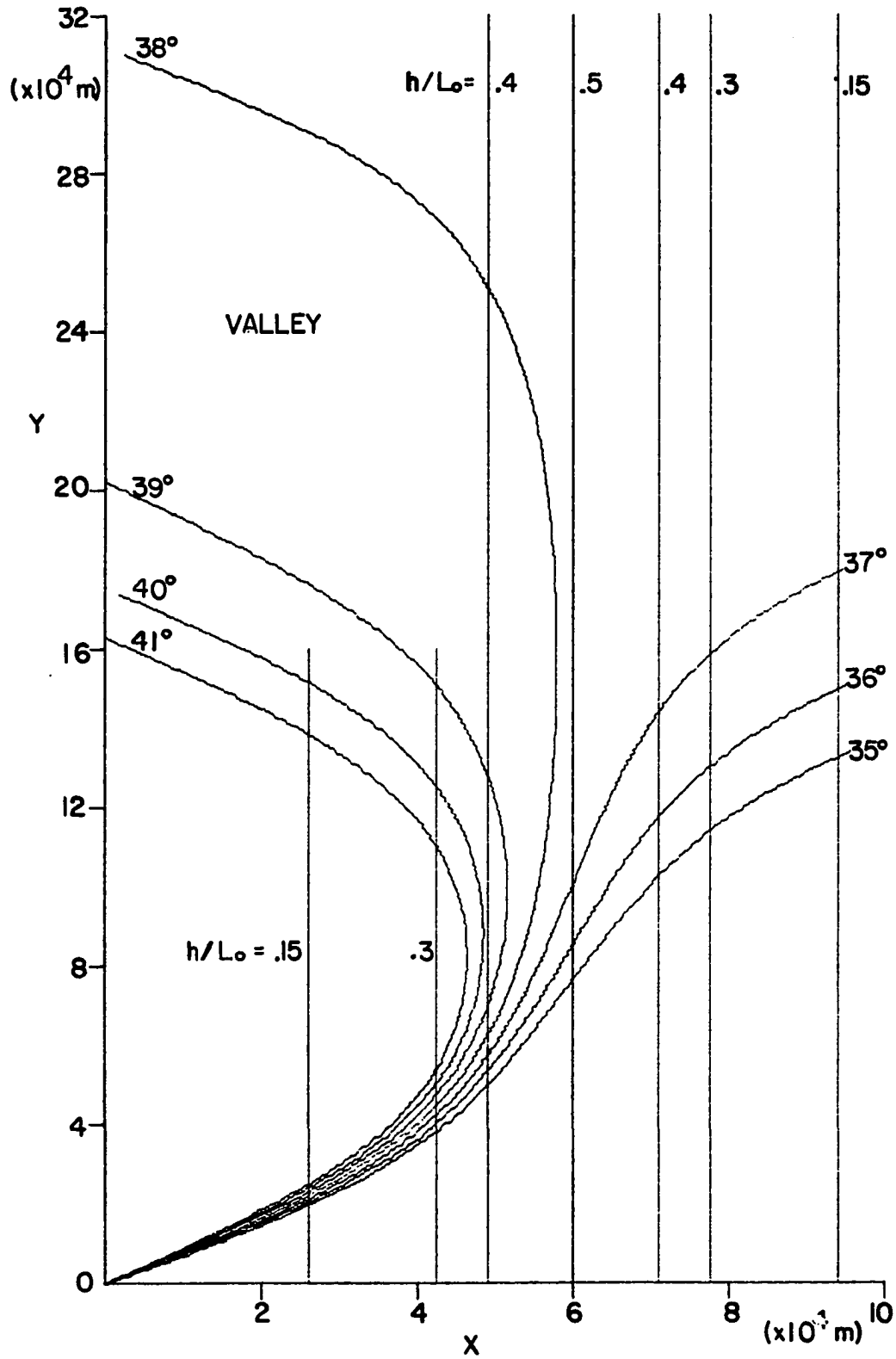

Fig. 16b. Ray trajectories using third order wave theory without energy dissipation (h_o/L_o = 1/10, H_o/L_o = 4/172.3).

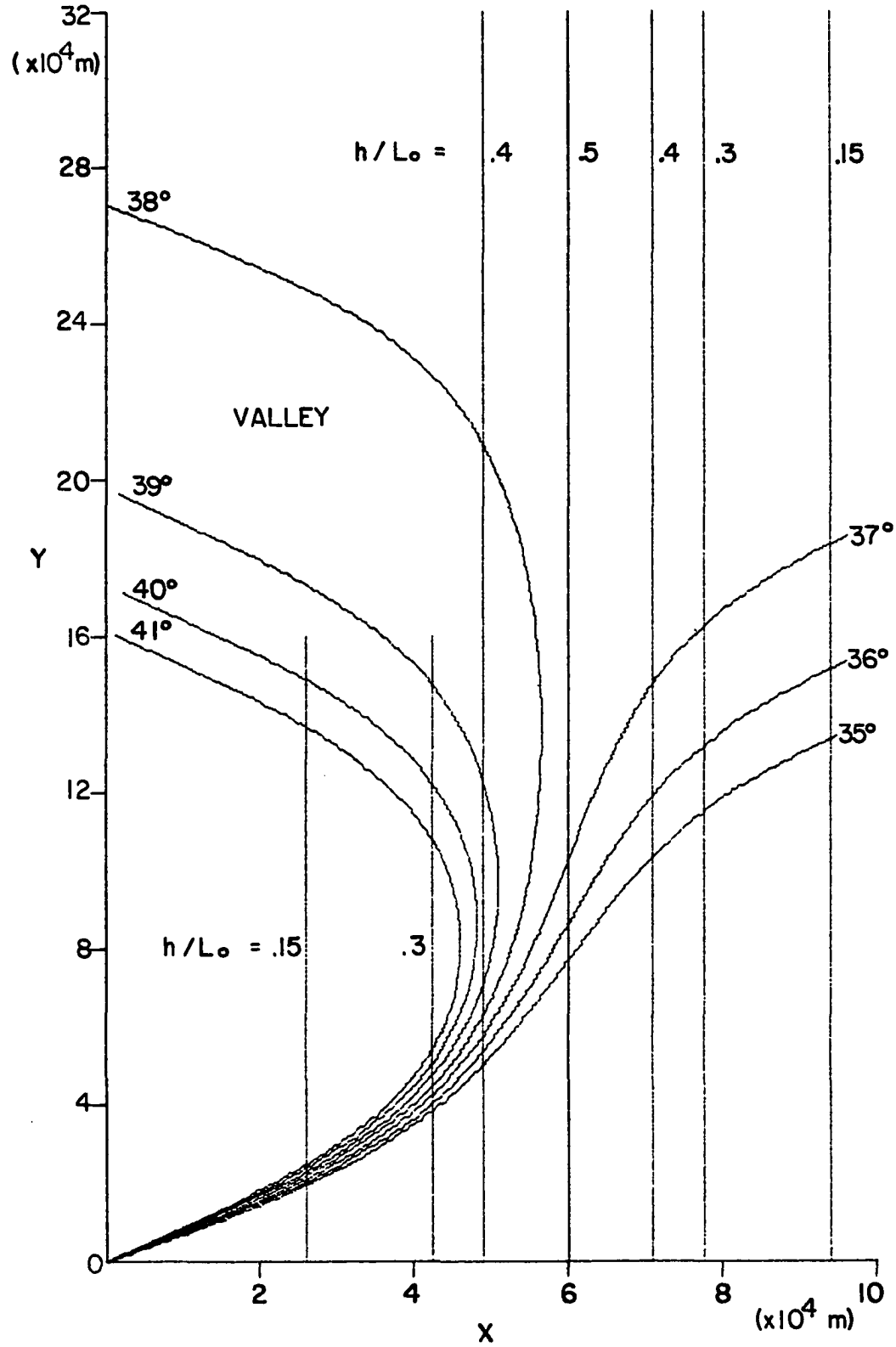

Fig. 16a. Ray trajectories using third order wave theory with energy dissipation (Model 2). (h_o/L_o = 1/10, H_o/L_o = 4/172.3).

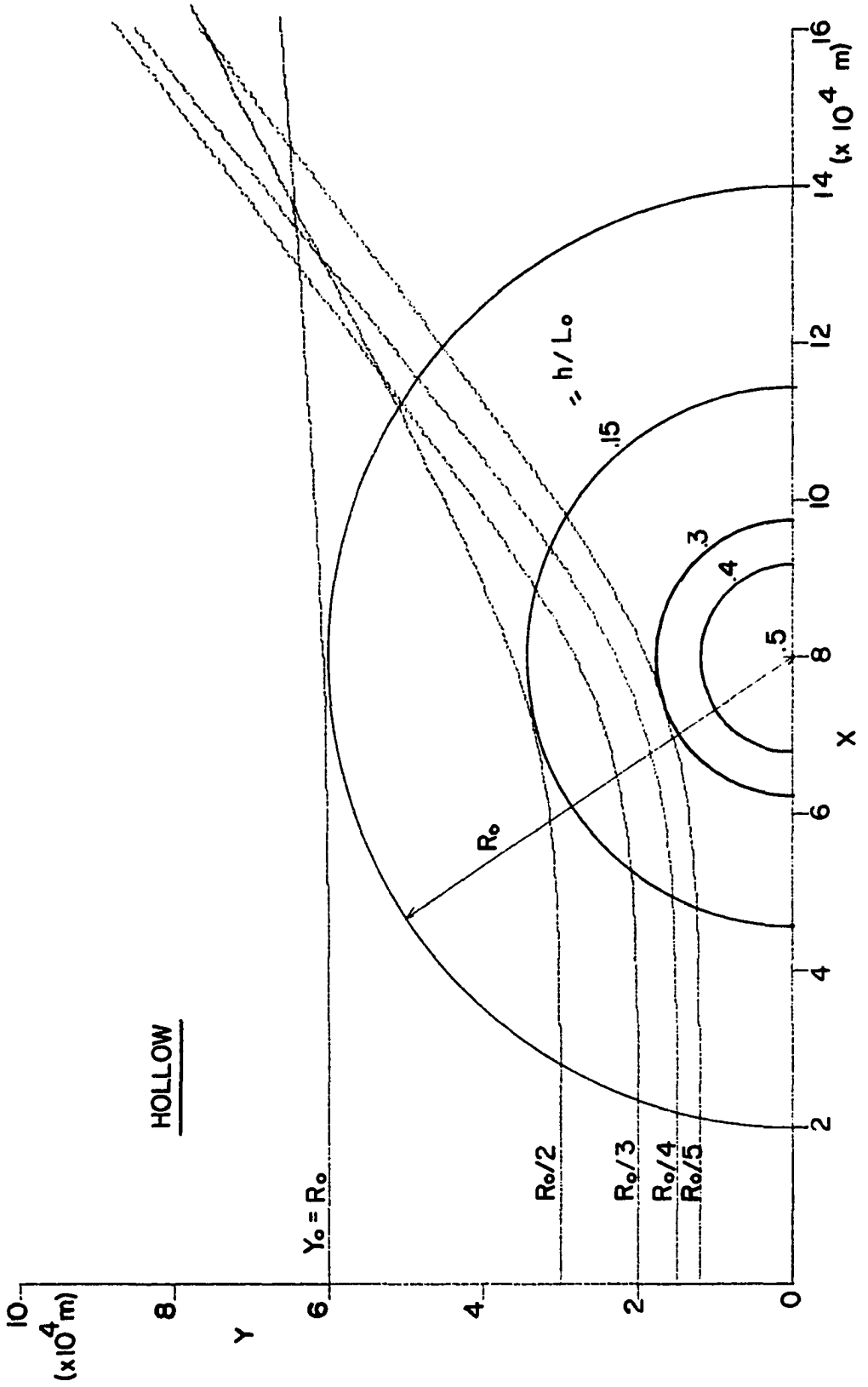

Fig. 19a. Ray trajectories using third order theory without energy dissipation ($h_{max}/L_o=1/2$, $H_o/h_{min}=1/4$).

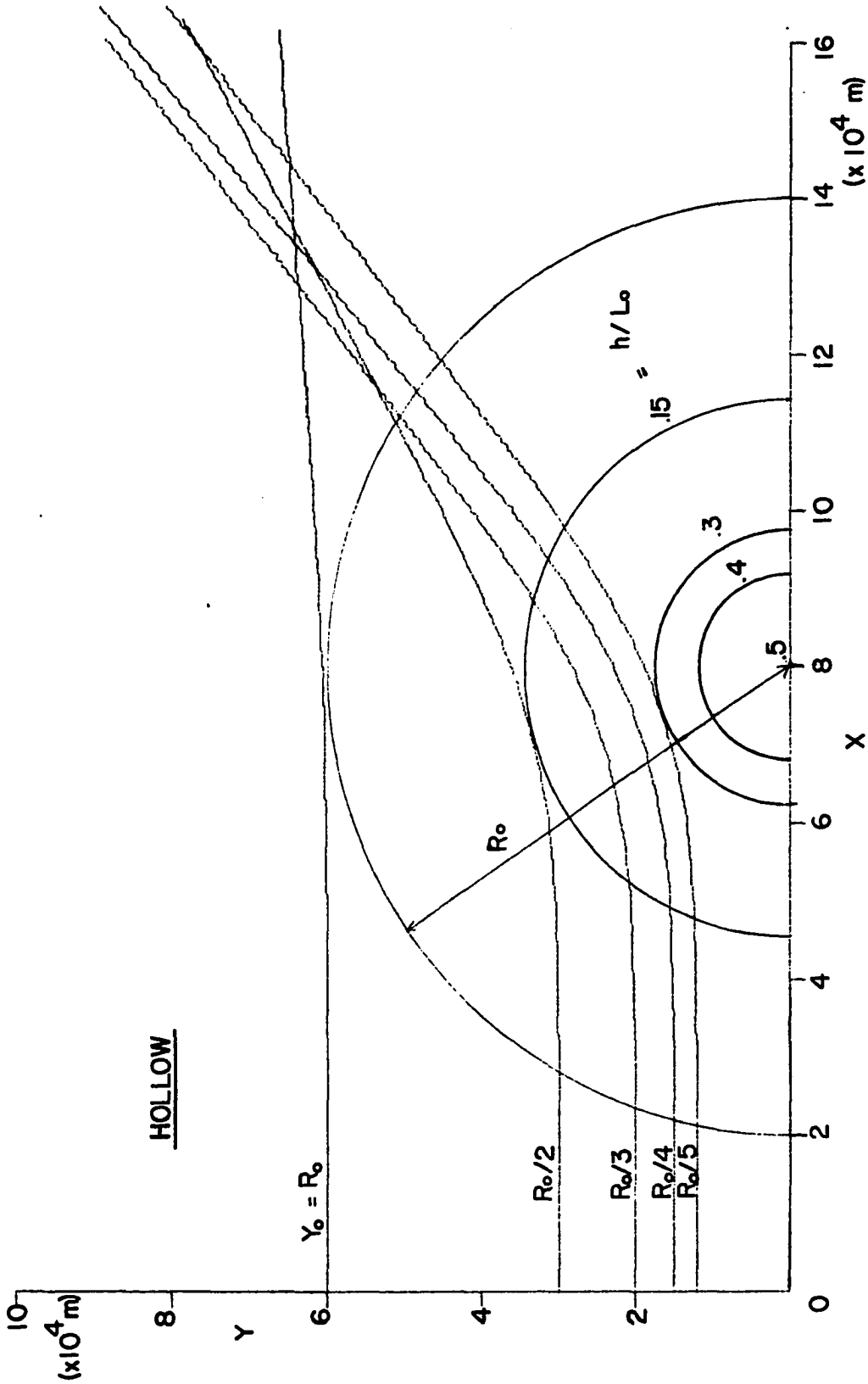

Fig. 19b. Ray trajectories using third order theory with energy dissipation ($h_{max}/L_o=1/2$, $H_o/h_{min}=1/4$).

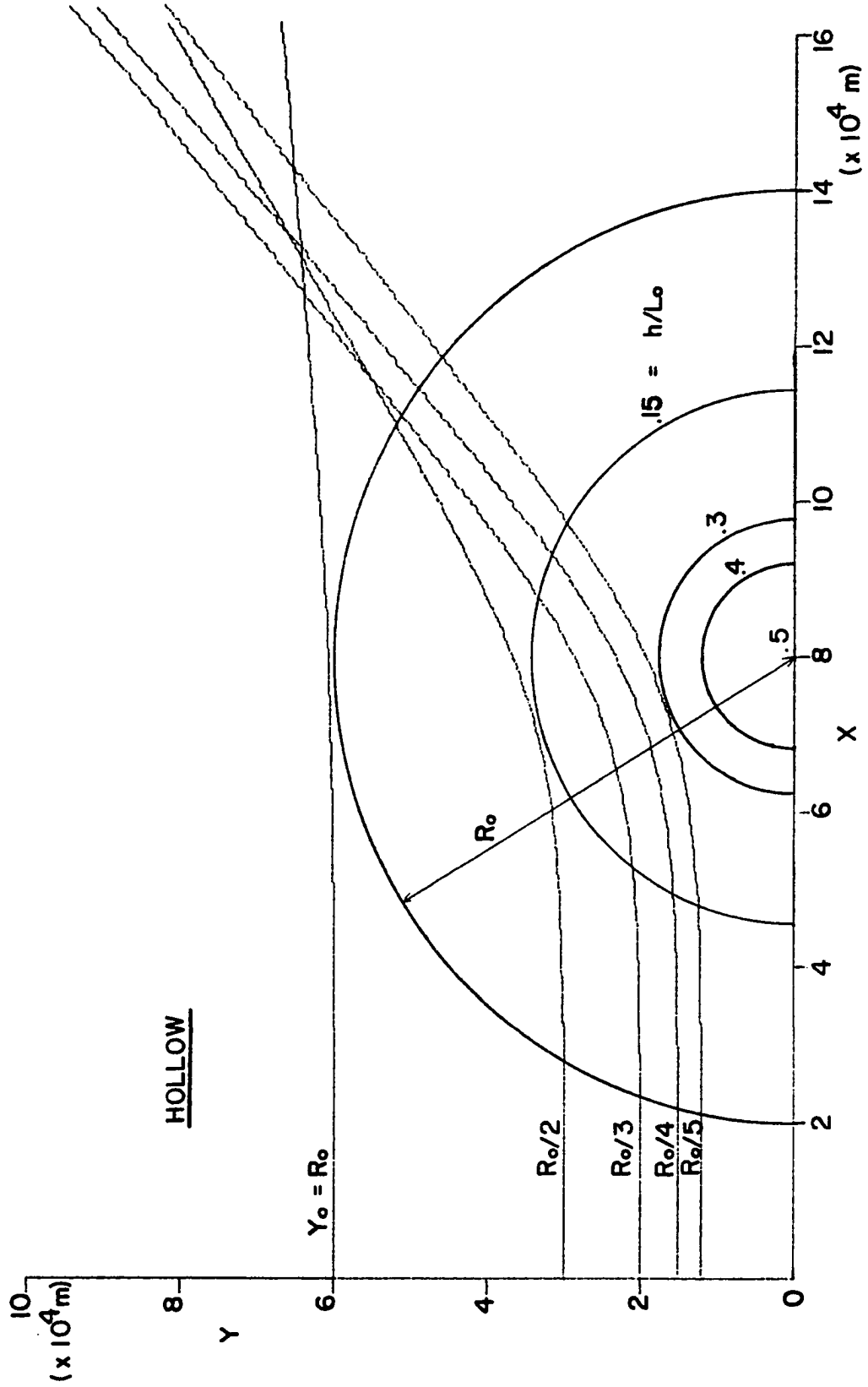

Fig. 19c. Ray trajectories using first order theory ($h_{max}/L_o=1/2$, $H_o/h_{min}=1/4$).

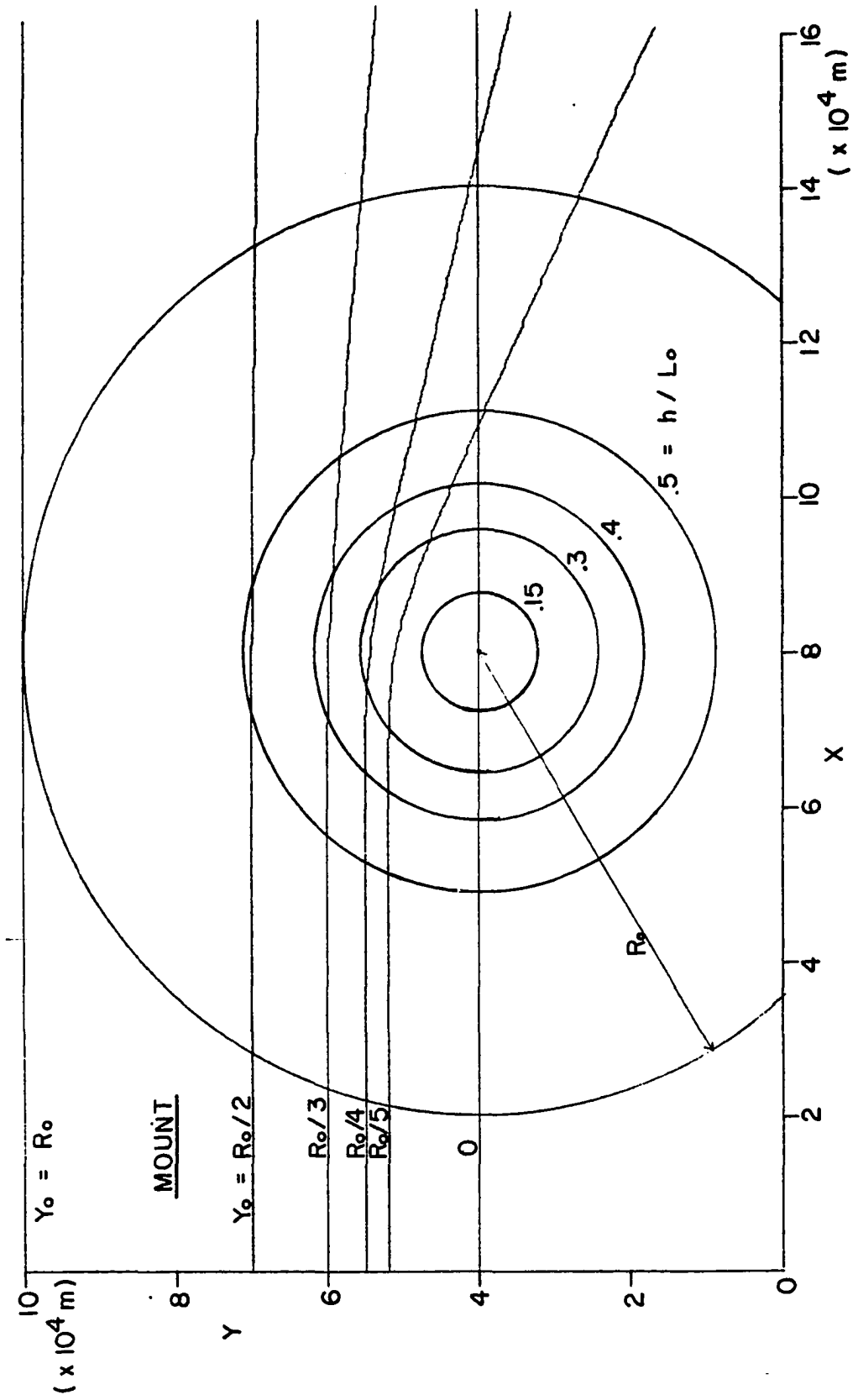

Fig. 20a. Ray trajectories using third order theory with energy dissipation (h_{max}/L_o=100/172.3, H_o/h_{min}=1/4).

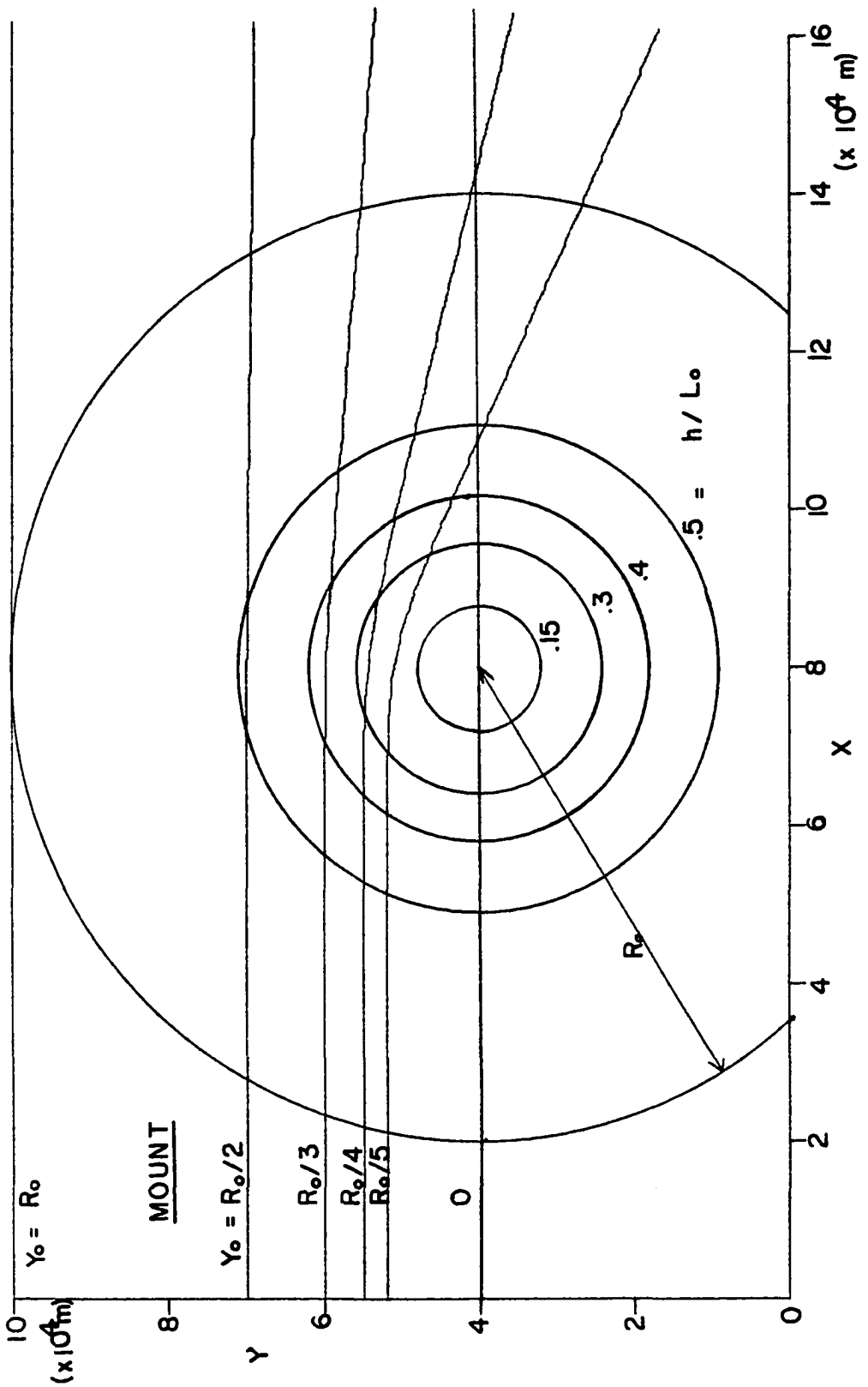

Fig. 20b. Ray trajectories using third order theory without energy dissipation (h_{max}/L_o=100/172.3, H_o/h_{min}=1/4).

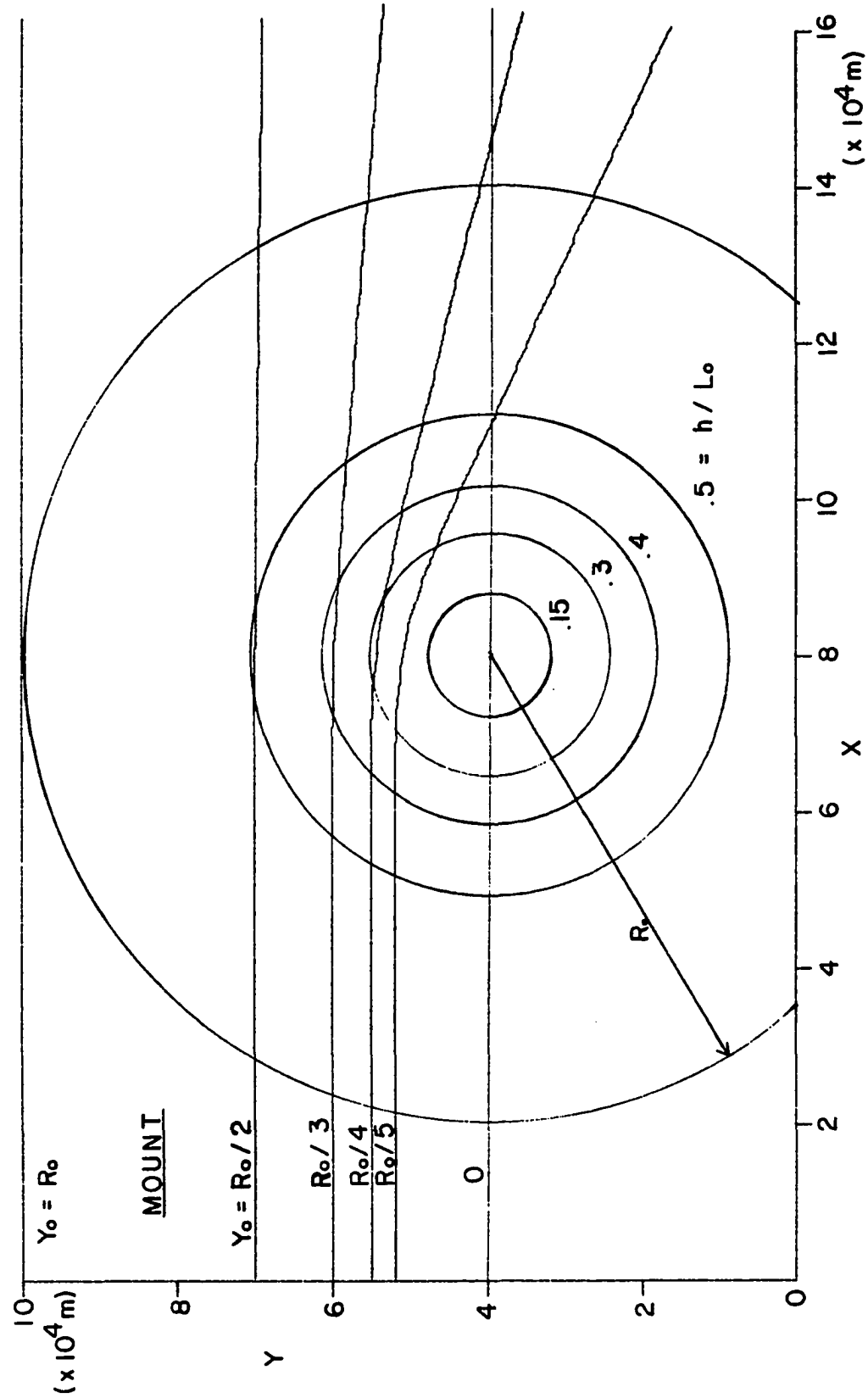

Fig. 20c. Ray trajectories using first order theory (h_{max}/L_o=100/172.3, H_o/h_{min}=1/4).

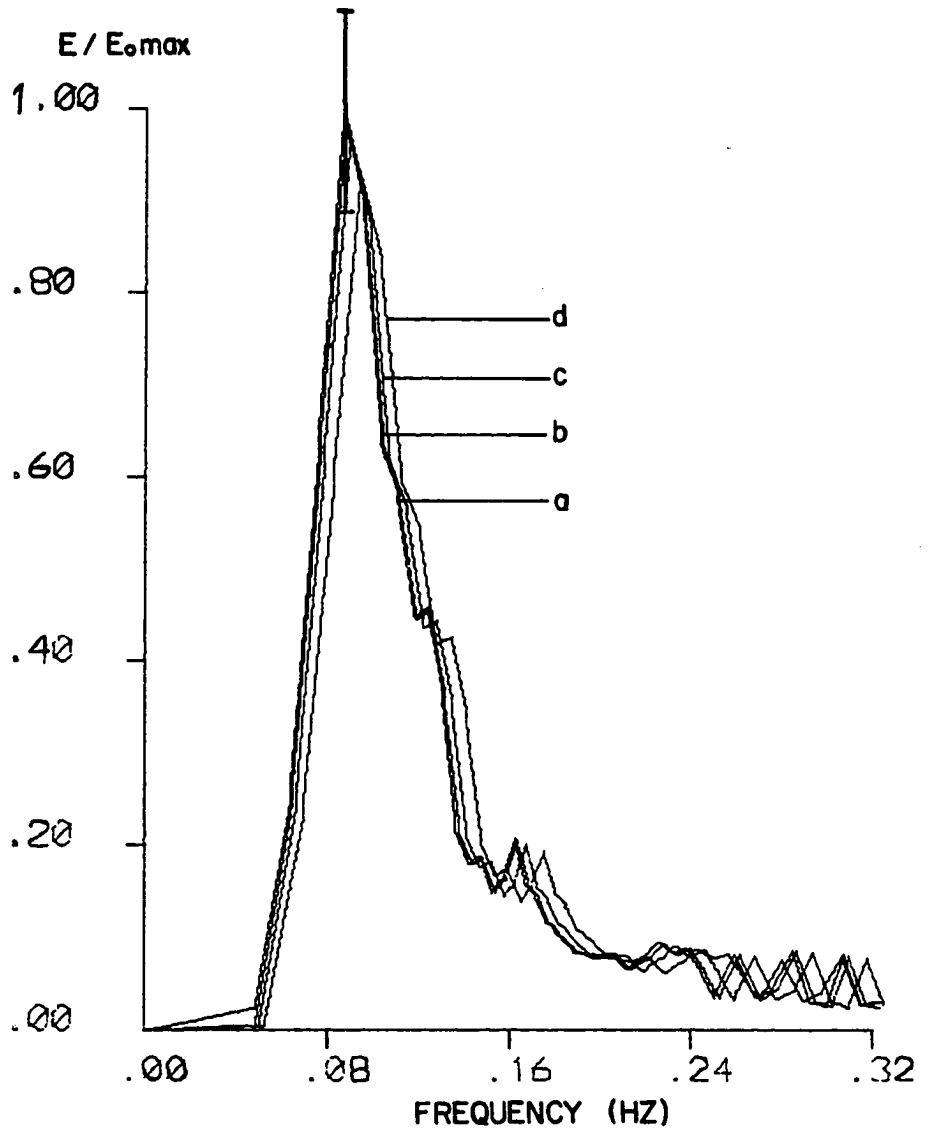

Fig. 21a. Distortion in the wave spectrum caused by ten degree shifts in the angle of measurement from true wave propagation direction, ø= a) 0°, b) 10°, c) 20°, and d) 30°. (Data segment 1 to 4; vertical bar denotes 80% confidence band.)

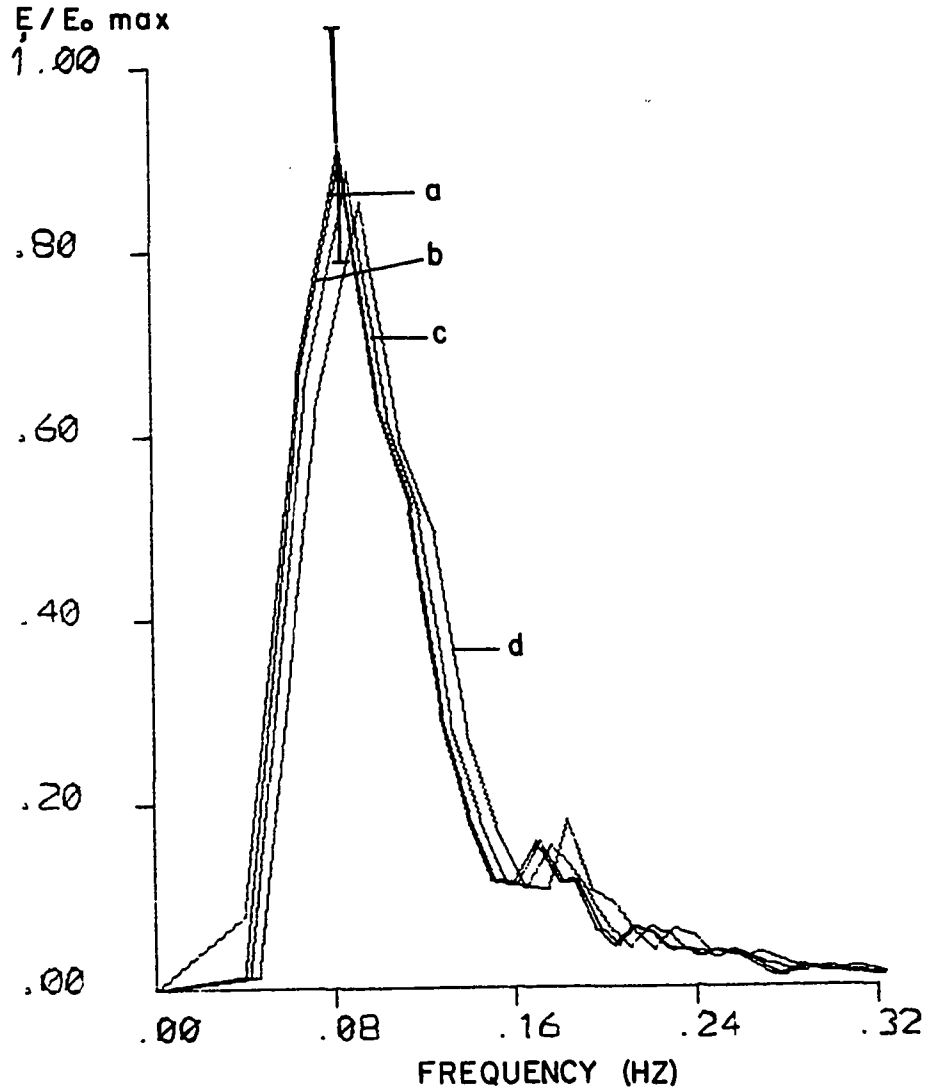

Fig. 21b. Distortion in the wave spectrum caused by ten degree shifts in the angle of measurement from true wave propagation direction, ϕ= a) 0^{o}, b) 10^{o}, c) 20^{o}, and d) 30^{o}. (Data segment 5; vertical bar denotes 80% confidence band.)

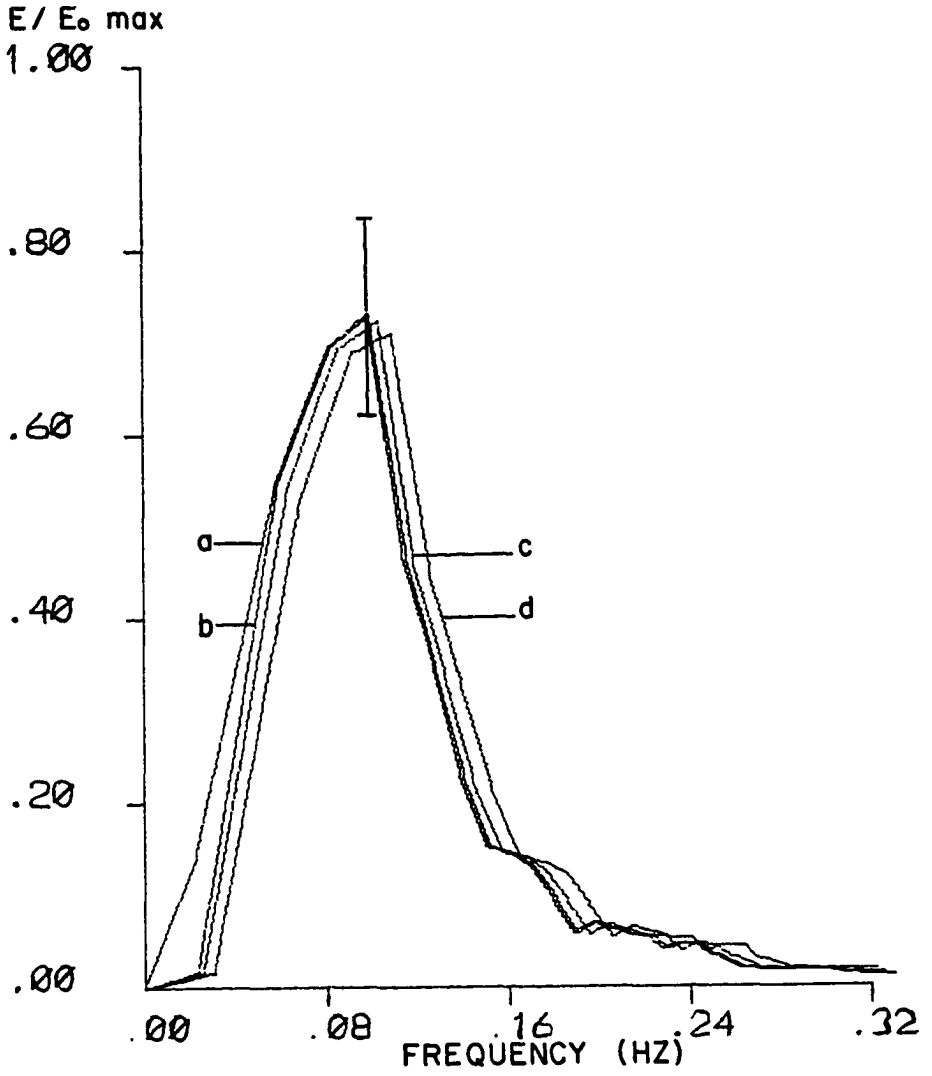

Fig. 21c. Distortion in the wave spectrum caused by ten degree shifts in the angle of measurement from true wave propagation direction, ϕ= a) 0^{o}, b) 10^{o}, c) 20^{o}, and d) 30^{o}. (Data segment 6; vertical bar denotes 80% confidence band.)

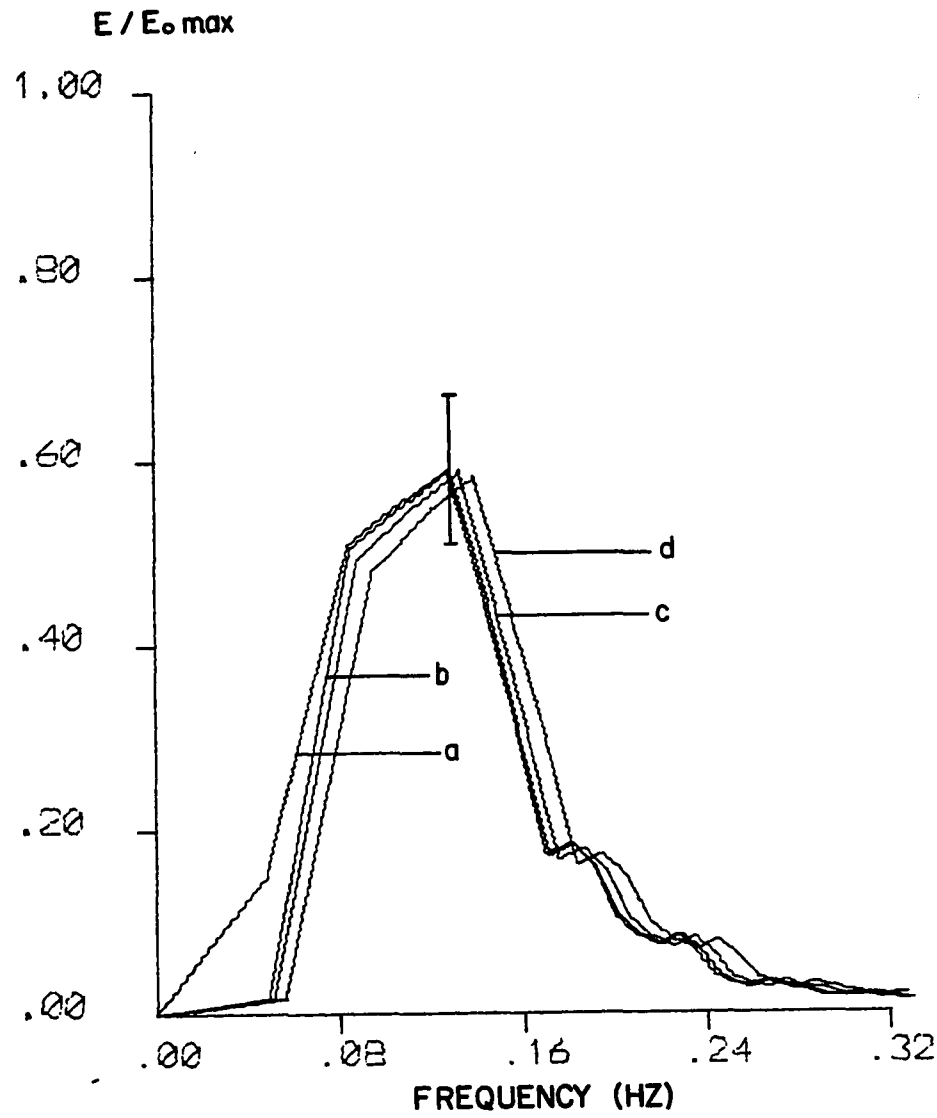

Fig. 21d. Distortion in the wave spectrum caused by ten degree shifts in the angle of measurement from true wave propagation direction, ø= a) 0°, b) 10°, c) 20°, and d) 30°. (Data segment 7; vertical bar denotes 80% confidence band.)

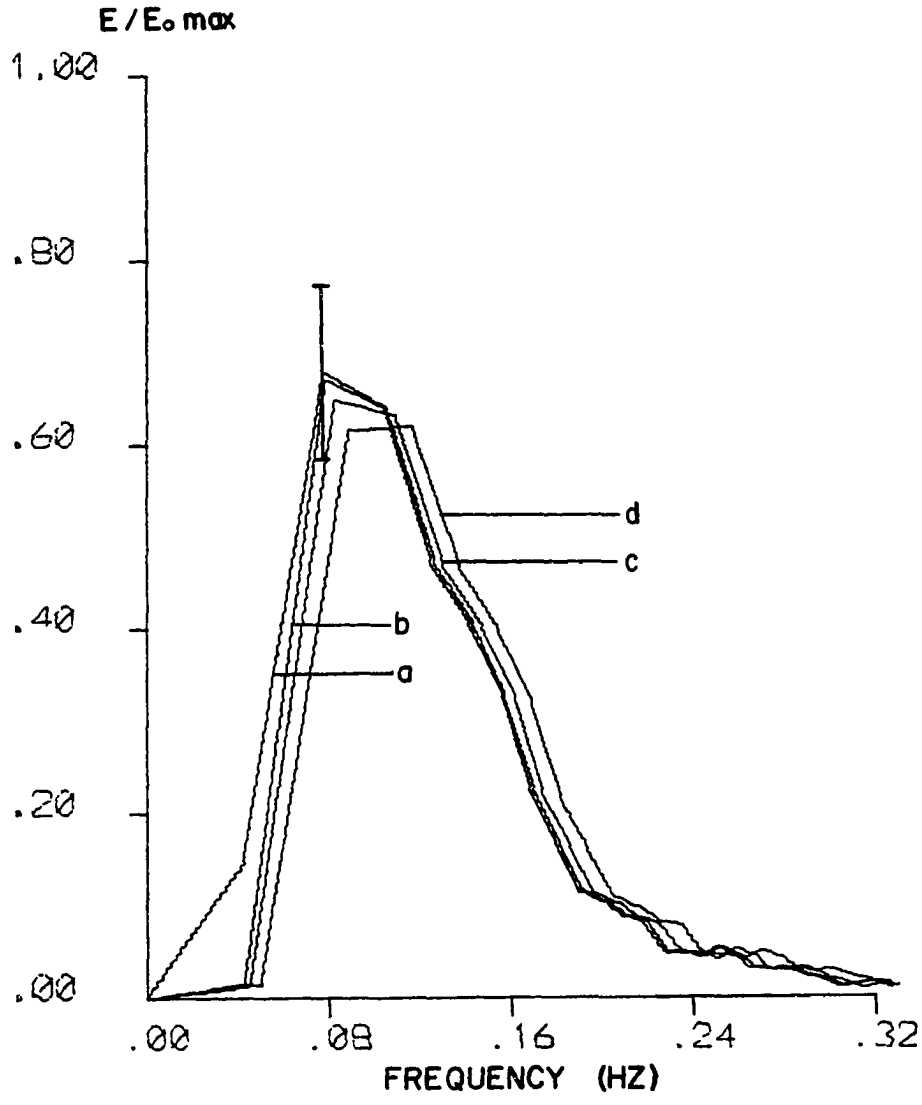

Fig. 21e. Distortion in the wave spectrum caused by ten degree shifts in the angle of measurement from true wave propagation direction, ø= a) 0°, b) 10°, c) 20°, and d) 30°. (Data segment 8; vertical bar denotes 80% confidence band.)

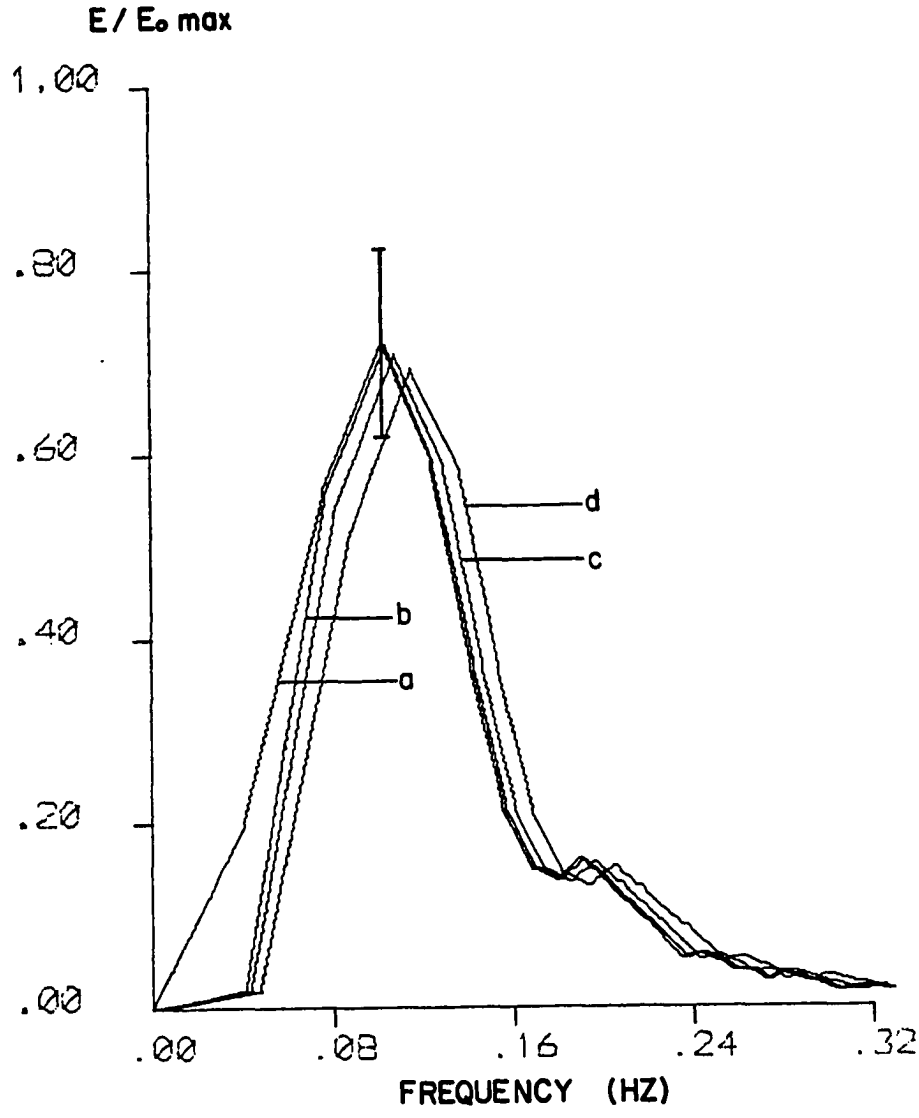

Fig. 21f. Distortion in the wave spectrum caused by ten degree shifts in the angle of measurement from true wave propagation direction, ϕ= a) 0^{o}, b) 10^{o}, c) 20^{o}, and d) 30^{o}. (Data segment 9; vertical bar denotes 80% confidence band.)

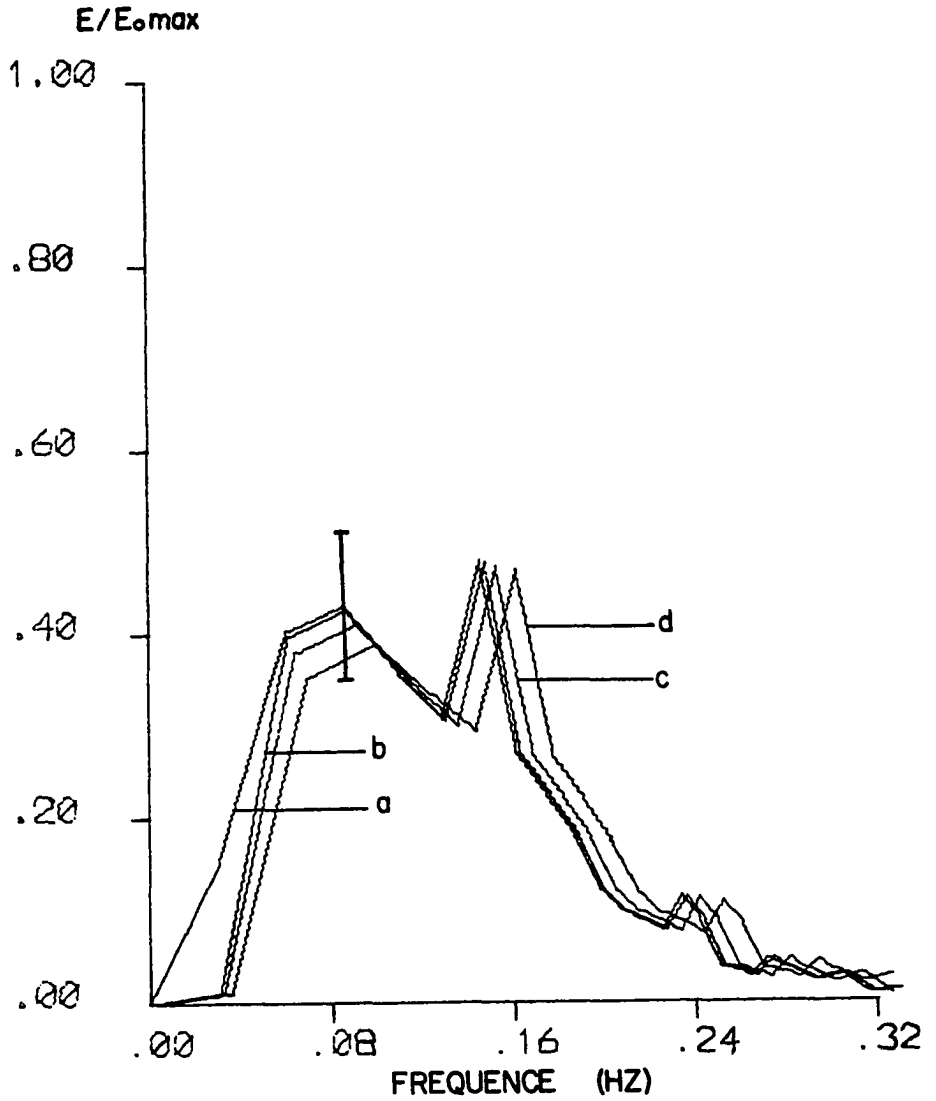

Fig. 21g. Distortion in the wave spectrum caused by ten degree shifts in the angle of measurement from true wave propagation direction, ϕ= a) 0^{o}, b) 10^{o}, c) 20^{o}, and d) 30^{o}. (Data segment 10; vertical bar denotes 80% confidence band.)

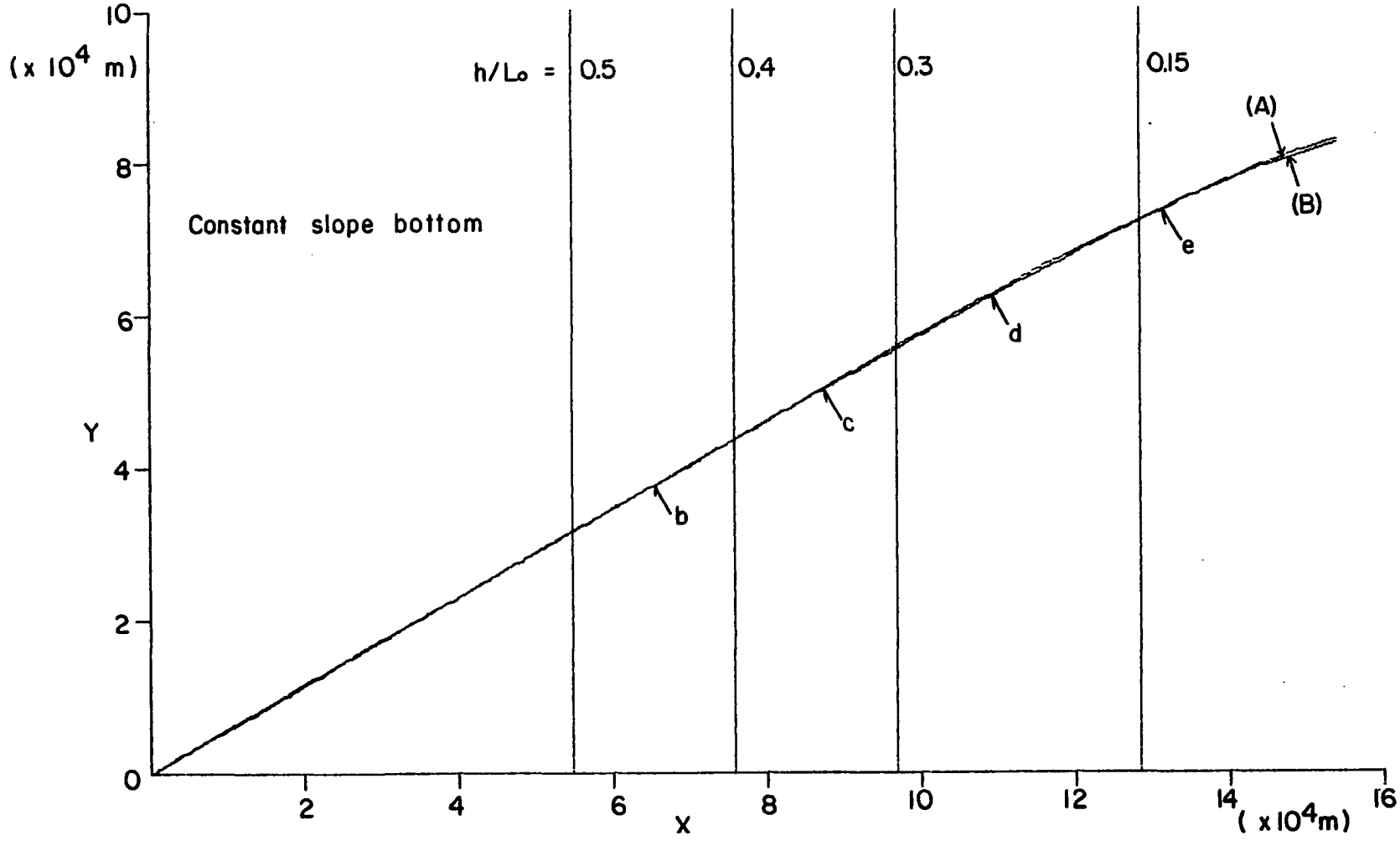

Fig. 22. Trajectories by standard ray theory(A) and by power refraction theory(B) over constant sloping bottom. (The marks b to e represent the locations where the spectra in Fig. 24 were calculated.)

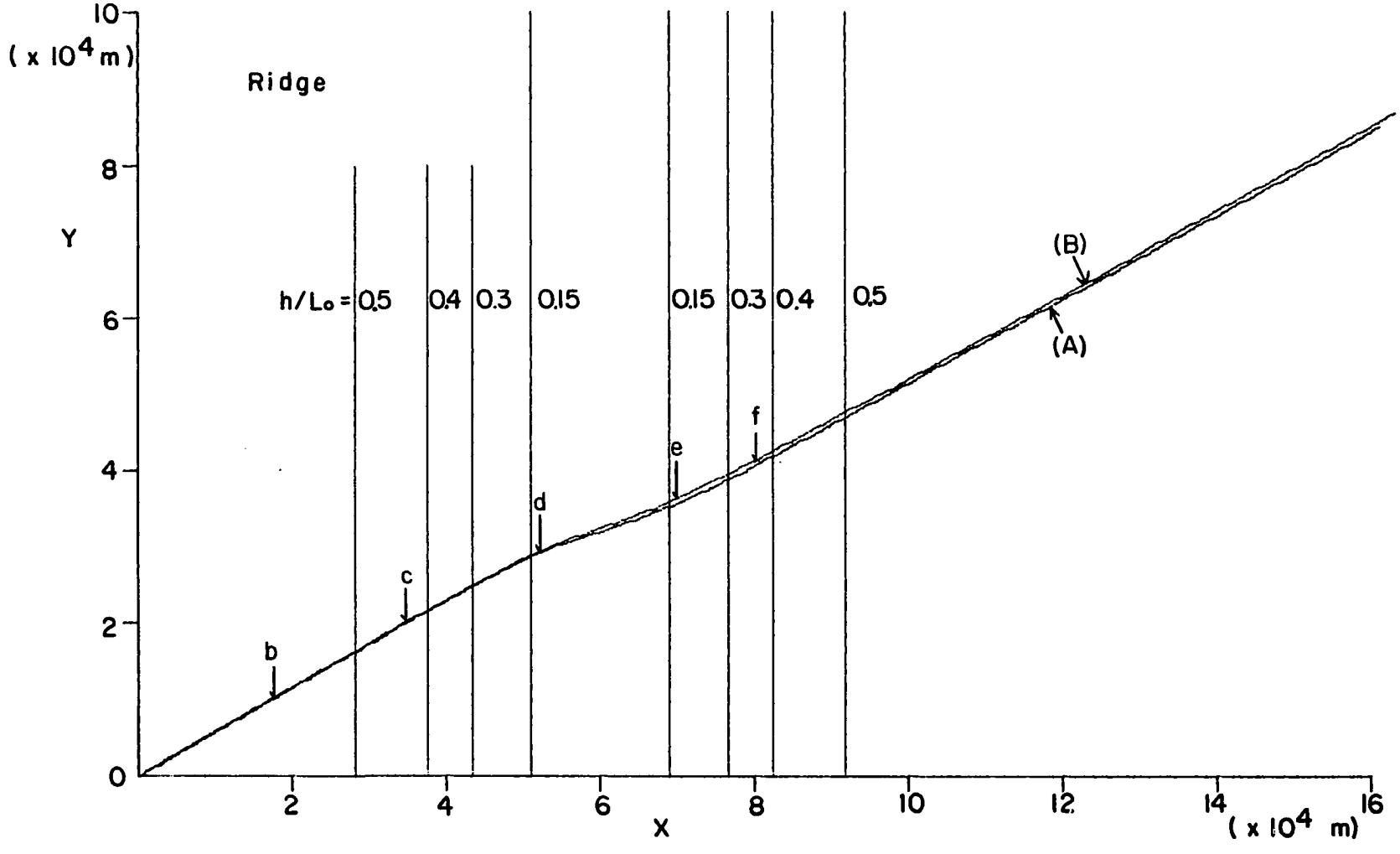

Fig. 23. Trajectories by standard ray theory(A) and by power refraction theory(B) over 'ridge'. (The marks b to f represent the locations where the spectra in Fig. 25 were calculated.)

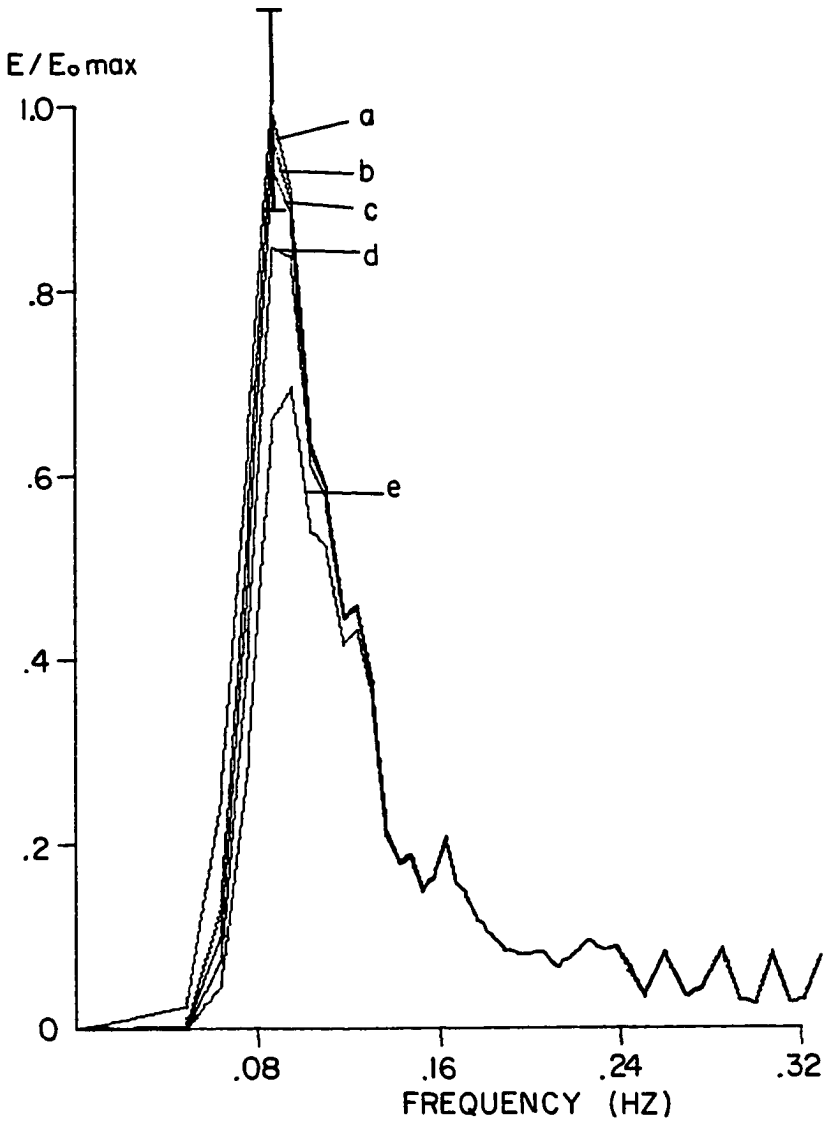

Fig. 24. Spectrum transformation over constant sloping bottom using third order power theory with energy dissipation(Model 2). (Vertical bar denotes 80% confidence band.) (Reference spectrum is denoted by 'a'; see Fig. 22 for the locations of spectra b to e.)

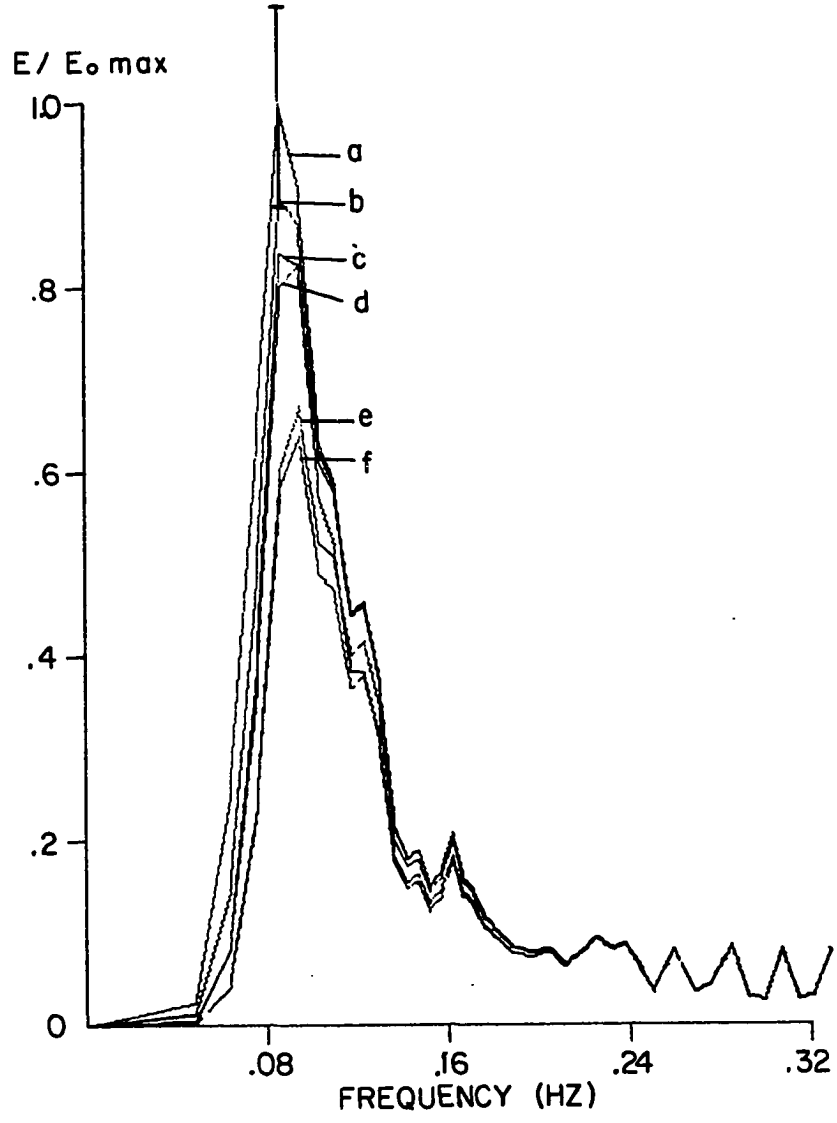

Fig. 25. Spectrum transformation over ridge using third order power refraction theory with energy dissipation. (Reference spectrum is denoted by 'a'; see Fig. 23 for the locations of spectra b to f.)

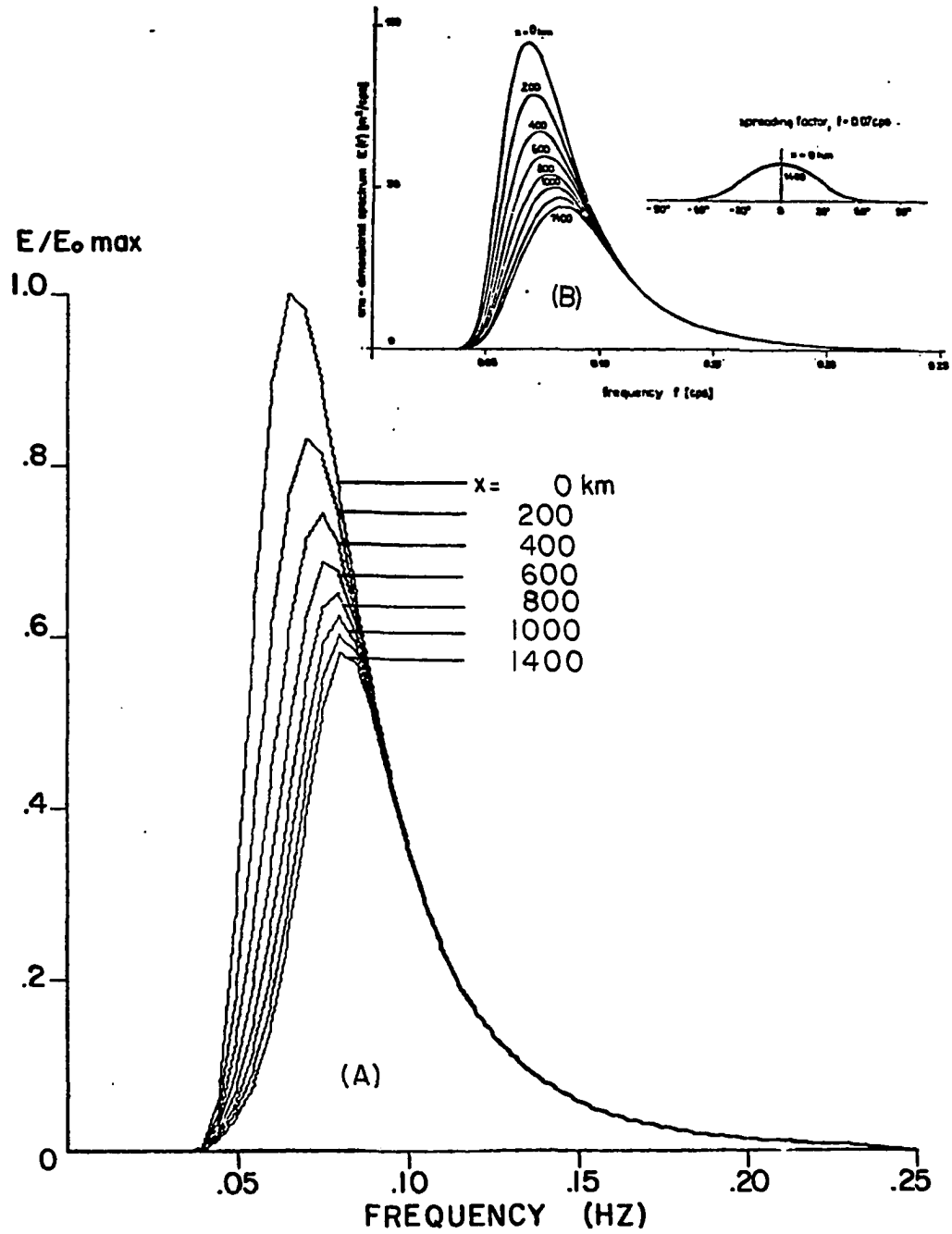

Fig. 26. Spectrum transformation over constant depth (100m) using the present power refraction model with equation (2.54)(A), and from Hasselmann and Collins(B). (Input spectrum is from Pierson and Moskowitz, 1964.)

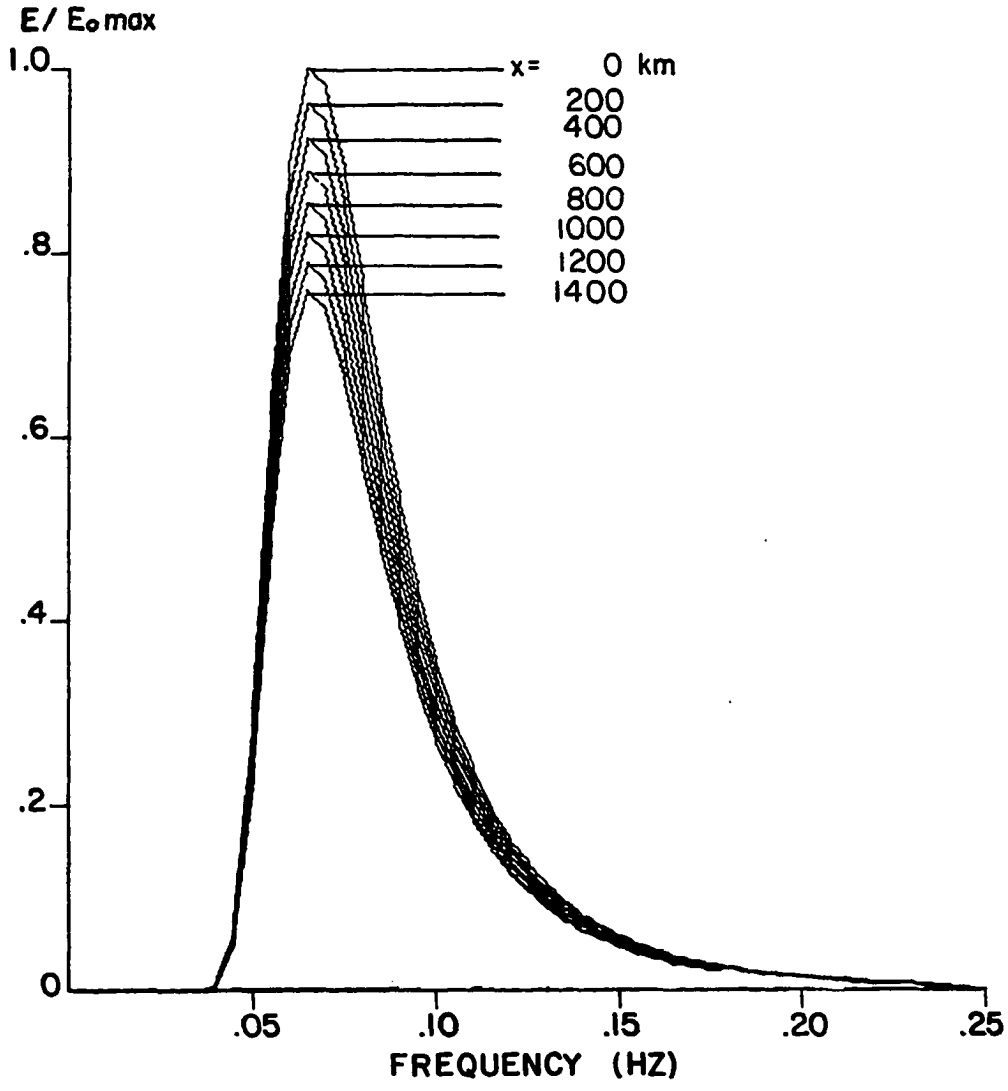

Fig. 27. Spectrum transformation over constant depth (100m) using the present power refraction model with equation (2.55). (Input spectrum is from Pierson and Moskowitz, 1964.)

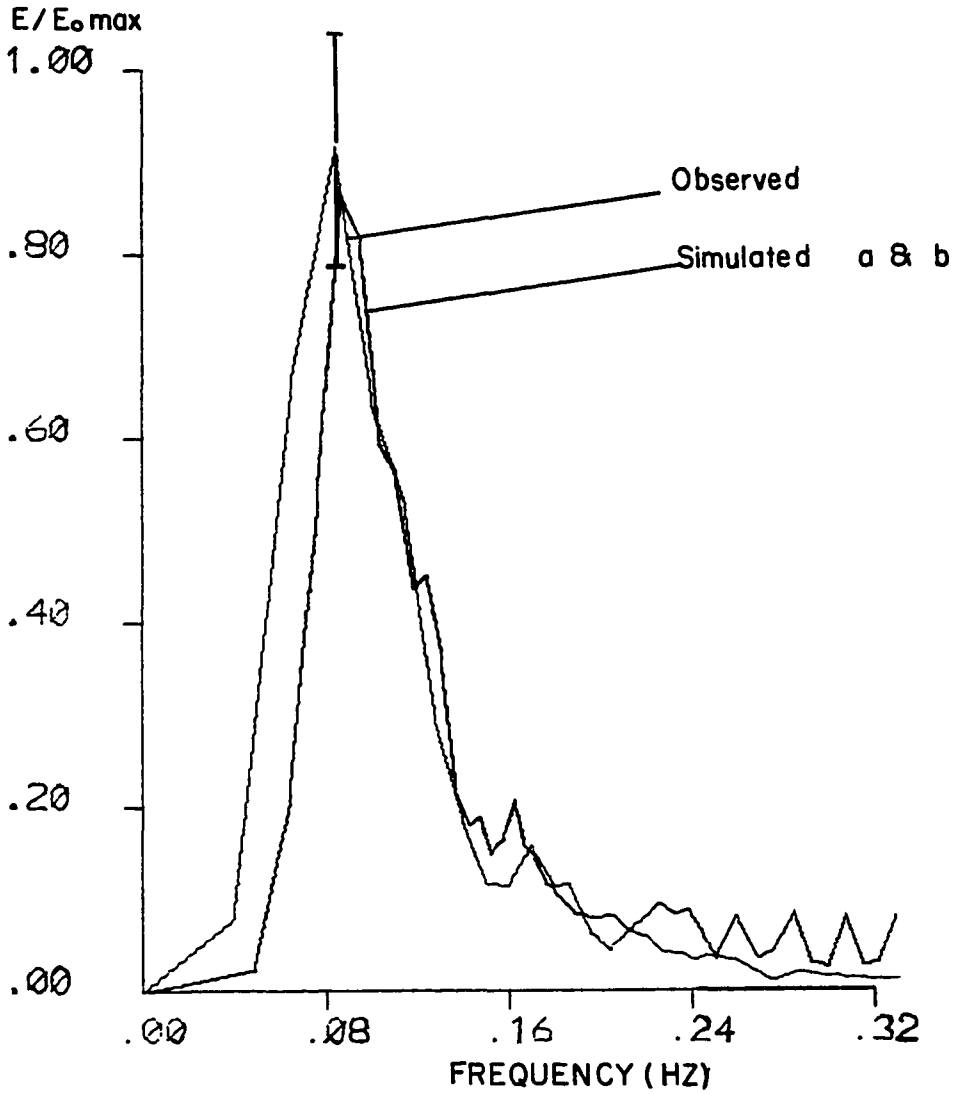

Fig. 28a. Comparison of observed and simulated spectra. (Data segment 5; vertical bar denotes 80% confidence band.) Simulated spectrum a is calculated by using Eq. (2.55), and b by Eq. (2.54).

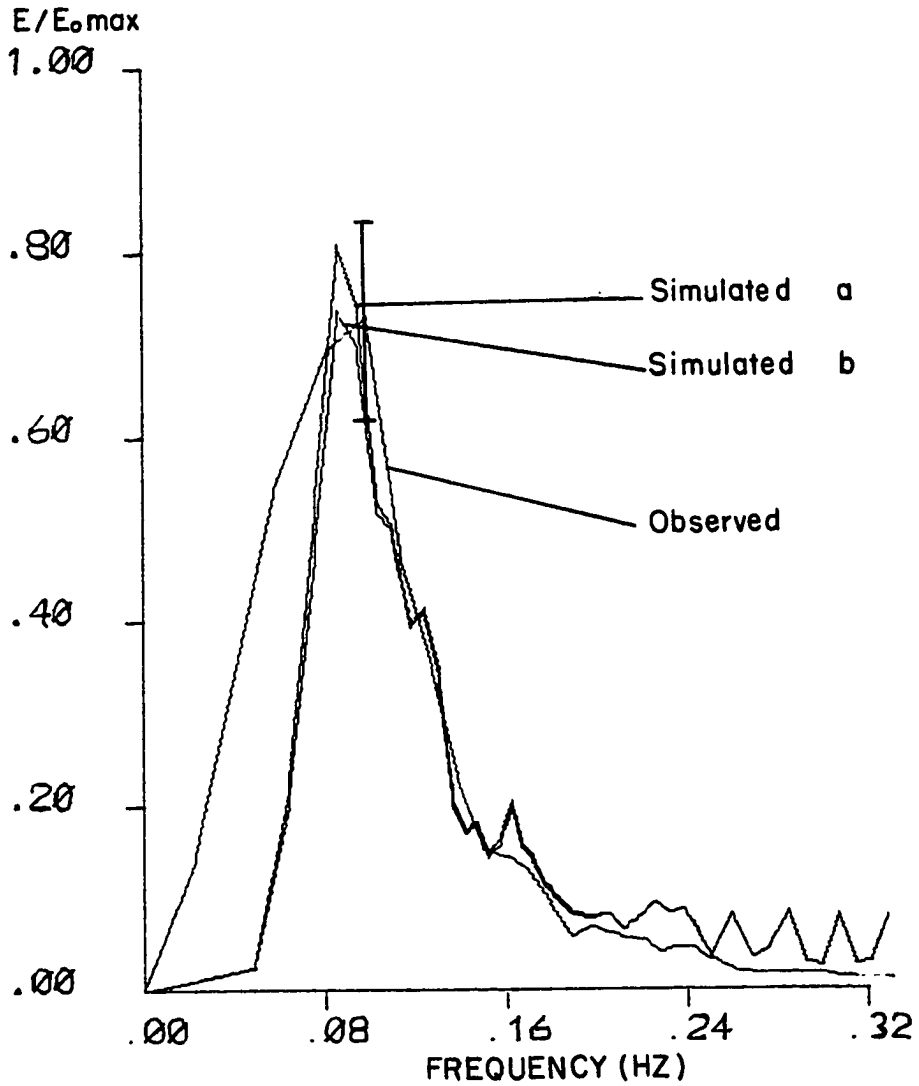

Fig. 28b. Comparison of observed and simulated spectra. (Data segment 6; vertical bar denotes 80% confidence band.) Simulated spectrum a is calculated by using Eq. (2.55), and b by Eq. (2.54).

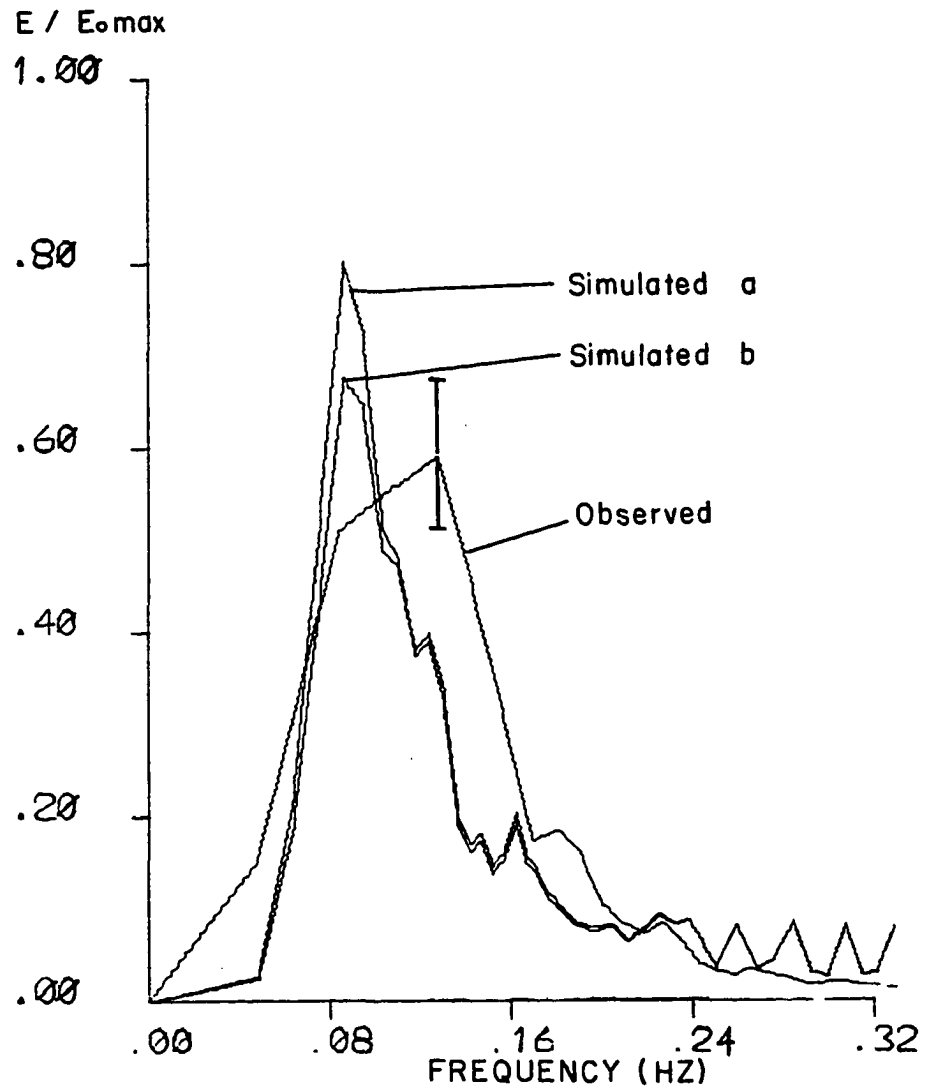

Fig. 28c. Comparison of observed and simulated spectra. (Data segment 7; vertical bar denotes 80% confidence band.) Simulated spectrum a is calculated by using Eq. (2.55), and b by Eq. (2.54).

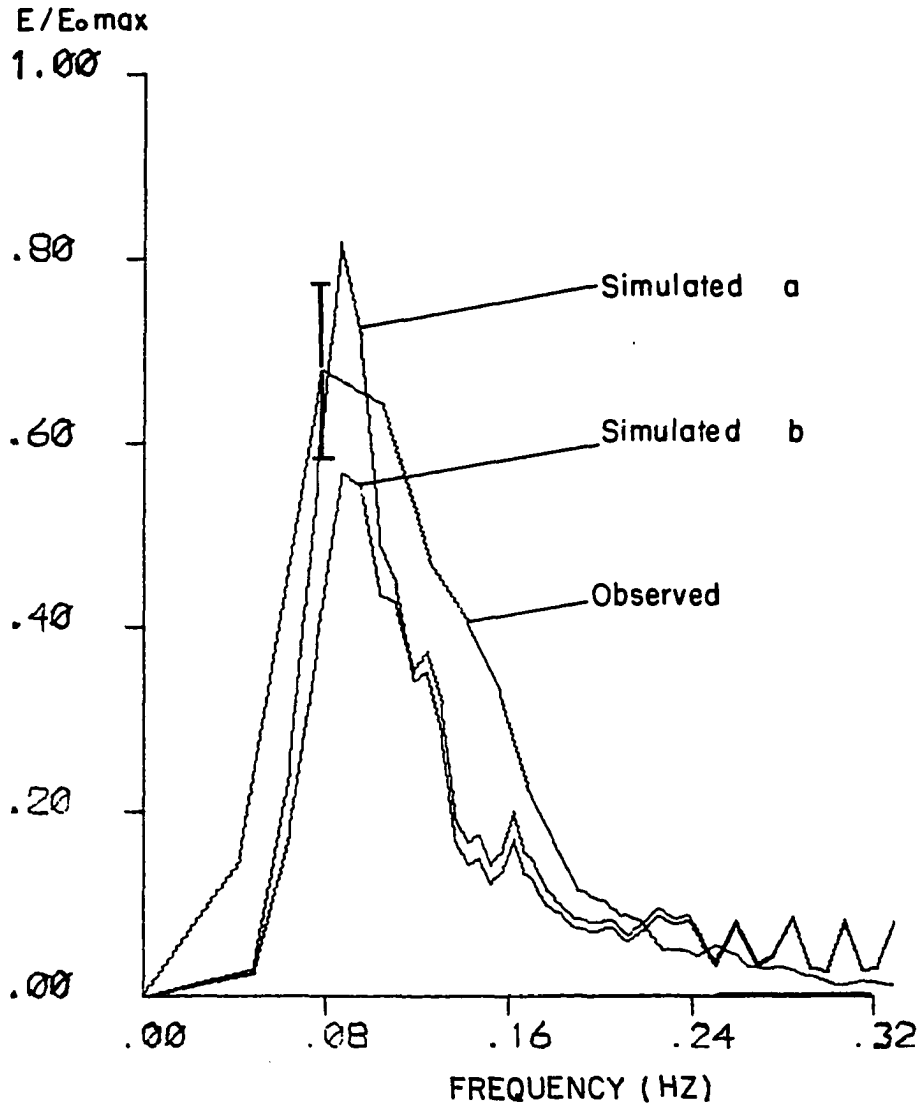

Fig. 28d. Comparison of observed and simulated spectra. (Data segment 8; vertical bar denotes 80% confidence band.) Simulated spectrum a is calculated by using Eq. (2.55), and b by Eq. (2.54).

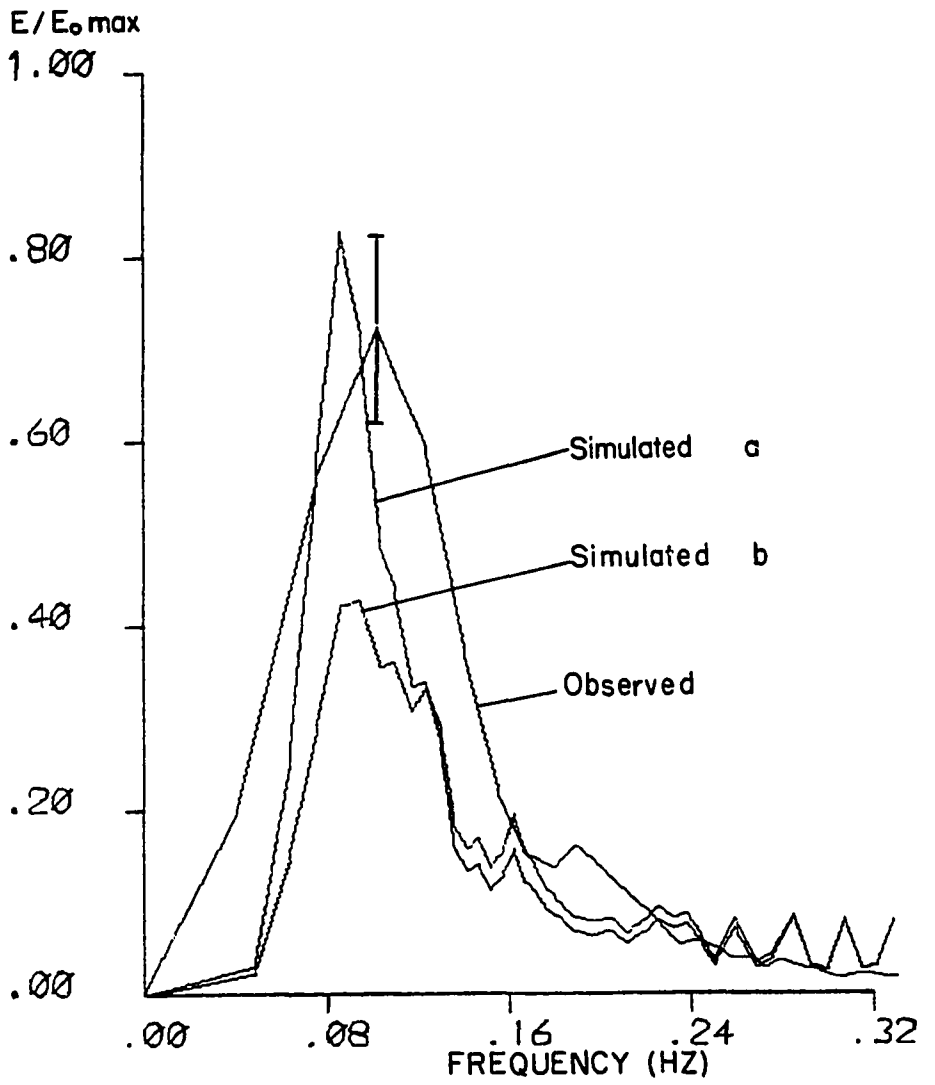

Fig. 28e. Comparison of observed and simulated spectra. (Data segment 9; vertical bar denotes 80% confidence band.) Simulated spectrum a is calculated by using Eq. (2.55), and b by Eq. (2.54).

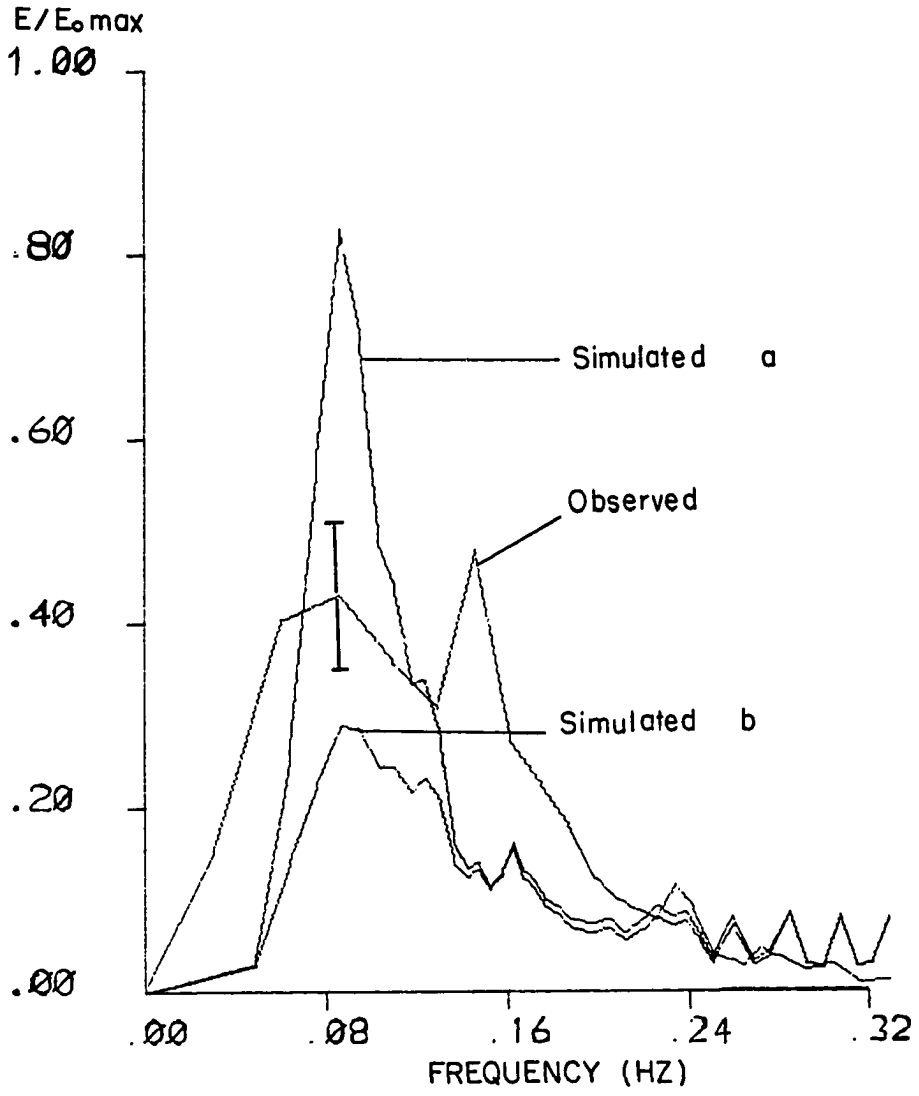

Fig. 28f. Comparison of observed and simulated spectra. (Data segment 10; vertical bar denotes 80% confidence band.) Simulated spectrum a is calculated by using Eq. (2.55), and b by Eq. (2.54).

REFERENCES

Abramowitz, M. and I. A. Stegun, 1970. Handbook of mathematical functions. Dover Pub. Inc., N.Y.

Arthur, R. I., W. H. Munk, and J. D. Issacs, 1952. The direct construction of wave rays. Trans. Am. Geophys. Un., 33:855-865.

Bendat, J. S. and A. G. Piersol, 1971. Random data: Analysis and measurement procedures. Wiley-Interscience, N.Y.

Breeding, J. E., Jr., 1978. Velocities and refraction laws of wave groups: A verification. J. Geophys. Res., 83(c6):2970-2976.

Bretschneider, C. L. and R. O. Reid, 1954. Modification of wave height due to bottom friction, percolation, and refraction. Tech. Memo. 45. Beach Erosion Board, Corps of Engineers, U.S.A.

Burden, R. L., J. D. Faires and A. C. Reynolds, 1980. Numerical analysis. Prindle, Weber and Schmidt, Boston, Massachusetts, 239-258.

Chao, Y. Y., 1971. An asymptotic evaluation of the wave field near a smooth caustic. J. Geop. Res., 76(30): 7401-7408.

_____ and W. J. Pierson, 1972. Experimental studies of the refraction of uniform wave trains and transient wave groups near a straight caustic. J. Geop. Res., 77(24):4545-4554.

Collins, J. I., 1972. Prediction of shallow water spectra. J. Geop. Res., 77(5):2693-2707.

_____ and W. Weir, 1969. Probabilities of wave characteristics in the surf zone. Tetra Tech. Report. No-TC 149.

Crapper, G. D., 1957. An exact solution for progressive capillary waves of arbitrary amplitude. J. Fluid Mech., 2:532-540.

Davies, T. V., 1952. Symmetrical finite amplitude gravity waves. Proc. NBS Semicent. Symp. on Gravity Waves. NBS Circular 521, 55-60.

Divoky, D., B. Le Mehaute, and A. Lin, 1970. Breaking waves on gentle slopes. J. Geophys. Res., 75:1681-1692.

Eagleson, P. S., 1962. Laminar damping of oscillatory waves. J. Hydraulic Div. Proc. ASCE., 88 (HY3):155-181.

Fox, M. J. H., 1976. On the nonlinear transfer of energy in the peak of a gravity wave spectrum-II. Proc. Roy. Soc., A348:467-483.

Galvin, C. J., Jr., 1972. Wave breaking in shallow water; in Waves on Beaches and Resulting Sediment Transport. ed. by R. E. Meyer. Academic Press., N.Y., 413-456.

Gerald, C. F., 1970. Applied numerical analysis. Addison-Wesley Pub. Co., Reading, MA.

Goldsmith, V., W. D. Morris, R. J. Byrne, and C. H. Whitlock, 1974. Wave climate model of the Mid-Atlantic shelf and shoreline (Virginia Sea) - Model development, shelf geomorphology, and preliminary results. VIMS SRAMSOE No. 38.

Grosch, C. E. and W. J. Comery, 1977. Finite amplitude wave refraction. Institute of Oceanography, Old Dominion University, Tech. Rep. No. 34.

Grosskopf, W. G., 1980. Calculation of wave attenuation due to friction and shoaling: An evaluation. Tech. Paper 80-8, U.S. Army Corps of Engrs., CERC.

Harrison, W. and W. S. Wilson, 1964. Development of a method for numerical calculation of wave refraction. Tech. Memo. 6. U.S. Army Corps of Engrs., CERC.

Hasselmann, K., 1962. On the nonlinear energy transfer in a gravity wave spectrum. Part 1. J. Fluid Mech., 12: 481-500.

_____, 1963a. On the nonlinear energy transfer in a gravity wave spectrum. Part 2. J. Fulid Mech., 15: 273-281.

_____, 1963b. On the nonlinear energy transfer in a gravity wave spectrum. Part 3. J. Fluid Mech., 15: 385-398.

Hasselmann, K. and J. I. Collins, 1968. Spectral dissipation of finite depth gravity waves due to turbulent bottom friction. J. Mar. Res., 26(1):1-12.

Hinich, M. J. and C. S. Clay, 1968. The application of the discrete transform in the estimation of power spectra, coherence, and bispectra of geophysical data. Rev. of Geophys. 6(3):347-363.

Isaacson, M. de St. Q., 1977. Second approximation to gravity wave attenuation. J. Waterway Port Coastal and Ocean Div. ASCE, Vol. 103(WW1):43-55.

Iwagaki, Y. and T. Kakinuma, 1967. On the bottom friction factors off five Japanese coasts. Coastal Engineering in Japan, 10:13-22.

_____ and Y. Tsuchiya, 1966. Laminar damping of oscillatory waves due to bottom friction. Proc. 10th Conf. on Coastal Engrn., Tokyo, Japan, 149-174.

Johnson, J. W., M. P. O'Brien, and J. D. Issacs, 1948. Graphical construction of wave refraction diagrams. U.S. Navy Hydrographic Office Publ., 605.

Kajiura, K., 1961. On the partial reflection of water waves passing over a bottom of variable depth. IUGG. Monogr., 24:205-230.

Karisson, T., 1968. Refraction of continuous ocean spectra. J. Waterways and Harbour Div., ASCE, 95:437-448.

Keller, J. B., 1958. Surface waves on water of non-uniform depth. J. Fluid Mech., 4:607-614.

Kenyon, K. E., 1971. Wave refraction in ocean currents. Depp Sea Res. and Ocean. Abs., 18:1023-1034.

Laitone, E. V., 1962. Limiting conditions of cnoidal and Stokes' waves. J. Geophys. Res., 67(4):1555-1564.

Lenau, C. W., 1966. The solitary wave of maximum amplitude. J. Fluid Mech., 26(2):309-320.

Linnette, H. M., 1961. Statistical filters for smoothing and filtering equally spaced data. U.S. Navy Electronics Lab., San Diego, California. Res. Report 1049.

Long, R. B., 1973. Scattering of surface waves by an irregular bottom. J. Geophy. Res., 78(33):7861-7870.

Longuet-Higgins, M. S., 1956. The refraction of sea waves in shallow water. J. Fluid Mech., 1(2):163-176.

_____, 1957. On the transformation of a continuous spectrum by refraction. Proc. Camb. Phil. Soc., 53(1): 226-229.

_____, 1963. The generation of capillary waves by steep gravity waves. J. Fluid Mech., 16:138-159.

_____, 1976. On the non-linear transfer of energy in the peak of a gravity wave spectrum: A simplified model. Proc. Roy. Soc. A., 347:311-328.

_____ and E. D. Cokelet, 1976. The deformation of steep surface waves on water. I. A numerical method of computation. Proc. Roy. Soc. Lond., A350:1-26.

Lukasik, S. J. and C. E. Grosch, 1963. Laminar damping of oscillatory waves, Discussion. J. Hydraulic Div. Proc. ASCI., 89(HY1):231-239.

Ludwick, J. C., 1975. Variation in the boundary-drag coefficient in the tidal entrance to Chesapeake Bay, Virginia. Mar. Geol., 19:19-28.

McCowan, J., 1894. On the highest wave of permanent type. Phil. Mag., 38(5):351-358.

McGoldrick. L. F., 1965. Resonant interactions among capillary-gravity waves. J. Fluid Mech., 21:305-331.

_____, 1970. An experiment on second order capillary-gravity resonant interactions. J. Fluid Mech., 42: 193-200.

Meyer, R. E., 1979. Theory of water-wave refraction. Adv. in Applied mech., 19:53-141.

_____, 1979b. Surface wave reflection by underwater ridges. J. Phys. Oceanogr., 9:150-157.

Miche, R., 1944. Mouvements ondutatoires des mers en profondeur constante on decroissant. Annals des points et Chaussees.

Monahan, E. C., 1971. Oceanic white caps. J. Phys. Oceanogr. 1:138-144.

Monin, A. S. and A. M. Yaglom, 1979. Statistical fluid mechanics: mechanics of turbulence. Vol. 1. 249-256. English ed. ed. by J. L. Lumley. The MIT Press, Massachusetts.

Morris, W. D., 1979. A comparison of simulated and experimental wave spectra in the near shore region. M.S. thesis. Department of Oceanography, Old Dominion University, Norfolk, Virginia.

Munk, W. H. and R. S. Arthur, 1952. Wave intensity along a refracted ray. Proc. NBS Semicent. Symp. on gravity waves. NBS Circular, 521.

_____ and M. A. Traylor, 1947. Refraction of ocean waves. J. Geol., 55:1-26.

Nath, J. H. and F. L. Ramsey, 1976. Probability distributions of breaking wave heights emphasizing the utilization of the JONSWAP spectrum. J. Phys. Oceanogr., 6:316-323.

Orr, T. E. and J. G. Herbich, 1970. Numerical calculation of wave refraction by digital computer. Texas A M Eng. Ex. State. Coastal and Ocean Eng. Div. Rep., 114.

Packham, B. A., 1952. The theory of symmetrical gravity waves of finite amplitude, II. The solitary waves. Proc. Roy. Soc., A213:238-249.

Perigrine, D. H., 1972. Equations for water waves and the approximation behind them. in Waves on beaches and resulting sediment transport. ed. by R. E. Meyer. Academic Press, N.Y.

Phillips, O. M., 1977. The dynamics of the upper ocean. Cambridge University Press, Cambridge, London.

Pierson, W. J., Jr., 1951. The interpretation of crossed orthogonals in wave refraction phenomena. Tech. Memo. 21. Beach Erosion Board. Corps of Engrs. U.S.A.

_____ and L. Mosckowitz, 1964. A proposed spectral form for fully developed wind seas based on the similarity theory of S.A. Kitaigorodskii. J. Geophys. Res., 69(24):5181-5190.

_____, G. Neuman and R. W. James, 1955. Observing and forecasting ocean waves by means of wave spectra and statistics. U.S. Naval Oceanographic Office. H. O. Pub. No. 603.

Poole, L. R., 1976. Transformation of apparent ocean wave spectra observed from an aircraft sensor platform. NASA Tech. Note. TN D-8246. Langley Res. Center, Hampton, Virginia.

Putnam, J. A. and J. W. Johnson, 1949. The dissipation of wave energy by bottom friction. Trans. Am. Geophys. Union, 30(1):67-74.

Rizzoli, P., R. Dacci, and M. Gacie, 1966. Numerical Calculation of wave refraction in the Adriatic Sea.

Coll. Inter. Sur L'Exploit des Oceans, Theme I, Vol. II, Proc., 1-9.

Shemdin, O., K. Hasselmann, S. V. Hsiao and K. Herterrich, 1978. Nonlinear and linear bottom interpolation effects in shallow water. Turbulent fluxes through the sea surface, wave dynamics and prediction. Ed. by A. Favre and K. Hasselmann. Plenum Publ. Co.

Shen, M. C. and J. B. Keller, 1975. Uniform ray theory of surface, internal and acoustic wave propagation in a rotating ocean or atmosphere. SIAM J. Appli. Math., 28(4):857-875.

Shepard, F. P., 1963. Submarine Geology. Harper, N.Y.

Stokes, G. G., 1880. Mathematical and physical papers, 1: 197-229 and 314-326. Cambridge University Press.

Sverdrup, H. U. and W. H. Munk, 1944. Wind, sea, and swell: Theory of relations for forecasting. U.S. Navy Hydrographic Office Publ., 601.

Walker, J. R., 1976. Refraction of finite-height and breaking waves. Proc. 15th Coastal Engr. Conf., 507-524.

Weggel, J. R., 1972. Maximum breaker height for design. Proc. 13th Conf. On Coastal Engr. ASCE., 1:419-432.

Wilson, W. S., 1966. A method for calculating and plotting surface wave rays. Dept. of Army Corps of Engineers. Tech. Memo No. 17.

APPENDIX A

INTERPOLATION OF WATER DEPTH

The depth data which are used for the present study are from Map 1000 and 12200 (edited in October 1980). Because a regular grid system is not used in the present study, the water depth must be interpolated along the wave rays. Several trial and error schemes have been tried for the interpolation. The first attempt was to fit the bottom depth data to cubic surface equations. The second try was made for the quadratic equation. However, both trials failed because they produced undesirable ridges and/or troughs. Then, by taking more points of depth data into the calculations at a given point, the least square fits to the cubic and quadratic surfaces were attempted, and found to be much more stable than the equation fitting methods described earlier. The method is not suitable for the present case, however, because first, it requires too much computing time, and second, the area of the data points used for this method is so wide that it was easy to generate an erroneous surface. Another method uses a least square fit to a linear surface, and reduces computing time greatly. (Similar comparisons of the above mentioned method were conducted by Harrison and Wilson (1964)).

The water depths interpolated by this least square fit to a linear surface are compared with the actual depth data. They show very high correlations. Further, since the wave refraction equation is a second order differential equation, the depth effect is averaged twice, thus minor changes of depth contour do not greatly affect the wave refraction of a large scale wave movement as in the present study.

The computational procedure used is as follows: at a given position, seven adjacent water depths are obtained from the above mentioned map data. (The reasons why there are seven are again due to the efficiency of computation and the availability of the data points.) These data points are used in the following equations.

$$Z_i = \sum_{i=1}^{7} f(x_i, y_i) \ , \qquad \text{(A1)}$$

where Z_i is the depth data corresponding to ith coordinates of x and y, and the function f is a function to be found. By setting ε_i to be the "difference" function at each point of data, we get

$$\varepsilon_i = Z_i - f(x_i, y_i), \quad i = 1,2,\ldots 7 \ . \qquad \text{(A2)}$$

Letting E be the sum of the squares of ε_i, and to make it be minimum, its differential with respect to the coefficients must be zero, thus

$$\frac{\partial E}{\partial a_j} = \sum_{i=1}^{7} \varepsilon_i \frac{\partial \varepsilon_i}{\partial a_j} = 0 \ . \qquad \text{(A3)}$$

This set of equations can be written in matrix form,

$$\mathbb{A}\, a_j = b_j \qquad \text{(A4)}$$

where a_j are the variables to be found which is a column vector (these are coefficients of function f), $\mathbb{A}$ is a matrix, and b_j is a column matrix. This equation is solved by taking the inverse transform of matrix $\mathbb{A}$. With these coefficients, the water depth f(x,y) is found. The subroutine for this process is listed in Appendix D.

APPENDIX B

INTEGRATION OF DISSIPATION RATE FUNCTION

For these functions, the fourth-order Runge-Kutta method is used (Gerald, 1970). The equation to be integrated has the following form,

$$\frac{dF}{ds} = - D_f \qquad \text{(A6)}$$

where D_f is the dissipation rate function, and s is the path of the wave ray. For this integration, finer steps of ds give a better approximation. However, we can not increase this number without bound, because we have to consider the calculation efficiency and the computer memory capacity. The 10 sub-divided points (per a step of a main program) show a good approximation for the present experiment.

The dissipation rate functions are written in the form of a multiple of the function F, which is a wave power for the present study. Then the water depth is interpolated by the linear equation, as

$$h_j(s) = \frac{d_i - d_{i-1}}{ds} s_j + d_{i-1}, \quad j = 0,1,2,\ldots 10 , \qquad \text{(A7)}$$

where ds is the distance per a step of a main program, d_{i-1} is the water depth of the previous calculation step of the main program, and d_i is the water depth when $s_j = s_{11}$; this depth is d_{i-1} for the next step calculation. This approximation can be justified by the following facts: (1) The interpolation method of the water depth is a plane fitting methods. (2) Initially a smooth bottom topography is assumed. Then equation (A6) can be written as

$$\frac{dF}{ds} = D_f\ (\ h(s),\ F)\ , \qquad \text{(A8)}$$

thus

$$F_{n+1} = F_n + (k_1 + k_2 + k_3 + k_4)\ /\ 6\ \ ,$$

where $k_1 = (ds/10)\ D_f(h_o, F_o)$,

$$k_2 = (ds/10)\ D_f(h_o + dh/2,\ F_n + k_1/2)\ ,$$

$$k_3 = (ds/10)\ D_f(h_o + dh/2,\ F_n + k_2/2)\ ,$$

and $k_4 = (ds/10)\ D_f(h_o + dh,\ F_n + k_3)$.

The accuracy of this method can be found in many articles (Burden et al., 1980; and Gerald, 1970).

APPENDIX C

TESTING OF ACCURACY IN NUMERICAL CALCULATION

Several tests for checking program accuracy have been made. First, a test of the reponse of the numerical model to the increment of the calculation step size over a constant sloping bottom is made. The y coordinates for each calculation step size are listed in Table C1. The variation in y coordinate due to changing step sizes is less than 0.1% of y.

Second, a test calculates the wave phase speed gradients with respect to x. Table C2 shows that the phase speed gradients--both the first and the second derivatives--are stable. For further comparison, the analytic derivation for the first derivative of wave speed using the linear wave theory has been made, and the values of dc/dx are listed in the same table. These values show very good agreement.

APPENDIX D

COMPUTER PROGRAM

This appendix contains a complete listing of the program for the first model. Most of the subroutines can alsc be used for the second model via slight modifications. The subroutine 'depth' for the actual sea bottom is listed at the end.

```
C   PROGRAM---REFCO.FOR---  MR. IMSANG OH   FEB/19/1981

C   PROGRAM REFRAC.CPY + DISSFN.SUB
C
C       A          THE SLOPE OF THE BOTTOM TOPOGRAPHY
C       HT         THE WAVE HEIGHT OF THE SURFACE WAVE
C       HTO        THE ORIGINAL VALUE OF THE SURFACE WAVE'S WAVE HEIGHT
C       DT         THE CHANGE IN THE TIME PER STEP
C       DTHET      THE CHANGE IN THE THET PER STEP
C       C          CELERITY
C       CC         CELERITY
C       DEL        RADIUS OF THE BUMP/HOLLOW; USED IN DEPTH CASE=4
C       DSR        PARAMETER OF DEPTH CASE=3,4
C       DSX        PARAMETER OF DEPTH CASE=3,4
C       KS         DUMMY VARIABLE TO KEEP TRACK OF KK
C       KHT        KEEPS TRACK OF KK WITH RESPECT TO THE RAYS
C       KAVER      AVERAGES THE VALUES OF KHT   USED IN WVHGT
C       KO         ORIGINAL VALUE OF K  CALC. FROM WL
C       KK         VALUE OF K-- THE WAVENUMBER
C       DISTO      THE DISTANCE BETWEEN THE ORIGINAL X AND Y POSITIONS
C       DIST       THE DISTANCE BETWEEN CORRES. X AND Y VALUES
C       G          GRAVITY
C       HO         THE WATER DEPTH COEFFICIENT
C       XO         THE SHORE BOUNDARY CONDITION
C       XEND       SAME AS XO MINUS 100 METERS
C       H,D        THE DEPTH OF THE WATER COLUMN
C       RTHET      THE ANGLE THET IN RADIANS
C       ICOUNT     PARAMETER CONTROLLING THE OUTPUT QUANTITY
C       KSLOPE     INPUT VARIABLE FOR THE HEIGHT GEOMETRY
C       GAMMA      DETERMINES THE +VE/-VE SLOPE OT THE  DEPTH GEOMETRY
C       WL         WAVELENGTH
C       OMEGA      2*PI/\; USED IN THIRD ORDER CALCULATIONS
C       DTHETA     DTHET IN DEGREES
C       DX         THE CHANGE IN THE X-DIR. PER STEP
C       DY         THE CHANGE IN THE Y-DIR. PER STEP
C       NPROB      THE NO. OF PROBLEMS: EACH ANGLE AND DS
C       NMSTP      CALCULATES THE NUMBER OF STEPS IN A DO LOOP
C       ONE-FIVE   CELERITY CALCULATIONS AT DIFFERENT POINTS ABOUT (X,Y)
C       WIDTH      RATIO OFORIGINAL RAY DIST. TO THE PRESENT VALUE
C       LENGTH     RATIO OF THE PRESENT WAVENUMBER TO THE ORIGINAL
C       RATIO      COEFFICIENT OF THE ORIGINAL WAVE HEIGHT TO CALC. HT
C       ORDER      THE ORDER TERM OF STOKES EQN.
C
C
C
      REAL KHT,KAVER,KO,KK,KS,LENGTH
      INTEGER ORDER
     COMMON/ANGLE/THET
     COMMON/HTLT/HT,HTO,DISTO
     COMMON/BC/A,G,HO,XO
     COMMON/BJC/H,CC
     COMMON/CJEG/DT,DTHET,TIME,N
     COMMON/COME/RTHET
     COMMON/COODR/X,Y
     COMMON/COUNT/ICOUNT
```

```
      COMMON/DISTAN/DIST
      COMMON/HEAD/DEL,DSX,DSR
      COMMON/INOUT/JIN,JOUT
      COMMON/PARA/DS,DSTOT,DIM1
      COMMON/PIE/P,DIVP,PI
      COMMON/STEP/ISTEP
      COMMON/TOPOG/KSLOPE,KDISS
      COMMON/UPDOWN/GAMMA
      COMMON/WAVEL/KAVER,LENGTH,WIDTH
      COMMON/WAVLEN/WL
      COMMON/WJC/KO,OMEGA,KK,BO
      COMMON/BBETA/B(3),BETA
      COMMON/WNINES/ONE,TWO,THREE,FOUR,FIVE,SIX,SEVEN,
     *          EIGHT,WNINE
      COMMON/FIX/XEND,ANG,ORDER
      COMMON/ENERGY/ETOTAL,POWER,ERATIO,FRIFC
      EQUIVALENCE (M,JOUT)
C
C      INPUT/OUTPUT DEVICES
C
        WRITE(5,333)
333     FORMAT(/,' ENTER INPUT/OUTPUT DEVICE : EX. FOR INPUT 22,
     1   FOR OUTPUT TTY=5, DSK=23,   ALSO ENTER KSLOPE AND KDISS')
        ACCEPT*, JIN,JOUT,KSLOPE,KDISS
C
        IF(JIN .EQ. 22) OPEN(UNIT=JIN,FILE='REFCO.DAT')
        IF(JOUT .EQ. 23) OPEN(UNIT=JOUT,FILE='REFCO.OUT')
C
C      READ THE NUMBER OF PROBLEMS: EACH PROBLEM IS AN ANGLE AND DS
C
        NPROB=1
      WRITE(JOUT,7000)  NPROB
C
C      READ DATA  **  NPROB TIMES
C
      DO 8877  IJKLM=1,NPROB
        IIKLM=IJKLM
        IF(IJKLM. GT. 1) OPEN(UNIT=JIN,FILE='REFCO.DAT')
      CALL REED(IIKLM)
        CLOSE(UNIT=JIN)
      P = PI/180.
      DIVP = 1.0/P
      KO = (2.*PI)/WL
      KK = KO
      DSTOT = 0.
      KHT = KO
      RTHET = P*THET
      DX = DS*COS(RTHET)
      DY = DS*SIN(RTHET)
    1 CONTINUE
      CALL DEPTH(X,Y,H)
        DIM1=H
      OMEGA = SQRT(G*KO*(TANH(KO*H)))
        ISTEP=1
        B(1)=1.0
```

```
        B(2)=1.0
      CALL WVHGT
      WRITE(JOUT,9000)OMEGA,KO
        KOO=KO
        ETOTAL=0.125*1.03*9.8*HTO*HTO
        CALL GRPV(OMEGA,CC,CG,KOO,H)
        POWER=CG*ETOTAL
      WRITE(M,50)
      I3 = ICOUNT
      CALL KNAME
        THETM1=90.
C
500   I3 = I3 + 1
    8 DSTOT = DSTOT + DS
C
      XX = X
      YY = Y
        CALL DEPTH(XX,YY,D)
      XPOS = XX + DX
      XNEG = XX - DX
      YPOS = YY + DY
      YNEG = YY - DY
      KS = KHT
      KK = KS
      ONE = C(XX,YY)
      KHT = KK
      KK = KS
      TWO = C(XPOS,YY)
      KK = KS
      THREE = C(XNEG,YY)
      KK = KS
      FOUR = C(XX,YPOS)
      KK = KS
      FIVE = C(XX,YNEG)
        KK=KS
        SIX=C(XPOS,YPOS)
        KK=KS
        SEVEN=C(XNEG,YPOS)
        KK=KS
        EIGHT=C(XNEG,YNEG)
        KK=KS
        WNINE=C(XPOS,YNEG)
        GO TO 98765
      CALL ROUND(ONE)
      CALL ROUND(TWO)
      CALL ROUND(THREE)
      CALL ROUND(FOUR)
      CALL ROUND(FIVE)
        CALL ROUND(SIX)
        CALL ROUND(SEVEN)
        CALL ROUND(EIGHT)
        CALL ROUND(WNINE)
98765   CONTINUE
C
      DT = DS/ONE
```

```
      TIME = TIME + DT
C
C     DTHET = THE CHANGE IN THETA CALC.
C
C
      DTHET  =  (1./(2.*ONE))*((SIN(RTHET)/COS(RTHET))*
     1             (TWO-THREE)-(COS(RTHET)/SIN(RTHET))*
     2             (FOUR-FIVE))
C
C     NEW THETA ANGLE IN RESPONSE TO CHANGES IN S,X,Y
C
      RTHET = RTHET + DTHET
      THET = RTHET*DIVP
      DTHETA = DTHET*DIVP
C
555      DX = DS*COS(RTHET)
      DY = DS*SIN(RTHET)
      X = X + DX
      Y = Y + DY
      XTEST =  X
      YTEST= Y
        CALL DEPTH(XTEST,YTEST,H)
        IF (XTEST.GE.XEND)  GO TO 61
        IF (YTEST.GE.4.*XEND) GO TO 61
        IF(XTEST.LT.-5000.) GO TO 61
  200 CONTINUE
      KAVER = KHT
      CALL WVHGT
        IF(I3 .LT. ICOUNT) GO TO 500
        I3=0
        WVLTH=2.*PI/KK
        DOVWL=H/WL
        HTOVWL=HT/WL
        WOVWL=WVLTH/WL
        GTSQRT=SQRT(LENGTH)
        WTSQRT=SQRT(ABS(WIDTH))
        DOVL=H/WVLTH
        WRITE(JOUT,48)X,Y,THET,DOVWL,WOVWL,HTOVWL,GTSQRT,WTSQRT,DOVL,CC
69      THETM1=THET
        GO TO 500
   61 CONTINUE
      WRITE(M,62)
      WRITE(M,50)
 1111 CONTINUE
10000 CONTINUE
 8877 CONTINUE
   50 FORMAT(1H1)
   48 FORMAT(1X,4E14.6,6(1X,E11.4))
   62 FORMAT(1X,'WE ARE AT THE SHORE')
  908 FORMAT(100X,I10)
  909 FORMAT(1X,6(E17.10,2X))
 7000 FORMAT(I10)
 8000 FORMAT(1X,10(I10,1X))
 9000 FORMAT(1X,'     OMEGA = ',E16.8,/,1X,'        KO = ',
     1          E16.8,//)
   99 CONTINUE
        CLOSE(UNIT=23)
```

```
      CLOSE(UNIT=22)
      STOP
      END

      SUBROUTINE KNAME
      COMMON/ANGLE/THET
      COMMON/HEAD/DEL,DSX,DSR
      COMMON/INOUT/JIN,JOUT
      COMMON/PARA/DS,DSTOT,DIM1
      COMMON/TOPOG/KSLOPE,KDISS
      COMMON/UPDOWN/GAMMA
      COMMON/FIX/XEND,ANG,ORDER
      EQUIVALENCE (M,JOUT)
C
      GO TO (105,205,305,405,505),KSLOPE
  105 WRITE(M,106)
      GO TO 505
  205 WRITE(M,206)
      GO TO 505
  305 WRITE(M,306)
      GO TO 505
  405 WRITE(M,406)
  106 FORMAT(1X,40H      SLOPING BOTTOM                          )
  206 FORMAT(1X,40H      RIDGE/VALLEY                           )
  306 FORMAT(1X,40H      TWO FLAT PLANES W/ SLOPE IN BETN.       )
  406 FORMAT(1X,40H     BUMP OR HOLLOW                          )
  505 CONTINUE
        WRITE(M,7) ORDER
    7   FORMAT(1H ,10H ORDER =     ,I2)
      WRITE(M,6)  DEL,DSX,DSR
    6 FORMAT(1X,10H   DEL =   ,E12.5,/,1X,10H   DSX =   ,E12.5,/,1X,10H
     1  DSR =   ,E12.5)
      WRITE(M,4)
    4 FORMAT(6X,'X',11X,'Y',15X,'THET',8X,'DTP/WL',8X,'L/WL',
     18X,'HT/WL',8X,'SH CO',7X,'RE CO',10X,' D/L',/)
      RETURN
      END

      SUBROUTINE REED(IJKLM)
C
C      READ ALL INPUT DATA FOR ONE PROBLEM, EXCEPT NPROB
C
        INTEGER ORDER
      REAL KO,KK
      COMMON/HTLT/HT,HTO,DISTO
      COMMON/ANGLE/THET
      COMMON/BC/A,G,HO,XO
      COMMON/CJEG/DT,DTHET,TIME
      COMMON/COODR/X,Y
      COMMON/COUNT/ICOUNT
      COMMON/HEAD/DEL,DSX,DSR
```

```
      COMMON/INOUT/JIN,JOUT
      COMMON/PARA/DS,DSTOT,DIM1
      COMMON/PIE/P,DIVP,PI
      COMMON/STEP/ISTEP
      COMMON/TOPOG/KSLOPE,KDISS
      COMMON/UPDOWN/GAMMA
      COMMON/WAVLEN/WL
      COMMON/WJC/KO,OMEGA,KK,BO
      COMMON/FIX/XEND,ANG,ORDER
      COMMON/ENERGY/ETOTAL,POWER,ERATIO,FRIFC
C
      READ(JIN,1)  ORDER
      READ(JIN,10)  DEL,DSR,DSX
      READ(JIN,10)  GAMMA,HO,XO,WL,HTO,FRIFC
      READ(JIN,10)  X
      READ(JIN,10)  Y
      READ(JIN,10)  THET
        READ(JIN,10) DS
        READ(JIN,10) XEND
        XEND=XO-DS
      READ(JIN,1)   ICOUNT
        PI=3.14159265
        G=9.80
        A=HO/XO
      WRITE(JOUT,101)
      WRITE(JOUT,2)  ORDER
      WRITE(JOUT,103)
      WRITE(JOUT,12)  DEL,DSR,DSX

      WRITE(JOUT,104)
        WRITE(JOUT,13)A,GAMMA,HO,XO,WL,HTO,FRIFC
        XEND=XO-DS
      WRITE(JOUT,109)
      WRITE(JOUT,12)  X
      WRITE(JOUT,110)
      WRITE(JOUT,12)  Y
      WRITE(JOUT,107)
      WRITE(JOUT,12)  THET
      WRITE(JOUT,111)
      WRITE(JOUT,12)  DS
      WRITE(JOUT,120)
      WRITE(JOUT,12)   XEND
      WRITE(JOUT,121)
      WRITE(JOUT,2) ICOUNT
      WRITE(JOUT,122)
      WRITE(JOUT,2)   KSLOPE,KDISS
    1 FORMAT(/,6I10)
    2 FORMAT(6(1X,I9),/)
   10 FORMAT(/,6F12.3)
   12 FORMAT(6(1X,F11.3),/)
   13   FORMAT(2F12.6,4F12.2,4F12.4)
  101 FORMAT(7X,5HORDER)
  102 FORMAT(10X,2HPI)
  103 FORMAT(9X,3HDEL,9X,3HDSR,9X,3HDSX)
  104 FORMAT(11X,1HA,7X,5HGAMMA,10X,2HHO,10X,2HXO,10X,2HWL,8X,
     1          4HHTO    )
```

```
  105 FORMAT(7X,5HDT(1),7X,5HDT(2))
  106 FORMAT(4X,8HDTHET(1),4X,8HDTHET(2))
  107 FORMAT(5X,7HTHET(1),5X,7HTHET(2))
  108 FORMAT(5X,7HTIME(1),5X,7HTIME(2))
  109 FORMAT(8X,4HX(1),8X,4HX(2))
  110 FORMAT(8X,4HY(1),8X,4HY(2))
  111 FORMAT(7X,2HDS)
  120 FORMAT(5X,5H XEND)
  121 FORMAT(1X,9HICOUNT     )
  122 FORMAT(5X,6HKSLOPE,5X,5HKDISS)
      RETURN
      END


      SUBROUTINE WVHGT
C
C      CALC NEW WAVE HEIGHT OF SURFACE WAVES IN REFERENCE TO HTO
C
      REAL K,KO,LENGTH
      REAL KAVER
      COMMON/HTLT/HT,HTO,DISTO
      COMMON/COME/RTHET
      COMMON/COODR/X,Y
      COMMON/DISTAN/DIST
      COMMON/STEP/ISTEP
      COMMON/WAVEL/KAVER,LENGTH,WIDTH
      COMMON/INOUT/JIN,JOUT
      COMMON/PARA/DS,DSTOT,DIM1
      COMMON/WJC/KO,OMEGA,KK,BO
      COMMON/ENERGY/ETOTAL,POWER,ERATIO,FRIFC
      COMMON/BBETA/B(3),BETA
C
      IF (ISTEP.NE.1)  GO TO 100
      ISTEP = 0
      DISTO = DIST
      HT = HTO
      RETURN
  100 K = KAVER
        CALL INTENS
        WIDTH=1./(ABS(BETA))
        CALL DEPTH(X,Y,D)
        CALL DISSFN(OMEGA,D,HT)
        DIM1=D
        LENGTH= 1/(TANH(K*D)*(1+2.*K*D/SINH(2.*K*D)))
      RATIO = LENGTH*WIDTH*ERATIO
      HT = HTO*SQRT(RATIO)
      RETURN
      END


      FUNCTION C(X,Y)

      REAL KK
      COMMON/BC/A,G,HO,XO
```

```
      COMMON/BJC/H,CC
      COMMON/INOUT/JIN,JOUT
      COMMON/TOPOG/KSLOPE,KDISS
      COMMON/WJC/KO,OMEGA,KK,BO
      EQUIVALENCE (M,JOUT)
      CALL CELER(X,Y,CC)
      C = CC
      RETURN
      END


      SUBROUTINE CELER(X,Y,C)
C
C      CALC CELERITY USING ITERATION AND CLR SUBROUTINES
C
        REAL KO,K1,K2,K3,K
        REAL KK
        INTEGER ORDER
      COMMON/HTLT/HT,HTO,DISTO
      COMMON/BC/A,G,HO,XO
      COMMON/BJC/H,CC
      COMMON/INOUT/JIN,JOUT
      COMMON/TOPOG/KSLOPE,KDISS
      COMMON/WJC/KO,OMEGA,KK,BO
      COMMON/FIX/XEND,ANG,ORDER
      EQUIVALENCE(M,JOUT)
C
        CALL DEPTH(X,Y,H)
1000    CALL CALCK(OMEGA,H,10.,K3)
      K = K3
      KK  = K
C
      CALL CLR(HT,K,ORDER,C)
      RETURN
      END


      SUBROUTINE CLR(HT,K,ORDER,C)
C
C      CALC THE VALUE OF C FOR ORDERS = 0,1,3
C
        REAL K,KK
        INTEGER ORDER
      COMMON/BC/A,G,HO,XO
      COMMON/BJC/H,CC
      COMMON/INOUT/JIN,JOUT
      COMMON/TOPOG/KSLOPE,KDISS
      COMMON/WJC/KO,OMEGA,KK,BO
      EQUIVALENCE (M,JOUT)
C
      IF (ORDER.EQ.0)  GO TO 200
      IF (ORDER.EQ.3)  GO TO 100
      C = SQRT((G/K)*TANH(K*H))
      RETURN
  100 CONST = G/OMEGA
```

```
        N=0
        ABKK=10.
588     HK=H*K
        COKH6=COSH(HK)**6
        COKH4=COSH(HK)**4
        COKH2=COSH(HK)**2
        SIKH6=SINH(HK)**6
        SIKH4=SINH(HK)**4
      PP = (3./64./4.)*(8.*(COKH6)+1.)/(SIKH6)
      QQ =(8.*((COKH4)-(COKH2))+9.)/(32.*(SIKH4))
        EKA = K*HT/PP
      RDCL = SQRT(0.25*EKA**2+1./(27.*PP**3))
      AA = (0.5*EKA+RDCL)**(1./3.)
        EKRD=0.5*EKA-RDCL
        IF(EKRD.LT.0.0)  GO TO 198
      BB = (0.5*EKA-RDCL)**(1./3.)
        GO TO 199
198     BB = -((-EKRD)**(1/3.))
199      ALPHA = AA  +  BB
        BO=ALPHA*0.5/K
        OMG=OMEGA/SQRT(1.+QQ*(ALPHA**2))
        CALL CALCK(OMG,H,10.,COMK)
      C = CONST*TANH(K*H)*(1.+QQ*(ALPHA**2))
        ABSKMK=ABS((AMAX1(K,COMK)/AMIN1(K,COMK)) -1.)
        IF((ABSKMK) .LT. 1.0E-06)  RETURN
        ABKK=ABSKMK
        K=COMK
        N=N+1
        IF(N.GT.100) RETURN
        GO TO 588
      RETURN
  200 C = SQRT(G*H)
      RETURN
      END


      SUBROUTINE DEPTH(X,Y,H)
C
C      SUBROUTINE DEPTH CALC. THE WATER DEPTH
C             WITH   X,XO,A

      COMMON/BC/A,G,HO,XO
      COMMON/HEAD/DEL,DSX,DSR
      COMMON/TOPOG/KSLOPE,KDISS
      COMMON/UPDOWN/GAMMA
C
      XX = (X-DSX)/DEL
C      SLOPING BOTTOM
C
C      A=SLOPE = HO/XO
        H=A*(XO-X)
        IF((XO-X) .LE. 0.0) H=0.0000001
        GO TO (1,2,3,4), KSLOPE
        IF(KSLOPE.EQ.7) GO TO 7
        GO TO 10
```

```
    1   CONTINUE
        RETURN
C
C       RIDGE/VALLEY
C         GAMMA > ZERO    RIDGE
C         GAMMA < ZERO    VALLEY
C
    2 H = HO*(1.+GAMMA*((TANH(XX)**2)-1.))
        RETURN
C
C       TWO FLAT PLANES W/ SLOPE IN BETN.
C         GAMMA < ZERO    SHALLOW TO DEEP
C         GAMMA > ZERO    DEEP TO SHALLOW
C
    3 H = HO*(1. - GAMMA*(TANH(XX)-1.))
        RETURN
C
C       BUMP OR HOLLOW
C         GAMMA > ZERO    BUMP
C         GAMMA < ZERO    HOLLOW
C
    4 R = SQRT(X**2+Y**2)
        PHI = ATAN2(Y,X)
        Z = DSR - R*COS(PHI)
        Q = SQRT(Y*Y+Z*Z)
        RR = Q/DEL
        H = HO*(1.+GAMMA*((TANH(RR)**2)-1.))
        RETURN
C
C       X IS LESS THAN ZERO
C
   10 H = 0.0
        RETURN
C**********************************
    7     H=A*X + 0.15*HO
          RETURN
C**********************************
        END
C
C
C
        SUBROUTINE ROUND(X)
C       *
C       ***      ROUNDS TO FIVE SIGNIFICANT FIGURES          ****
C       *
        IX = IFIX(X)
        IF (IX.LE.0)  GO TO 100
C   IX > 0
        I = 1
        IZ = 10
    5 IF (IX.LT.IZ)  GO TO 20
        I = I + 1
        IZ = IZ*10
        GO TO 5
```

```
   20 K = 6- I
      Z = (10.0**K)*X
      Z = (Z + 5.0)*0.1
      IZ = IFIX(Z)
      X = FLOAT(IZ)*(10.0**(1-K))
      RETURN
C    IX = 0
  100 I = 0
      Y = 10.0
   25 Z = Y*X
      IZ = IFIX(Z)
      IF(IZ.GT.0)  GO TO 500
      I = I +1
      Y = 10.0*Y
      GO TO 25
  500 K = 6 + I
      Z = (10.0**K)*X
      Z = (Z + 5.0)*0.1
      IZ = IFIX(Z)
      X = FLOAT(IZ)*(10.0**(1-K))
      RETURN
      END
C
CCCCC
C
      SUBROUTINE DISSFN(FREQ,D,WH)
C
C   CALC. BOTTOM FRICTION BY THREE DIFFERENT FORMULA USING
C   RUNGE-KUTTA TECHNIQUE.
      DIMENSION X(11),Y(11),YC(11),YE(11)
      COMMON/PARA/DS,DSTOT,DIM1
      COMMON/INOUT/JIN,JOUT
      COMMON/TOPOG/KSLOPE,KDISS
      COMMON/ENERGY/ETOTAL,POWER,ERATIO,FRIFC
      COMMON/BBETA/B(3),BETA
      COMMON/WJC/KO,OMEGA,KK,BO

      COMMON/WAVEL/KAVER,LENGTH,WIDTH
C   DEFINE THE THREE FORMULA

      DP(D,YP)=-8*0.01/3./9.8*FREQ*FREQ*WH*YP/((SINH(WK*D)**3
     *          )*CG)*BETA

      DC(D,YP)=-BT*WKIVIS/9.8*C*C*SUM*YP/(D*D*CG)*BETA

      DE(D,YP)=-2.*BT*WKIVIS*WK*YP/CG/SINH(2.*WK*D)*BETA

C
C   CONSTANTS
C
      IF(KDISS.NE.0)GO TO 8
      ERATIO=1.0
      RETURN
8     WKIVIS=1.3/1.03/1000000.
      BT=SQRT(FREQ*.5/WKIVIS)
```

```
      DH=DS*0.1
      ALPHA=(DIM1-D)/DS
      ADH=ALPHA*DH
      PI=3.14159265

      XO=DIM1
      YO=POWER

      X(1)=0.
      Y(1)=YO

      DO 10 I=2,11
      CALL GRPV(FREQ,C,CG,WK,XO)
      GO TO (1,2,3), KDISS
1     FK1=DH*DP(XO,YO)
      FK2=DH*DP(XO+0.5*ADH,YO+.5*FK1)
      FK3=DH*DP(XO+0.5*ADH,YO+.5*FK2)
      FK4=DH*DP(XO+ADH,YO+FK3)
      Y(I)=YO+(FK1+2.*FK2+2.*FK3+FK4)/6.
      YO=Y(I)
      GO TO 100

2     WL=2.*PI/WK
        SUM=1.+1.4142136*(3./(16.*PI*PI)*BO*WL*WL/(D**3))**2+
     - 1.7320508*(27./1024./(PI**4)*BO*BO*(WL**4)/(D**6))**2


      FK1C=DH*DC(XO,YO)
      FK2C=DH*DC(XO+0.5*ADH,YO+.5*FK1C)
      FK3C=DH*DC(XO+0.5*ADH,YO+.5*FK2C)
      FK4C=DH*DC(XO+ADH,YO+FK3C)
      YC(I)=YO+(FK1C+2.*FK2C+2.*FK3C+FK4C)/6.
      YO=YC(I)
      GO TO 100

3     FK1E=DH*DE(XO,YO)
      FK2E=DH*DE(XO+0.5*ADH,YO+.5*FK1E)
      FK3E=DH*DE(XO+0.5*ADH,YO+.5*FK2E)
      FK4E=DH*DE(XO+ADH,YO+FK3E)

      YE(I)=YO+(FK1E+2.*FK2E+2.*FK3E+FK4E)/6.
      YO=YE(I)

100   X(I)=X(I-1)+DH
      XO=X(I)*ALPHA+DIM1
10    CONTINUE

101   FORMAT(10X,'    X        LINEAR              CHET',/,
     1  11(4E16.8,/))
      POWER=YO
      EE=POWER/CG
      ERAT=EE/ETOTAL
      ERATIO=ERAT
      RETURN
      END
```

```
      SUBROUTINE GRPV(FREQ,C,CG,WK,D)
C     THIS SUBROUTINE CALCULATE CERELITY AND GROUP VELOCITY AND
C     WAVE NUMBER AT A GIVEN POSITION AND GIVEN FREQUENCY.

      CALL CALCK(FREQ,D,10.E+1,WK)
      C=SQRT(9.8*TANH(WK*D)/WK)
      WN=0.5+WK*D/SINH(2.*WK*D)
      CG=C*WN
      RETURN
      END



      SUBROUTINE CALCK(WW,D,KK,WK)
C
C     THIS PROGRAM IS SUBROUTINE FOR FINDING WAVE NUMBER BY
C     ITERATION METHOD FROM DISPERSION RELATION.
C
      REAL KK,K3,K4

      K3=KK
      K4=1.0E-8

      W=WW
      N=0
1     N=N+1
      IF(N .GT. 100) GO TO 30
      FK3=W*W-9.8*K3*TANH(K3*D)
      FK4=W*W-9.8*K4*TANH(K4*D)

      IF(ABS(FK3) .LT. 1.0E-6) GO TO 10
      IF((FK3*FK4) .GT. 0.) GO TO 20
      K3=(K3+K4)*.5
      GO TO 1

20    K4=(K3-K4) + K3
      GO TO 1

10    WK=K3
      GO  TO 50
30    CONTINUE
C30   WRITE(5,999) N
999   FORMAT(' IETERATION DOES NOT CONVERSE AT N =', I5)
C     STOP
50    RETURN
      END
```

```
      SUBROUTINE INTENS
C
C
C   THIS SUBROUTINE CALCULATES THE WAVE INTENSITY ALONG THE
C   WAVE RAY, BY FINITE DIFFERENCE METHOD.
C
      COMMON/COME/RTHET
      COMMON/PARA/DS,DSTOT,DIM1
      COMMON/BBETA/B(3),BETA
      COMMON/WNINES/ONE,TWO,THREE,FOUR,FIVE,SIX,SEVEN,
     *          EIGHT,WNINE
C
      DX=DS*COS(RTHET)
      DY=DS*SIN(RTHET)

      DCDX=(TWO-THREE)/(2.*DX)
      DCDY=(FOUR-FIVE)/(2.*DY)

      DC2DX=(TWO+THREE-2.*ONE)/(DX*DX)
      DC2DY=(FOUR+FIVE-2.*ONE)/(DY*DY)

      DC2DXY=(SIX-SEVEN+EIGHT-WNINE)/(4.*DX*DY)
      CDIV=1./ONE

C
C   CALC. P AND Q
C
      PEE=(COS(RTHET)*DCDX+SIN(RTHET)*DCDY)*(-CDIV)
      QUE=(SIN(RTHET)*SIN(RTHET)*DC2DX - 2.*SIN(RTHET)*COS(
     1          RTHET)*DC2DXY + COS(RTHET)*COS(RTHET)*DC2DY)*CDIV
C
C   CALC. BETA(=WAVE INTENSITY)
C
      B(3)=((PEE*DS-2.)*B(1)+(4.-2.*QUE*DS*DS)*B(2))/(PEE*DS+2)
C
      B(1)=B(2)
      B(2)=B(3)
      BETA=B(3)
C
      RETURN
      END
```

```
      SUBROUTINE DEPTH(X,Y,D)
C     PROGRAM---COMDT1.SUB-- BY IMSANG OH  JAN/23/1981
C     SUBPROGRAM FOR COMPLEX DEPTH
C     CONVERTING THE RANDOM DEPTH TO REGULAR INTERVAL GRID.
C     LEAST SQUARE FIT OF DEPTH DATA TO LINEAR EQUATION.

      DIMENSION ICX(7),ICY(7),N(7),A(3,4),C(3),CONST(3),CO(3)
      COMMON/OLDCO/ICXO(7),ICYO(7)
      COMMON/DEEP/DPT(1816)
      COMMON/CODPT/IX(1816),IY(1816)

C     CONVERTING THE INCOMING DATA INTO THE GRID POINTS WHICH
C     ARE USED IN THIS SUBROUTINE.(UNIT=1 KN, I.E., 1852M=1KN).
C     ALSO CORRECTION FOR LATITUDE VARIATION ALONG RAY.

      TY=Y/1852.
      TX=X/1852./COS( (37.-TY/60.)*3.14159265/180.)
      PX=TX-AINT(TX)
      PY=TY-AINT(TY)

      IXX=AINT(TX)
      IYY=AINT(TY)
      IF(PX.GT.0.5) IXX=IXX+1
      IF(PY.GT.0.5) IYY=IYY+1



      DO 15 I=1,7
      ICX(I)=-1
15    ICY(I)=-1

      ICOUNT=0
      DO 20 I=1,20
      II=I-1
      DO 30 J=1,1816
      IF(ABS(IXX-IX(J)).GT.II) GO TO 30
      IF(ABS(IYY-IY(J)).GT.II) GO TO 30

      DO 25 KKK=1,6
      IF((IX(J).EQ.ICX(KKK)).AND.(IY(J).EQ.ICY(KKK))) GO TO 30
25    CONTINUE
      ICOUNT=ICOUNT+1
      ICX(ICOUNT)=IX(J)
      ICY(ICOUNT)=IY(J)
      N(ICOUNT)=J
      IF(ICOUNT.EQ.7) GO TO 400
30    CONTINUE
20    CONTINUE

400   CONTINUE
C400  WRITE(5,97) IXX,IYY,((ICX(I),ICY(I),DPT(N(I))),I=1,7),N
97    FORMAT(///12X,2I12,/,7(/,12X,2I12,F15.0),7I5)
```

```
      IN=0
      DO 555 I=1,7
      DO 777 J=1,7
      IF(ICX(I).NE.ICXO(J)) GO TO 777
      IF(ICY(I).NE.ICYO(J)) GO TO 777
      IN=IN+1
777   CONTINUE
      IF(IN.EQ.7) GO TO 444
555   CONTINUE

      CALL MAKEA(A,ICX,ICY)
CC          TYPE101,((A(KKK,LLL),LLL=1,4),KKK=1,3)
C         TYPE*,N
101   FORMAT(//10E12.5)
      CALL MAKECT(DPT,ICX,ICY,CONST,N,ZIM1)
C           TYPE101,CONST,XIM1,YIM1,ZIM1

      CALL GAUSS(A,C,CONST,CO,3)
C           TYPE*,C
C444  XIM1=FLOAT(IXX)
C     YIM1=FLOAT(IYY)
444   XIM1=TX
      YIM1=TY
      D=Z(XIM1,YIM1,C)
C   CONVERT THE UNIT OF FATHOM INTO METER
      D=1.8288*D
      ZIM1=D
      DO 333 I=1,3
333   CO(I)=C(I)
      AAA=D
C     WRITE(5,91) IXX,IYY,AAA
91    FORMAT(2I10,F17.3)

      DO 77 I=1,7
      ICXO(I)=ICX(I)
77    ICYO(I)=ICY(I)

      RETURN
      END

      REAL FUNCTION Z(X,Y,C)
      REAL C(3)

C     Z=C(1)+C(2)*Y+C(3)*Y*Y+C(4)*X+C(5)*X*Y+C(6)*X*X
      Z=C(1)+C(2)*Y+C(3)*X

      RETURN
      END
```

```
      SUBROUTINE MAKEA(A,ICX,ICY)
C  MAKEING THE MATRIX A BY GIVEN POSITION AND DPT

      DIMENSION A(3,4),ICX(7),ICY(7)

      DO 30 I=1,3
      DO 30 K=1,3
      A(K,I)=0.0
      DO 30 J=1,7
      X=ICX(J)*1.0
      Y=ICY(J)*1.0
      KK=K
      II=I
      A(KK,II)=A(KK,II)+XYN(X,Y,KK)*XYN(X,Y,II)
30    CONTINUE

      RETURN
      END


      SUBROUTINE MAKECT(DPT,ICX,ICY,CONST,N,ZIM1)
C   GENERATING THE COLUMN VECTOR OF RIGHT HAND SIDE OF EQ.

      DIMENSION DPT(1816),ICX(7),ICY(7),CONST(3),N(7)

      DO 10 I=1,3
      SZXY=0.0

      DO 20 J=1,7
      X=ICX(J)*1.0
      Y=ICY(J)*1.0
      IK=I
      ZXY=DPT(N(J))*XYN(X,Y,IK)
C     IF(J.EQ.7) ZXY=ZIM1*XYN(X,Y,IK)
20    SZXY=SZXY+ZXY
      CONST(I)=SZXY
10    CONTINUE
C       TYPE101,(CONST(I),I=1,3)
101   FORMAT(// 3E12.5)
      RETURN
      END
```

```
      SUBROUTINE GAUSS(A,C,CONST,CO,M)
C   EVALUATING THE CONSTANT BY GAUSSIAN ELLIMINATION.

      DIMENSION T(4),C(3),CO(3)
      DIMENSION A(3,4)
C     COMMON C(3)
      DIMENSION CONST(3)
      MP1=M+1
      MM1=M-1
      DO 55 I=1,M
55    A(I,MP1)=CONST(I)
C        TYPE101 ,((A(I,J),J=1,MP1),I=1,M)
101   FORMAT(//,3F12.2)
      K=1
1     CONTINUE
      DO 20 I=K,M
      IF(A(I,K).EQ.0.) GO TO 20
      DO 30 J=K,MP1
      T(J)=A(K,J)
      A(K,J)=A(I,J)
      A(I,J)=T(J)
30    CONTINUE
20    CONTINUE

      KP1=K+1
      DO 50 I=KP1,M
      CONV=A(I,K)/A(K,K)
      DO 60 J=K,MP1
      A(I,J)=A(I,J)-CONV*A(K,J)
60    CONTINUE
C       TYPE101,((A(KK,LL),LL=1,5),KK=1,4)
50    CONTINUE

      K=K+1
      IF(K.LT.M) GO TO 1

      C(M)=A(M,MP1)/A(M,M)
200   DO 70 I=1,MM1
      II=MP1-I
      IM1=II-1
      HAP=0.0
      DO 80 J=II,M
      HAP=HAP+A(IM1,J)*C(J)
80     CONTINUE
      C(IM1)=(A(IM1,MP1)-HAP)/A(IM1,IM1)
70    CONTINUE
      RETURN
      END
      REAL FUNCTION XYN(X,Y,M)

      GO TO (1,2,3),M

1     XYN=1.
      RETURN
2     XYN=Y
      RETURN
3     XYN=X
      RETURN
      END
```

AUTOBIOGRAPHICAL STATEMENT

IM SANG OH

BORN:

25 June 1948, Pohang, Korea

EDUCATION:

B.S. February 1972, Seoul National University

M.S. August 1976, Seoul National University

APPOINTMENTS AND POSITIONS:

Part Time Instructor, 1979, Department of Mathematics and Computing Science, Old Dominion University

Graduate Research Assistant, 1978-1981, Department of Oceanography, and Department of Mathematics, Old Dominion University

PUBLICATIONS:

Coastal/Offshore Positioning by Optical Methods, 1979, Tech. Rep. TR 79-5, Old Dominion University (with C. H. Blair)

The Polycheatous Annelids and Environments in the tidal flat, Inchon, Korea. J. Oceanolo, Soc. Korea, 11(2):71-76 (with W. S. Kim)

MEMBERSHIP IN PROFESSIONAL SOCIETY:

Member of Oceanological Society of Korea
Associate Member of Sigma Xi
Student Member of American Meteorological Society